Universitá degli Studi di Trieste

XXXI Ciclo del Dottorato di Ricerca in

Fisica

The effect of the Initial Mass Function (IMF) on the chemical evolution of elliptical galaxies.

Astronomia e Astrofisica

Dottorando:
Carlo M. De Masi
Supervisore:
Prof. F. Matteucci
Coordinatore:
Prof. L. Lanceri

ANNO ACCADEMICO 2017/2018

Summary

In this Thesis, we describe our work on the chemical evolution of elliptical galaxies, with a particular focus on the effect of the Initial Mass Function (IMF).
Generally, ellipticals are systems characterized by old stellar populations, showing little or no sign of ongoing star formation. Due to the lack of gas and star formation, chemical element abundances in these objects can only be derived from the study of absorption lines in their integrated spectra.
We adopted a modified version of the multi-zone model of chemical evolution for elliptical galaxies by Pipino and Matteucci (2004), taking into account both Type Ia and II SN feedback, where galaxies are assumed to form after the initial infall of a gas cloud. After this gas accretion, the galaxy produces its stellar population through a strong burst, which is eventually quenched by the thermal energy produced by stellar winds and SNe feedback (***galactic wind***), which drives the remaining gas away from the galaxy. Detailed stellar nucleosynthesis prescriptions are adopted to compute the formation of chemical elements.
The model allows us to follow the detailed evolution with time of 21 chemical elements, and we focused on reproducing the observed trends with mass of a number of abundance ratios, with the aim at deriving constraints on the formation and evolution of galaxies.
Specifically, we focused on reproducing the mass-metallicity and the $[\alpha/Fe]$-mass relations. In doing so, we investigated the effect of several recipes for the Initial Mass Function. The IMF has a strong influence on the evolution of chemical abundances, and we tested the most recent suggested IMFs for ellipticals.
We present the comparison of our results with (1) the dataset by Thomas et al. (2010), containing information on the chemical abundance patterns for $\approx$ 3000 galaxies extracted from the DR4 of the SDSS, and (2) with a sample of early-type galaxies selected from the SPIDER-SDSS catalog, whose abundances have been derived from averaged spectra, obtained by a stacking procedure of individual spectra according to their central velocity dispersion

(La Barbera et al., 2010; Rosani et al., 2018).
In previous works, the considered abundance trends could be reproduced by means of the so-called "inverse wind" model, namely assuming a larger efficiency of star formation in more massive ellipticals (also known as "downsizing" in star formation, see Matteucci, 1994).
The comparison with the first of these catalogs, however, showed the necessity to modify this scenario by adopting an IMF varying with galactic stellar mass. Specifically, we found that the observed increase of the total metallicity and the overabundance of α-elements with respect to Fe in more massive galaxies could only be reproduced by assuming a top-heavier IMF, i.e. a mass distribution of new-born stars skewed towards massive stars in galaxies with a higher total mass.
We tested both an arbitrarily varying IMF and the Integrated Galactic IMF (IGIMF), both becoming top-heavier for higher galactic masses, and, to different degrees, both IMFs were able to reproduce the trends. This is in contradiction with claims, diffused in literature, for the need of a bottom-heavy IMF for ellipticals (Cenarro et al., 2003; Auger et al., 2010; Grillo and Gobat, 2010; van Dokkum and Conroy, 2010, 2011; Conroy and van Dokkum, 2012a,b; Ferreras et al., 2013; La Barbera et al., 2013).
We repeated this analysis on the second catalog, and extended it by introducing new forms for the IMF; specifically, we tested a low-mass tapered ("bimodal") IMF.
The analysis of the second catalog, though not confirming the necessity of a top-heavier IMF (the trends in this catalog could be reproduced by assuming the inverse wind model only), strongly confirmed our rejection of bottom-heavier IMFs, which provided the worst agreement with data in our models.
As a way of reconciling our results with the observational claim of bottom-heavy IMFs, we finally tested a scenario with an explicitly time-dependent form of the bimodal IMF, switching from an initial top-heavy phase to a bottom-heavy one at a certain galactic time. This solution gave a good agreement with observed data as well, provided that the switching occurred in the early stages of the galactic evolution.
Our results are new, since it was previously concluded that ellipticals should have either a top-heavy (Fontanot et al., 2017), or a bottom-heavy IMF, whereas we found that the best agreement is given by a combination of the two.
The IMF is a crucial parameter in galaxy evolution, and is still highly unknown in galaxies outside the Milky Way. With our Thesis, we have put important constraints on the IMF in ellipticals, and on their chemical evolution.

The Thesis is organized as follows.
In Chapter 1, we summarize some fundamental basic concepts about chemical evolution of galaxies, by providing a brief overview of the various different nucleosynthesis processes taking place in stars, and by detailing the commonly adopted conventions and units of measure.
Chapter 2 outlines the main properties of elliptical galaxies, which are the main object of study in this Thesis. In Sec. 2.2 we present the main observational relations that are known to exist in these systems and that we tried to reproduce with our model, specifically the mass-metallicity and the $[\alpha/Fe]$-mass relations, while in Sec. 2.3 we tackle the topic of the dependence of these properties on environment.
In Chapter 3, the chemical evolution model we used is presented; we describe the basic equations and principles of the model, we introduce the treatment of the energetics, and we finally describe how to relate the model predictions to the observable quantities in the datasets.
The datasets we used to test the predictions of our model are presented in Chapter 4.
Chapter 5 reports the results originally presented in De Masi et al. (2018), and summarizes our tests to reproduce observed data by the use of downsizing only (Sec. 5.2), a variable IMF (Sec. 5.3) or the IGIMF (Sec. 5.4). The extension of this analysis, and the inclusion of the bimodal IMF are summarized in Chapter 6, from De Masi et al. (2019).
Finally, in Chapter 7 we summarize and comment our results.

Contents

Chapter 1

Introduction to chemical evolution

Chemical evolution models aim at studying how the various chemical elements formed and dispersed in galaxies.
The most common approach to the problem, which is also the one we followed in our work, is to study galaxy formation and evolution "from within", or "backwards". In this scenario, galaxies are assumed to form following the initial collapse of a gas cloud (even though later merging episodes can still be considered) and, after establishing the initial conditions, the presence of inflows/outflows and the nucleosynthesis prescriptions, the model evolves freely under these assumptions. The physics "ingredients" of the model, such as the star formation law (describing the rate of conversion of gas mass into stars), the stellar initial mass function (IMF, describing the mass distribution of new stars) and the properties of the initial gas infall episode, are all characterized by some free parameters. The values of these parameters are eventually constrained by reproducing as many observable quantities in real galaxies as possible, which in turn allows us to shed some light on the processes regulated by the parameters themselves (Matteucci, 2012).
It goes without saying that the focal point of these models is related to the production itself of the various chemical elements. According to the current cosmological models, primordial nucleosynthesis is only responsible for the creation of light elements such as Hydrogen (^1H), Deuterium (^2H), Helium (^3He and ^4He), and a small fraction of Lithium (^7Li) (Cyburt et al., 2016). The following elements with atomic mass number up to 11, namely ^6Li, ^9Be, ^{10}B and ^{11}B (considering no stable nuclei with $A = 5$ and $A = 8$ exist in nature) are produced by spallation, i.e. interaction between cosmic rays and interstellar atoms of C, N and O (Meneguzzi et al., 1971).
Beyond this point, and up to the Fe-peak elements (so, for $12 \leq A \leq 60$),

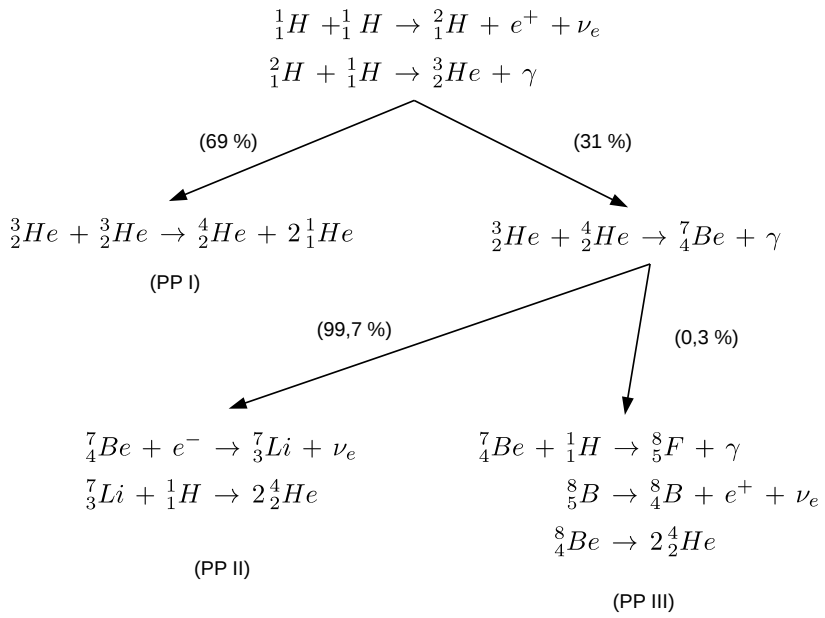

Figure 1.1: The three possible branches of the p-p chain with their ratios, relative to the conditions in the core of the Sun.

all existing nuclei are the product of various thermonuclear reactions taking place in star interiors (Matteucci, 2012; Carroll and Ostlie, 2017).

The first important nuclear reactions in stars, the so-called *p-p chain* and *CNO cycle*, both have the overall effect of converting four protons into a nucleus of ^4He (see Fig. 1.1 and 1.2 for the complete series of reaction, with the various branches and their relative ratios). Due to its weaker dependence on temperature, the p-p chain dominates in lower mass stars, while the CNO cycle takes over for $T > 2 \times 10^7\ K$, typically in stars slightly more massive than the Sun.

At $T \approx 10^8\,K$, the burning of ^4He into ^{12}C takes place through a three-particle process, the so-called 3α *process*:

$$\begin{aligned} ^4_2He + ^4_2He &\rightarrow ^8_4Be \\ ^8_4Be + ^4_2He &\rightarrow ^{12}_6C + \gamma \end{aligned} \tag{1.1}$$

The produced Carbon can then capture α-particles to yield ^{16}O, which in turn can produce small amounts of ^{20}Ne by the same mechanism.

$$\begin{aligned} ^{12}_6C + ^4_2He &\rightarrow ^{16}_8O \\ ^{16}_8O + ^4_2He &\rightarrow ^{20}_{10}Ne + \gamma \end{aligned} \tag{1.2}$$

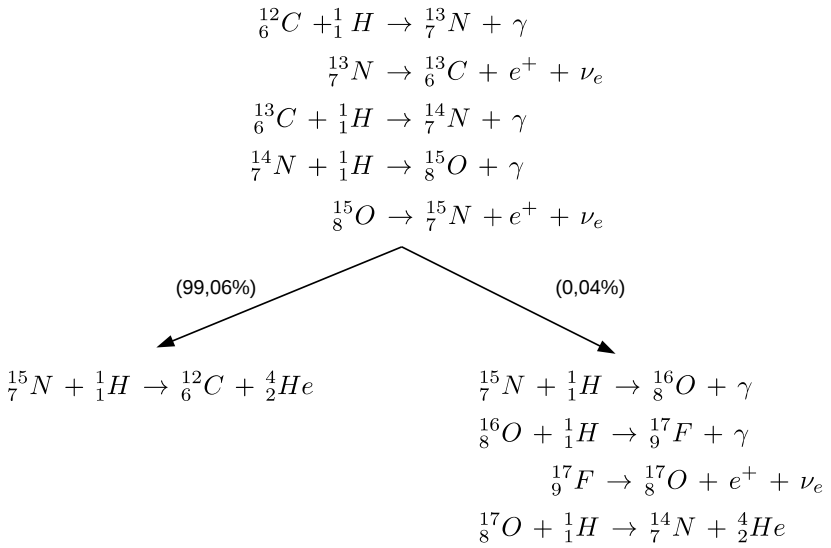

Figure 1.2: Same as Fig. 1.1, but for the CNO cycle.

For $T \approx 6 \times 10^8 - 10^9 K$, Carbon and Oxygen burning are ignited, with the former producing nuclei of ^{20}Ne, ^{23}Na, ^{24}Mg (in negligible quantities), and the latter mainly leading to the creation of ^{28}Si, ^{31}P:

$$^{12}_{6}C + ^{12}_{6}C \rightarrow \begin{cases} ^{16}_{8}O + 2\,^{4}_{2}He \\ ^{20}_{10}Ne + ^{4}_{2}He \\ ^{23}_{11}Na + p^{+} \\ ^{23}_{12}Mg + n \\ ^{24}_{12}Mg + \gamma \end{cases} \tag{1.3}$$

$$^{16}_{8}O + ^{16}_{8}O \rightarrow \begin{cases} ^{24}_{12}Mg + 2\,^{4}_{2}He \\ ^{28}_{14}Si + ^{4}_{2}He \\ ^{31}_{15}P + p^{+} \\ ^{31}_{16}P + n \\ ^{32}_{16}S + \gamma \end{cases} \tag{1.4}$$

At $T \approx 3 - 5 \times 10^9\, K$, once equilibrium between production and capture of α-particles is reached, starting from ^{24}Mg and ^{28}Si, there is production of ^{36}Ar, ^{40}Ca, ^{44}Sc, ^{48}Ti, ^{52}Cr and mainly ^{56}Ni. The latter finally β^+ decays into ^{56}Co and ^{56}Fe.

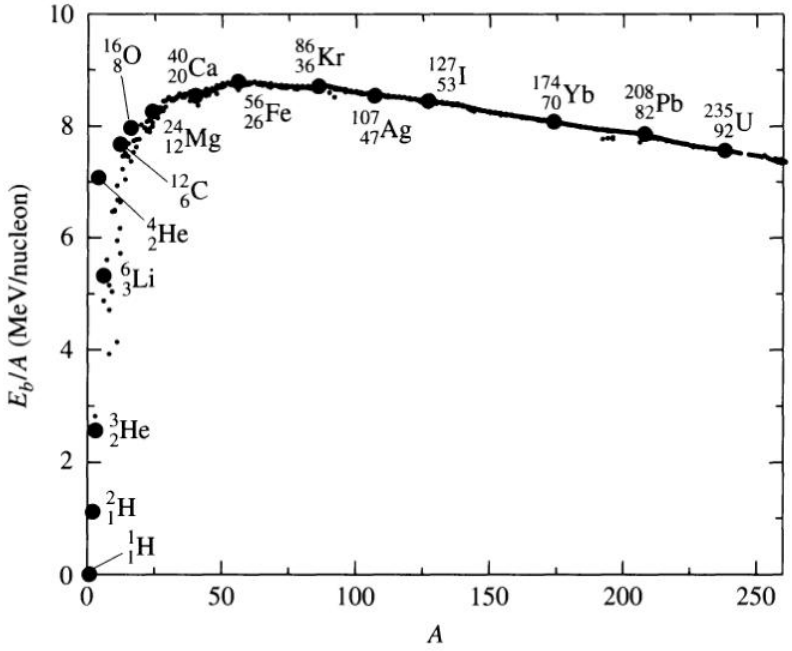

Figure 1.3: From Carroll and Ostlie (2017) - The binding energy per nucleon, E_b/A, as a function of mass number A. ^{56}Fe, the most stable nucleus, exhibits a clear peak, which is the reason why no further nuclear burning processes are possible beyond the production of this element.

Once this stage of the evolution is reached, the production of heavier elements via further nuclear burning reactions is halted, since the binding energy per nucleon peaks for ^{56}Fe and decreases for heavier nuclei (see Fig. 1.3). Elements with $A > 60$, finally, are formed by the so-called *s/r (slow/rapid) processes*, namely reactions involving the neutron capture by seed nuclei (mainly ^{56}Fe), followed by a β-decay (see Fig. 1.4). The two processes are differentiated by the ratio between the neutron capture and the decay time-scales. In the s-process, generally taking place during the He-burning phase of low-mass stars, neutron capture is slow with respect to the β-decay. On the other hand the r-process, due to high free neutrons density, is characterized by a capture fast enough to allow for multiple events before the decay, so that the process can take place until neutron-rich nuclei cannot add other neutrons anymore; the conditions for this to happen are believed to be met during explosive phases of stellar lifetimes, such as the Helium flash, next to the surface of neutron stars relics after core-collapse SNe, or in neutron stars mergers.

The scheme depicted so far shows how all of these processes are strongly

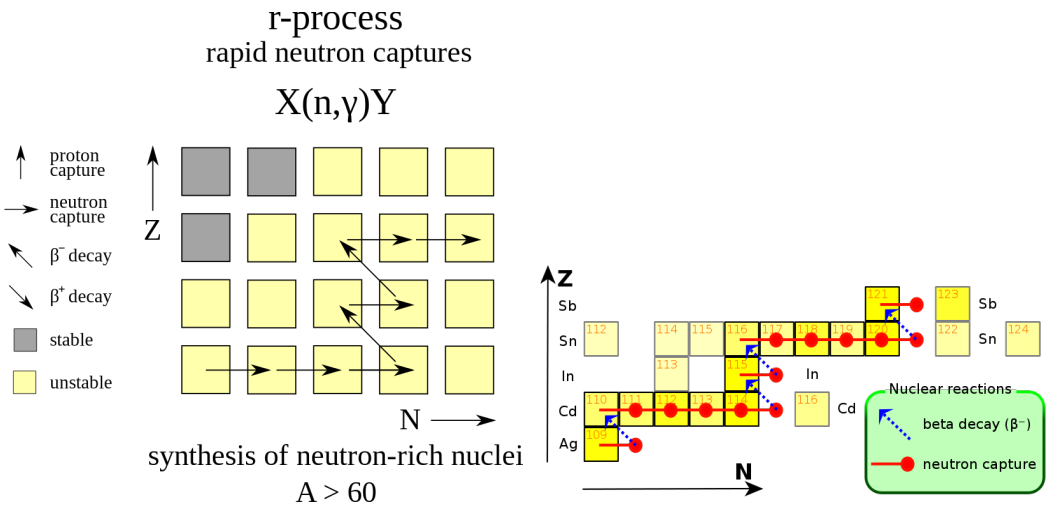

Figure 1.4: Both rapid (left panel) and slow (right panel) process involve neutron captures by a seed nuclei, followed by a β-decay; in the former, the capture time-scale is short enough to allow multiple captures before the decay, which, on the other hand, happens immediately in the s process.

dependent on their environment, since the various described nuclear reactions can only take place once the right conditions, such as temperature, pressure, and the abundances of other particles, are met in stars. For this reason, there are significant variations between the output elements produced by stars in different mass ranges or phases of their evolution, which are characterized by different values of said properties of temperature, pressure, etc. (Hoyle, 1946; Suess and Urey, 1956; Burbidge et al., 1957; Clayton et al., 1961; Seeger et al., 1965; Bodansky et al., 1968; Salaris and Cassisi, 2005; Goswami and Reddy, 2010; Carroll and Ostlie, 2017).
The final chemical properties of a galaxy, then, result from the combination of the different nucleosynthesis processes that take place during its evolution, and are further affected by the star formation history characteristic of the galaxy itself, which is generally observed to be related to the morphological type (late-type galaxies appear to have undergone a long period of star formation, while ellipticals show signs of having formed their stellar population in short, intense bursts - Matteucci, 1994; Matteucci et al., 1998; Thomas et al., 2010).
The combination of all of these factors determines the presence of characteristic trends in the abundances of different elements in galaxies, and in their relative ratios. In particular, it is of great interest in the study of galaxy evolution to analyze the abundance ratio between the so-called α-elements (O, Mg, Si, S, Ca) and Fe.

The reason why this ratio can provide us with useful information is that α-elements are produced, by subsequent addition of α-particles, in massive stars ($M > 10M_{\odot}$) on a short time-scale; on the other hand, Fe is mostly produced by Type Ia SNe, on a much longer time-scale. As a result of the delay in the production of these elements, as we will detail in the following, the ratio between their abundances can be used as "cosmic clocks", providing indications on the length of the star formation process in the galaxy.
The study and interpretation of these trends, then, is the very aim of chemical evolution models.

1.1 General definitions and units of measure

To begin with, while in Chemistry the term "metal" usually indicates particular elements or alloys presenting peculiar properties (such as a high electrical and thermal conductivity), in Astrophysics and Cosmology it assumes a somewhat broader meaning.
Since stars and the Interstellar Medium (**ISM**) are mainly composed of Hydrogen and Helium, in fact, all the other elements only account for a small percentage of the baryonic mass of the Universe, so that any element heavier than He is referred to as "heavy element" or "metal".
In this sense, we define the **metallicity** of an object (usually designated by the letter **Z**) as the percentage of the object's mass composed by any element heavier than He:

$$Z = \sum_{i>He} \frac{m_i}{M} = 1 - X - Y \tag{1.5}$$

where, as it is common practice, we defined X and Y as the Hydrogen and Helium mass fraction, respectively.
Generally, the abundance by mass of the i-th element is defined as:

$$X_i \equiv \frac{M_i}{M_{gas}} \tag{1.6}$$

so that, clearly

$$\sum_{i=1,N} X_i = 1$$

When measuring the heavy elements abundance in astrophysical objects, it is convenient to:

- use a logarithmic scale, because of the small absolute values of the quantities involved;

Parameter	Solar value
H mass fraction	$X_\odot \approx 0.7381$
He mass fraction	$Y_\odot \approx 0.2485$
Metallicity	$Z_\odot \approx 0.0134$

Table 1.1: Mass fractions of H (X), He (Y) and metals (Z) in the Sun, from Asplund et al. (2009).

- refer to the analogous abundances in the Sun (solar values of X, Y and Z as provided in Asplund et al., 2009 are shown in Table 1.1).

For this reason, the abundance of a given element (say, Fe) in a star or galaxy is usually expressed using the so-called "square-brackets" notation:

$$[Fe/H] \equiv \frac{Log\left(\frac{N_{Fe}}{N_H}\right)_*}{Log\left(\frac{N_{Fe}}{N_H}\right)_\odot} = Log\left(\frac{N_{Fe}}{N_H}\right)_* - Log\left(\frac{N_{Fe}}{N_H}\right)_\odot \quad (1.7)$$

where N_{Fe} and N_H are the number of Fe and Hydrogen atoms per unit of volume, and * and $\odot$ indicate the object and the Sun, respectively.
As a matter of fact Fe, which appears in the example above, is generally assumed as a proxy for the total metallicity in stars and stellar populations in galaxies, since it is easy to detect spectroscopically, and because stars rich in Fe tend to be rich in other metals too.
Analogously, the abundance of Oxygen, which generally dominates the chemical composition of the ISM, is a commonly adopted indicator for the ISM global metallicity, and is usually measured through the notation $12+Log(O/H)$.

1.2 Galaxy formation models in a cosmological context

As mentioned in the previous Sec., other ways to model galaxy formation and evolution do not purely rely on their chemical properties, although generally including them, at least to some extent.
Observations over the last decade converged into the development of the so-called "ΛCDM model" for structure formation. Within this theoretical framework, ≈75% of the energy density is given by a yet unknown form of dark energy, increasing the expansion rate of the Universe, about 21% by nonbaryonic cold dark matter that has yet to be detected in the laboratory, while the remaining 4%, constituted of baryonic matter, forms stars and

galaxies (Peebles, 1980; Blumenthal et al., 1984). In this scenario, dark matter halos, deriving from small fluctuations in the primordial density field of the Universe, form by following mergers of smaller ones. This mechanism is then extended to galaxies as well, which form following the collapse of baryonic matter in the potential well created by dark matter halos. As a consequence of this mechanism, more massive ellipticals result form mergers of smaller galaxies, possibly spirals or dwarf galaxies, thus implying that the most massive ones have formed last (Kauffmann and White, 1993; Baugh et al., 1996; Kauffmann and Charlot, 1998). Moreover, galaxies are assumed to form continuously over the whole redshift range, whereas in the "backward" approach described in the previous Sec. it is assumed that they all started forming at the same time (Matteucci, 2012).
In the hierarchical scenario, galaxy formation results from the interaction of complex and nonlinear processes, spanning a wide range of physical (from the scale of black holes to that of massive galaxy clusters) and time scales.
In particular, three major approaches have been proposed to describe this process (Oswalt and Keel, 2013):

- **Halo Occupation Distribution Method**
  In this method, the link between dark matter haloes and galaxies is derived in a purely statistical fashion (Neyman and Scott, 1952; Benson et al., 2000; Berlind and Weinberg, 2002).
  Specifically, the model is created by specifying the probability that a halo of mass M contains N galaxies of a particular class, and by assuming a spatial distribution of galaxies inside dark matter halos (most commonly, the distribution of galaxies is assumed to follow that of the dark matter). The halo occupation distribution is then constrained using galaxy clustering data (Oswalt and Keel, 2013).

- **Hidrodynamical simulations:** These models provide an explicit description of the gas dynamics in N-body simulations, which however generally makes them time- and memory demanding in computational terms; moreover, complex physical processes such as star formation, feedback, have to be included as "subgrid physics" (Oswalt and Keel, 2013).
  Current state-of-the-art full hydrodynamic cosmological simulations include the Galaxies-Intergalactic Medium Interaction Calculation project-GIMIC (Crain et al., 2009) and the OverWhelmingly Large Simulations project - OWLS (Schaye et al., 2010);

- **Semianalytic Models:** Semianalytic model provide a statistical representation of the growth of dark matter haloes ("merger tree"), to

which galaxy formation and evolution is coupled by using analytic laws based on theoretical and/or observational arguments to describe processes like star formation, supernovae and AGN feedback processes (Oswalt and Keel, 2013). This way, the full galaxy formation process is described through a set of differential equations describing the variation in mass of the different galactic components; these equations contain a number of free parameters, which are constrained by comparison with observations in the local Universe (White and Rees, 1978; White and Frenk, 1991; Baugh, 2006).

The ability of the ΛCDM model to explain a number of observational, large-scale measurements, such as:

- the power spectrum of low-redshift galaxies;
- the structure that is seen in the Lyman Îś forest at z≈3;
- the present acceleration of the cosmic expansion, as inferred from SNe observations;
- the polarization of the CMB;
- the temperature fluctuations in the cosmic microwave background;

allowed to constraint the parameters of the model with uncertainties of only a few percent (Peebles, 1980; Nusser and Dekel, 1992; Kovac et al., 2002; Perivolaropoulos, 2011; Komatsu et al., 2011; Planck Collaboration, 2016). On the other hand, however, the hierarchical clustering approach presents a number of downfalls when trying to explain some of the observational properties of real galaxies:

- the faint end of the luminosity function, since semianalytic models need a relatively strong SN feedback to suppress the large excess of faint galaxies (White and Frenk, 1991; Benson et al., 2000; Guo et al., 2011; Oswalt and Keel, 2013);
- similarly, the bright end of the luminosity function, which can only be reasonably matched by assuming a relatively strong form of "radio-mode" AGN feedback (Croton et al., 2006; Monaco et al., 2007), even if there are still some issues to be fixed concerning this model (Fontanot et al., 2011). In general, "radio-mode" AGN feedback allows to keep the stellar populations of massive galaxies old, but the observed trend for shorter star formation time-scale in more massive ellipticals, which in turn can account for the $[\alpha/Fe]$ overabundance in massive ellipticals

(see Sec. 2.2.4), can only be reproduced qualitatively (De Lucia et al., 2006; Fontanot et al., 2009; De Lucia et al., 2011);

- the very tight relation between star formation rate, metallicity, and galactic mass (Mannucci et al., 2010);
- the relation between the mass of the central black hole and the luminosity (mass) of the parent galaxy (Kormendy et al., 2011);

Chapter 2

Elliptical galaxies

This Thesis presents the study we performed on the chemical properties of elliptical galaxies, with the aim of obtaining indications on their origin and evolution.
In this Chapter, we briefly summarize some of the general properties of these galaxies, and we present two fundamental observational properties we tried to reproduce: the mass-metallicity and the $[\alpha/Fe]$-mass relations.

2.1 General properties of elliptical galaxies

The classification of galaxies into ellipticals, spirals, and irregulars dates back to the scheme proposed by Hubble (1936) (see Fig. 2.1). This division, originally purely based on a morphological classification only, still stands today because the morphology of a galaxy is observed to actually correlate with its stellar, kinematics and spectral properties.

Elliptical (or early-type) galaxies, in fact, are systems generally characterized by old stellar populations and redder colors, showing little or no sign of ongoing star formation (Renzini, 2006). Due to the lack of gas and star formation activity, no nebular emissions are generally observed, so that abundances in these objects can only be derived from the study of absorption lines in their integrated spectra (see Section 2.2).
Because of the correspondence between morphology and these other internal properties, the "early-type" label is often generally extended to galaxies selected on the basis of more or less automated methods, usually relying on spectroscopic and/or photometric parameters, such as the radial light profile, color and variously defined concentration indexes (see Bamford et al., 2009 and references therein), regardless of their morphology.
Different classification criteria, however, are obviously not completely equiv-

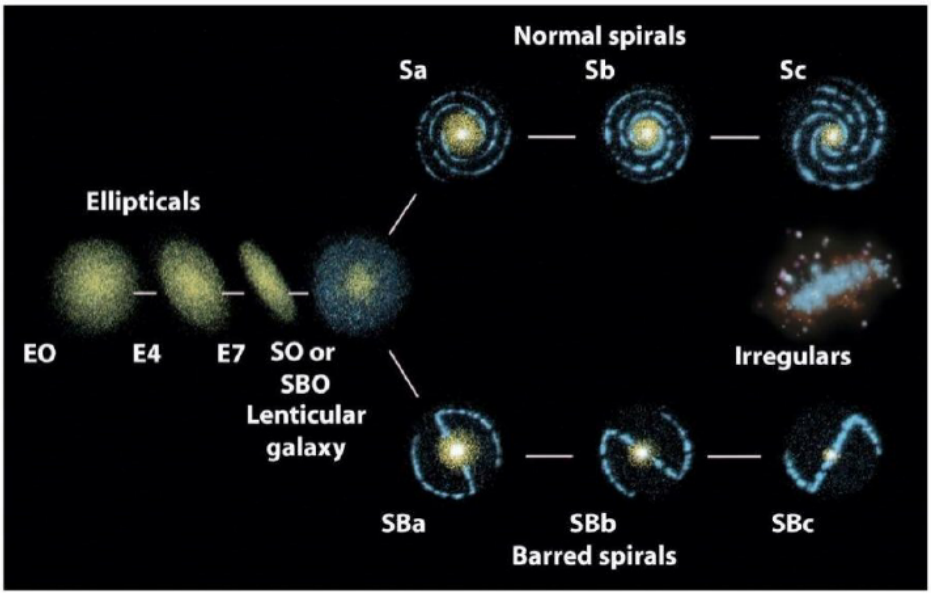

Figure 2.1: Hubble classification scheme. Image credit to: http://www.physast.uga.edu.

alent. The review by Renzini (2006) reports the overlap percentage between the morphological, spectroscopic and photometric criteria adopted by Bernardi et al. (2006), indicating that, out of the morphologically selected sample, $\approx 70\%$ of the objects also satisfy the color selection, and $\approx 81\%$ the spectroscopic one.

Delgado-Serrano et al. (2010) tried to link the present-day Hubble sequence to its 6 Gyr old counterpart, by selecting samples of nearby galaxies from the SDSS and of distant galaxies from the GOODS survey.

In this work, a morphological classification was performed by adopting a semi-automatic decision tree (see Fig. 2.2), taking into account a number of different properties (B/T, half light radius, disk-bulge-galaxy profile, two color-maps, and three-color images); the process was manually performed buy the authors, and the results confronted between each other. Fig. 2.3, reproducing Table 3 from Delgado-Serrano et al. (2010), reports the fraction of the different morphological types for both their local and distant samples. The classification confirmed that the local Universe is dominated by spirals galaxies, representing the 72% of the population, and that the fraction of E/S0 is 18%, while 10% of galaxies have peculiar morphologies.

On the other hand, Thomas et al. (2010) obtained a classification of "early-type (roundish, elliptically shaped)" for 16502 out of 48023 galaxies extracted from the SDSS DR4, by applying a strict morphological criteria, adopted to avoid selection against objects with recent star formation activity.

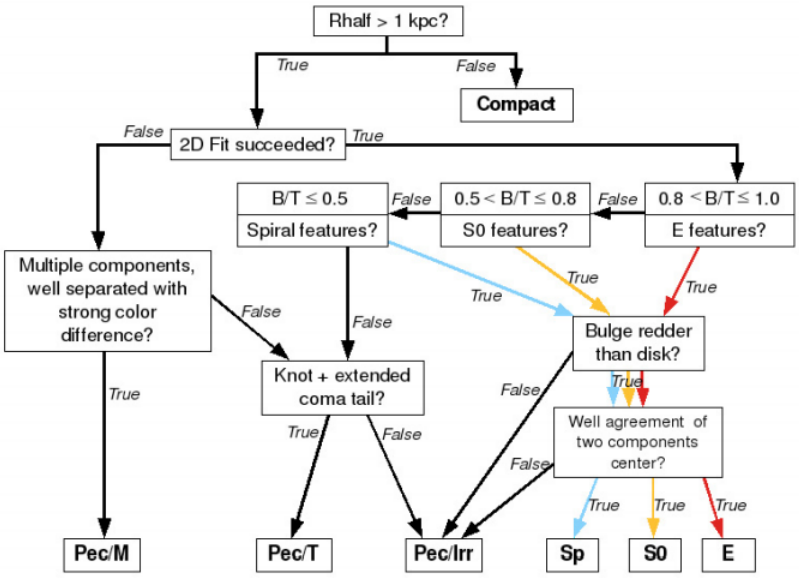

Figure 2.2: From Delgado-Serrano et al. (2010) - Semi-automatic decision tree used in the morphological classification process of the local and distant samples.

	Local			Distant		
Type	Total (%)	Quiescent (%)	Starburst (%)	Total(%)	Quiescent (%)	Starburst (%)
E	3 ± 1	3 ± 2	0 ± 0	4 ± 1	11 ± 3	0 ± 0
S0	15 ± 4	14 ± 4	20 ± 10	13 ± 2	33 ± 6	0 ± 0
Spiral	72 ± 8	76 ± 10	55 ± 17	31 ± 7	31 ± 6	31 ± 8
Peculiar[a]**:**	10 ± 3	7 ± 3	25 ± 11	52 ± 9	25 ± 5	69 ± 12
P/Irr	4 ± 2	2 ± 1	15 ± 9	26 ± 7	21 ± 5	29 ± 8
P/Tad	0 ± 0	0 ± 0	0 ± 0	6 ± 3	0 ± 0	10 ± 5
P/Mer	4 ± 2	4 ± 2	5 ± 5	20 ± 6	4 ± 2	30 ± 8
P/C	2 ± 1	1 ± 1	5 ± 5	0 ± 0	0 ± 0	0 ± 0

[a] Fractions in the peculiar class are simply addition of the fraction of peculiar subclasses.

Figure 2.3: From Delgado-Serrano et al. (2010) - Fraction of the different morphological types for local and distant samples.

2.2 Observational properties

As previously stated, ellipticals are generally gas poor systems, without ongoing star formation, so that observations only reveal hints on the chemical composition of stars dominating in the visual light (Matteucci, 1997; Pipino and Matteucci, 2004; Matteucci, 2012).
Stellar abundances are usually obtained by measuring the so-called ***spectral indices***, namely quantities expressing the strength of absorption lines in the integrated spectra of galaxies; commonly adopted indices are the $< Fe >$ and Mg_2 (Faber et al., 1985; Burstein et al., 1986; Worthey et al., 1994).
Indices can then be converted to abundances in two ways:

1. by performing a fitting procedure between the observed absorption features and libraries of spectro-photometric models generated by evolutionary population synthesis (EPS) codes, each characterized by different stellar parameters (Bruzual A., 1983; Renzini and Buzzoni, 1986; Chiosi et al., 1988; Buzzoni, 1989; Charlot and Bruzual, 1991; Bruzual A. and Charlot, 1993; Worthey et al., 1994; Tantalo et al., 1996; Maraston, 1998; Brocato et al., 2000; Bruzual and Charlot, 2003; Maraston, 2003; Thomas et al., 2003; Peletier, 2013). This procedure is generally carried out by looking for the combination of parameters that minimizes the χ^2 between model and observational data, either for a selected group of indices (Thomas et al., 2005), or for the whole set of available indices (Thomas et al., 2010);

2. in a simplified approach, through the adoption of calibration relations (Tantalo et al., 1998). These calibrations are, however, an approximation of the use of stellar population models, hence less accurate.

This exercise is further complicated by the uncertainties intrinsic to population synthesis techniques, due either to our incomplete knowledge of stellar evolution or to limitations in available stellar libraries (Charlot et al., 1996), and by the so-called age-metallicity degeneracy (Worthey et al., 1994), namely the fact that age and chemical composition have a similar effect on photometry and spectral features, so that particular care must be taken when choosing the features to analyze in order to separate the two effects. Moreover, it is useful to stress that star abundances observed at the present time result from the contribution of all the previous stellar generations, each of which gradually enriched the ISM out of which the new stars were born, through the evolution of the galaxy up to the present day. For this reason, when talking about abundance in ellipticals we generally refer to quantities resulting from an average, either with respect to mass or luminosity (see

later), over the various stellar generations that appeared in the galaxy evolution, and we can indicate them as $[< Fe/H >]$.
Generally, ellipticals are metal-rich; observed mean stellar metallicities are in the range $-0.8 \leq [< Fe/H >] \leq 0.3$ dex, and the characteristic ratio between α-elements and Fe is usually high (0.05-0.3 dex) - see Matteucci (2012).
These galaxies are known to present a certain number of common observational features, whose presence seems to favor a somewhat regular formation scenario, to the detriment of claims that these objects should have formed as a consequence of successive merging of spirals (see later discussion).
In the following, we summarize the most relevant of these observational properties.

2.2.1 Fundamental Plane

Elliptical galaxies exhibit a tight correlation between their central velocity dispersion σ_0, their surface brightness and their effective radius R_{eff}, generally referred to as the ***Fundamental Plane - FP*** (Dressler et al., 1987; Djorgovski and Davis, 1987; Bender et al., 1992; Jorgensen et al., 1996; Burstein et al., 1997). Fig. 2.4, from Bernardi et al. (2003), shows the FP in a magnitude-limited sample of nearly 9000 early-type galaxies, in the redshift range $0.01 \leq z \leq 0.3$, from the SDSS.
This relation extends the Faber and Jackson (1976) relation, which is then found to constitute a projection of the FP itself (hence, the bigger scatter characterizing the Faber-Jackson relation). The existence and the properties of the FP have two immediate applications:

1. **Distance indicator:** In the FP, the effective radius R_e is measured in physical units (kpc). For this reason, if the velocity dispersion and effective surface brightness (both of which are distance independent) can be obtained, the FP can be exploited to derive a measure of the physical size of the galaxy, which in combination with its angular size provides constraints on its distance (Carroll and Ostlie, 2017);

2. **M/L ratios, Galaxy Structure and Evolution:** Theoretically, the very existence of the FP can be derived by assuming that:

   - galaxies are in virial equilibrium;
   - they form an homologous photometric family, e.g. they all follow a $R^{1/4}1$ profiles (de Vaucouleurs, 1948), and M/L is a regular function of L;

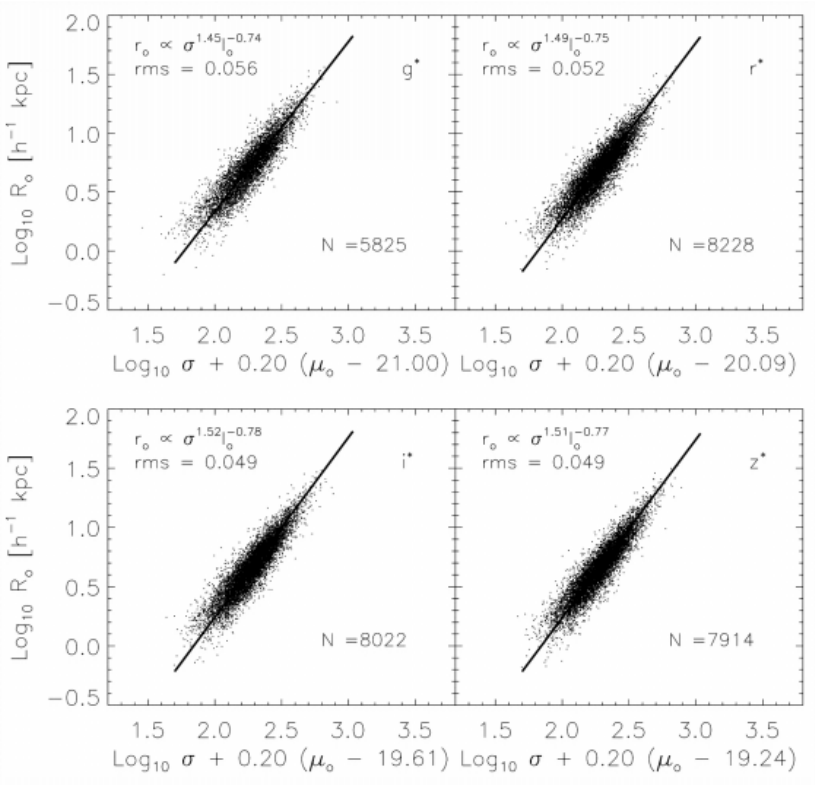

Figure 2.4: From Bernardi et al. (2003) - The Fundamental Plane in the four SDSS bands. Coefficients shown are those which minimize the scatter orthogonal to the plane, as determined by the maximum-likelihood method. Surface-brightnesses have been corrected for evolution.

- the mean value of the mass-to-light ratio does not vary from galaxy to galaxy;

Within this constraints, it can easily be found that a relation should exist between R_e, σ and $< I_e >$, of the form:

$$R_e \propto \sigma^2 < I_e >^{-1} \tag{2.1}$$

Real galaxies do follow this kind of behaviors, but the observed exponents deviate slightly from the above theoretical expectations; for instance, Virgo galaxies are found to obey the relation:

$$R_e \propto \sigma^{1/4} < I_e >^{-0.85} \tag{2.2}$$

within a small dispersion (Dressler et al., 1987).
This departure is called "**tilt**" of the FP; if we assume homology, and attribute all of the FP tilt to the changes in (M/L) ratio, one has to assume a relation between (M/L) and L of the form:

$$\left(\frac{M}{L}\right) \propto L^{0.2} \tag{2.3}$$

which, in turn, could be attributed to systematic changes in $M_{visible}/M_{dark}$, in their relative concentrations, or in variations of the stellar IMF (Cappellari et al., 2006).

The intrinsic scatter of the FP in ellipticals has been found to only sum up to a few %, independently of their star formation and merging history, their environment, the details of their internal structure and dynamics and projection effects (Djorgovski, 1995); this remarkable tightness basically means that, for any elliptical galaxy today, just two numbers determine to within a few percent or less a vast number of the properties of the galaxy:

- Mass, luminosity (in any OIR band);
- any consistently defined radius;
- surface brightness, or projected mass density;
- derived 3-d luminosity, mass, or phase-space density;
- central projected radial velocity dispersion.

The implication is that elliptical galaxies occupy only a small, naturally selected, subset of all dynamical structures which are in principle open to them; explaining the origin of this small scatter (or, equivalently, the narrow range of the dynamical structures accessible to ellipticals) is an outstanding problem Robertson et al. (2006).

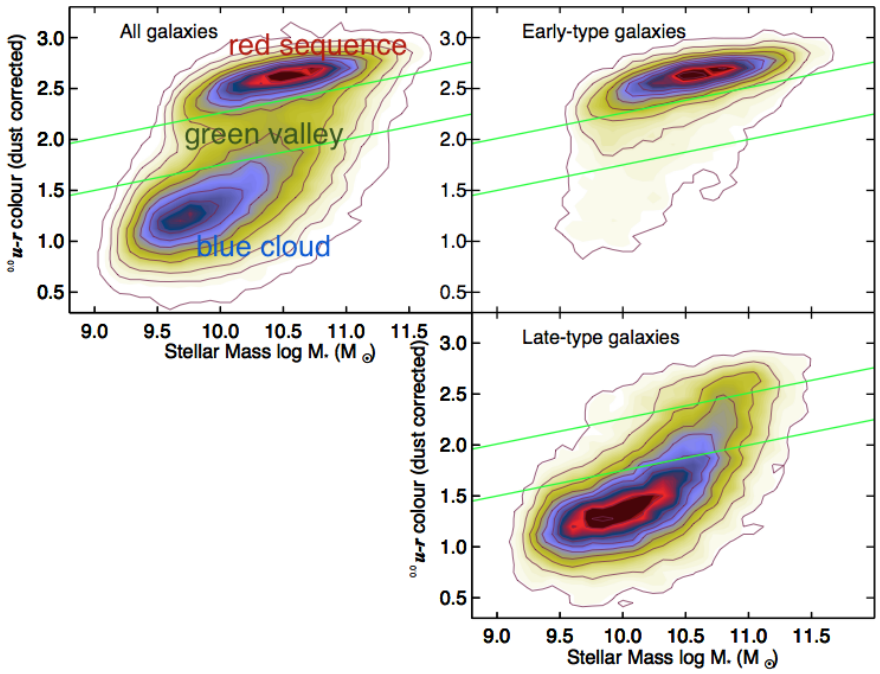

Figure 2.5: From Schawinski et al. (2014) - (u-r) color-mass diagram for all galaxies (top left), early-types (top) and late-types galaxies (bottom); green lines show the green valley defined by the all-galaxy diagram.

2.2.2 Color-magnitude relation (CMR)

At low redshift, a clear bimodality in the colors of cluster galaxies is evident, with spirals and irregulars populating the so-called "blue cloud", and ellipticals being grouped in an area referred to as "red sequence" (see Fig. 2.5). In the local Universe, cluster ellipticals populating the red sequence show a trend between luminosity and color, with more luminous galaxies being redder, as discussed by Baum (1959), Faber (1973) and Caldwell (1983). This correlation is common to both S0s and ellipticals (Sandage and Visvanathan, 1978a,b; Bower et al., 1992), and has been found to hold up to redshift $z \approx 1.4$ (Sandage and Visvanathan, 1978a,b; Ellis et al., 1997; Stanford et al., 1998; Van Dokkum et al., 2001; Lidman et al., 2008) with a very small scatter (Sandage and Visvanathan, 1978a,b), which makes it a powerful scaling relation characterizing early-types.
The CMR is usually regarded as a metallicity effect, with the increased metallicity leading to the reddening of galaxies; in this sense, it is regarded as a consequence of the existence of a mass-metallicity relation.

2.2.3 Mass-metallicity relation (MZR)

The mass-metallicity relation is a well know property characterizing galaxies of every morphologic type, consisting in the apparent increase in the strength of metal absorption/emission lines (according to the galaxy type) with mass; this is regarded as an increase of the metal content in more massive galaxies. First presented by Lequeux et al. (1979), it has been observed both in active galaxies (in the local universe by Garnett and Shields, 1987; Zaritsky et al., 1994; Garnett, 2002; Pilyugin et al., 2004; Tremonti et al., 2004; Kewley and Ellison, 2008; Mannucci et al., 2010, and at high redshift by Erb et al., 2006; Henry et al., 2013; Arabsalmani et al., 2018), and in ellipticals (de Carvalho and Djorgovski, 1990; Arimoto and Kobayashi, 1999; Thomas et al., 2010).
In the literature, the existence of the MZR is usually explained by assuming one or a combination of the following scenarios:

1. a larger star formation efficiency (i.e., a larger rate of star formation per unit mass of gas - see Sec. 3.1.1) in more massive galaxies (Pipino and Matteucci, 2004; Calura et al., 2009; De Masi et al., 2018);

2. a selective loss of metal by stellar winds, which would be more effective at expelling metals in low-mass galaxies (Larson, 1974; Arimoto and Yoshii, 1987; Tremonti et al., 2004; Kobayashi et al., 2007)

3. a combination of effects due to infall/outflow, star formation, IMF (Spitoni et al., 2010; Dayal et al., 2013);

Fig. 2.6, from Tremonti et al. (2004), shows the relation they found between stellar mass and gas-phase oxygen abundance for $\approx 53,400$ star-forming galaxies in the SDSS; Fig. 2.8 (top panel), from Thomas et al. (2010), shows the MZR for the 3360 early-type galaxies, with redshift range $0.05 < z < 0.06$, of the MOSES (Morphologically Selected Early types in SDSS) catalogue, extracted from the Data Release 4 (DR4) of the Sloan Digital Sky Survey (SDSS).

Lian et al. (2017) analized the mass-metallicity relations for the gaseous (MZR_{gas}) and stellar components (MZR_{star}) of local star-forming galaxies based on a representative sample from SDSS DR12. Fig. 2.7, from Lian et al. (2017), shows the comparison between gas metallicity measured by the N2 and R23 methods (Kewley and Dopita, 2002; Tremonti et al., 2004; Kewley and Ellison, 2008) with the mass-weighted stellar metallicity.
The plot shows how metallicity in the ISM of star-forming galaxies is generally higher than the one of the stellar population, and that this difference decreases with mass, so that the MZR_{star} is much steeper than the MZR_{gas}. This is attributable to the fact that metal enrichment is generally

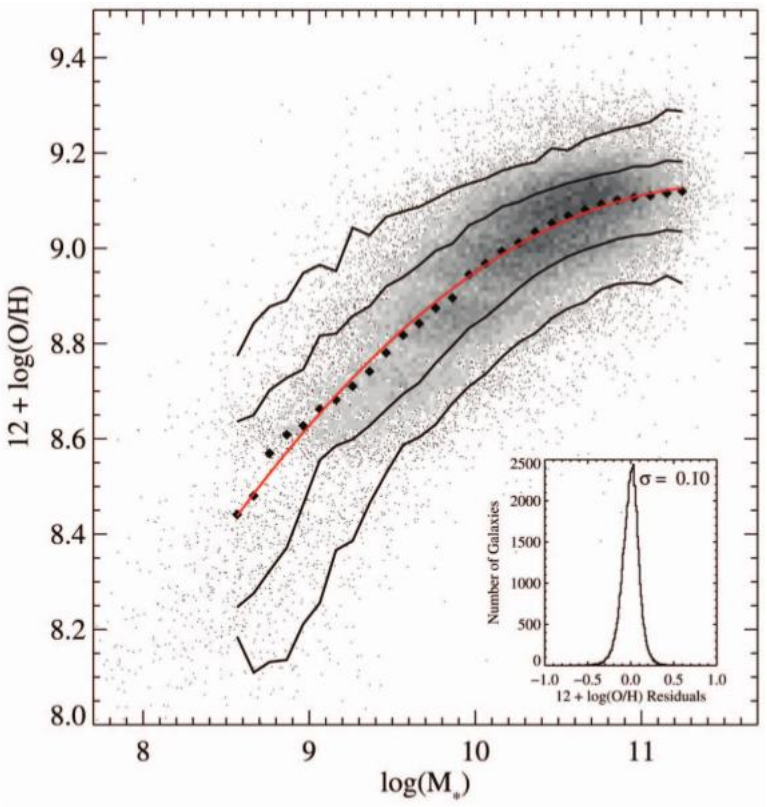

Figure 2.6: From Tremonti et al. (2004) - Relation between stellar mass, in units of solar masses, and gas-phase oxygen abundance for ≈ 53,400 star-forming galaxies in the SDSS. The large black filled diamonds represent the median in bins of 0.1 dex in mass that include at least 100 data points. The solid lines are the contours that enclose 68% and 95% of the data. The red line shows a polynomial fit to the data. The inset plot shows the residuals of the fit. Data for the contours are given in Table 3 of Tremonti et al. (2004).

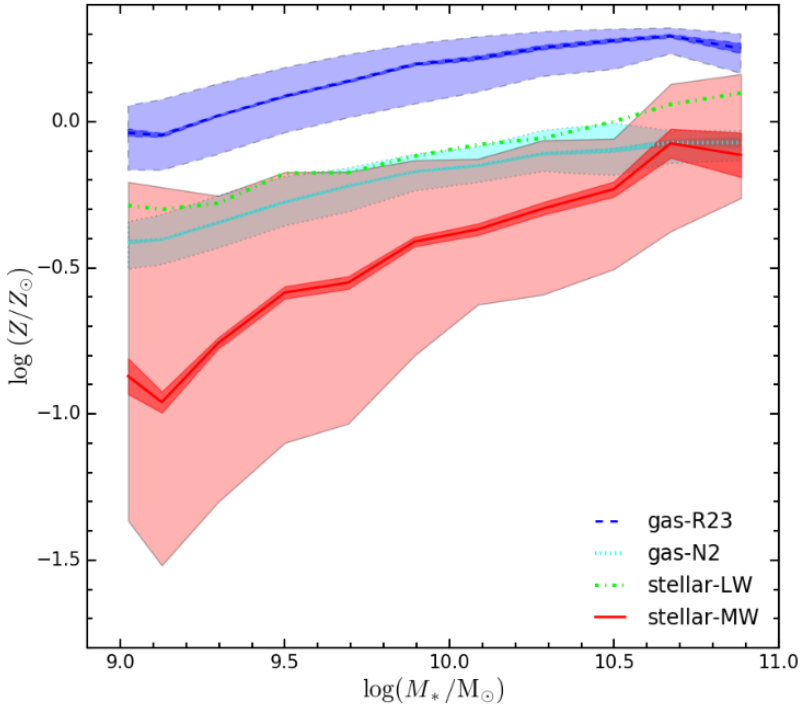

Figure 2.7: From Lian et al. (2017) - Comparison between the gas and stellar metallicity of local star-forming galaxies. Gas metallicities derived by the N2 and R23 methods are shown as cyan and blue colour, respectively. The mass-weighted MZR star is shown in red colour. The light shaded regions indicate the 16 and 84 percentiles while dark shaded regions represent the error of median metallicity..

monotonous, and while stellar metallicity is the product of the early epochs of chemical enrichment, the gas metallicity reflects more recent evolutionary processes (Tremonti et al., 2004; Lian et al., 2017).

2.2.4 $[\alpha/Fe]$-mass relation

Indications hinting towards supersolar $[\alpha/Fe]$ ratios have been observed in the core regions of elliptical galaxies, and the value of these ratios has been found to present a positive correlation with mass (Faber et al., 1992; Worthey et al., 1992; Carollo et al., 1993; Davies et al., 1993; Carollo and Danziger, 1994a,b); this trend has been confirmed in recent works by Thomas et al. (2010); de La Rosa et al. (2011); Johansson et al. (2012); Conroy et al. (2013); La Barbera et al. (2013); Segers et al. (2016); Rosani et al. (2018).
These observations are particularly interesting, since they can be exploited to discriminate between the two different formation scenarios proposed for elliptical galaxies. Specifically some models, based on hierarchical clustering cosmologies, suggest that ellipticals formed following subsequent, stochastic mergers of smaller systems; in this picture, massive ellipticals would need a major fraction of the cosmological time to complete the formation of their stellar population (Kauffmann and White, 1993; Baugh et al., 1996; Kauffmann and Charlot, 1998).
Alternative models present early-type galaxies as the result of the fast collapse of a gas cloud (Larson, 1974; Arimoto and Yoshii, 1987; Bressan et al., 1994; Matteucci, 1994). In this theoretical framework, the collapse episode is followed by a period of intense star formation, powered by the increased gas density, which is eventually quenched by the thermal energy produced by stellar winds and SNe feedback ("galactic wind"), which drives the remaining gas away from the galaxy.

Abundance ratios, then, can be used to discriminate between these two scenarios. As mentioned in the Introduction, the production of $[\alpha]$-elements by massive stars is much faster than the production of Fe, which is mostly provided by Type Ia SNe on a long time-scale. Taking this into account, the observed overabundance of $[\alpha]$-elements with respect to Fe in the stellar populations of massive ellipticals can be interpreted as a sign of the so-called "downsizing" in star formation, namely the fact that more massive galaxies formed their stars in a shorter period of time, as first suggested by Matteucci (1994) (see Fig. 2.9, from Thomas et al., 2010). As a consequence, in these galaxies the bulk of Fe would be formed only after the end of the star formation period (while some Fe is produced by massive stars as well, $\approx 2/3$ of the total Fe abundance is produced by Type Ia SNe on long time-scale), thus preventing Fe from "contaminating" the chemical composition of stars.

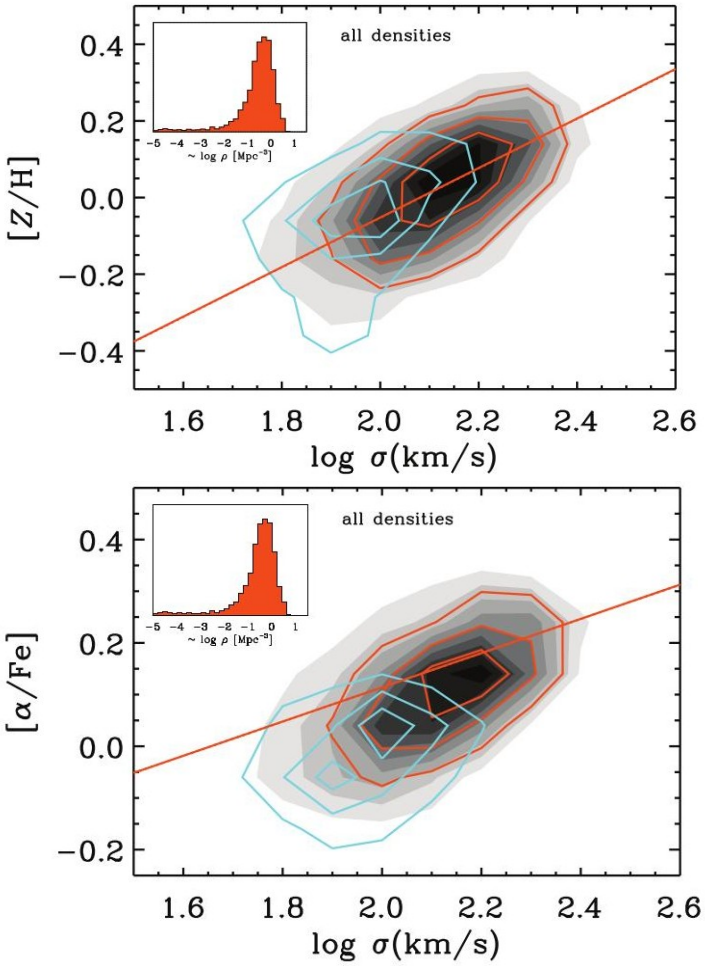

Figure 2.8: From Thomas et al. (2010) - Mass-metallicity relation (top panel) and $[\alpha/Fe]$-mass relation (bottom panel).

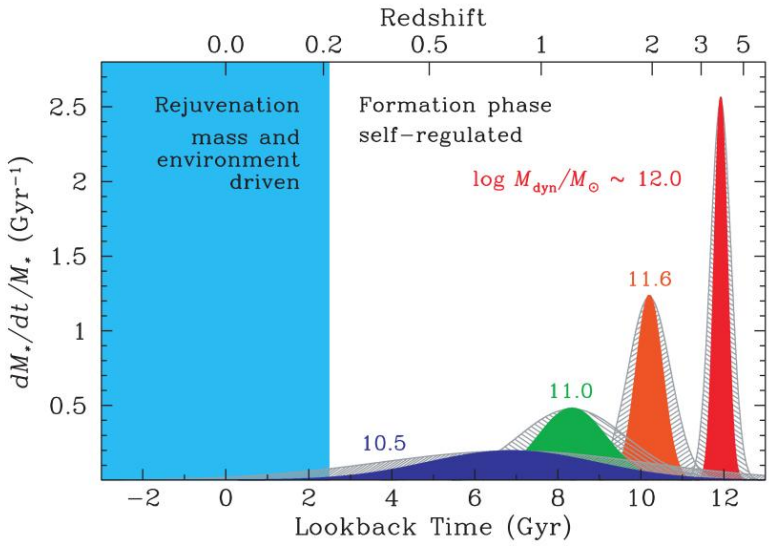

Figure 2.9: From Thomas et al. (2010) - Specific star formation rate as function of look-back time for early-type galaxies of various masses as indicated by the labels.

This hypothesis is further validated from the observations of $[\alpha/Fe]$ ratios $<$ 0 in the ICM (Matteucci and Vettolani, 1988; Matteucci and Gibson, 1995), due to the Fe produced after the end of star formation that cannot be locked up into stars, and is expelled into the intergalactic medium, lowering the ratio with α-elements.

2.3 Environment dependence

A correlation between morphology and environment, with ellipticals being more common in high-density environments, has been established to exist both at low and intermediate redshift (see Thomas et al., 2010 and references therein).
Conversely, it is still a matter of debate whether the environment can play a role in determining the properties of galaxies of a given morphology, for example by regulating the type and rate of mergers that galaxies may be subject to.
This question is, again, of interest in order to discriminate between the two formation scenarios we described. A number of works studying ellipticals in clusters dated the formation of most of their stars at redshift $z \geq 3$, based on the tightness of the color-σ and of the color-magnitude relation (Bower et al., 1992; Aragon-Salamanca et al., 1993; Stanford et al., 1998) and on the weak redshift dependence of the zero-point for the fundamental plane,

$Mg_2 - \sigma$ and color-magnitude relations of ellipticals in clusters (Ellis et al., 1997; Bernardi et al., 1998; van Dokkum et al., 1998).
These age estimations can actually be still justified within the framework of hierarchical formation for ellipticals in clusters, which are believed to form under conditions characterized by high star formation and merging rates (Kauffmann and Charlot, 1998). Conversely, confirming the old age of the stellar populations for ellipticals in lower density environments would provide an observational test against the hierarchical merger model (Bernardi et al., 1998).
The problem of studying the effect of environment is made somehow fuzzier by the uncertainties related to how the local environment of a galaxy could be best characterized; some works rely on various ways of determining the local density of galaxies (Eisenstein, 2003; Balogh et al., 2004; Strauss et al., 2002; Schawinski et al., 2007; Thomas et al., 2010), while others are based on catalogs of clusters and groups of galaxies (Bernardi et al., 1998; Yang et al., 2007; Wang et al., 2014; Rosani et al., 2018).
Longhetti et al. (2000); Poggianti et al. (2001); Terlevich and Forbes (2002); Denicolo et al. (2005); Thomas et al. (2005); Collobert et al. (2006); Rakos et al. (2007) estimated that ellipticals of a given mass appeared younger by ≈ 2 Gyr when found in lower density environments.
On the other hand, Bernardi et al. (1998) performed an analysis of the $Mg_2 - \sigma_0$ relation in different environments, finding only weak variations. Due to the Mg_2 dependence on both age and metallicity, this offset could be converted into an age difference between cluster and field elliptical by adopting simple stellar population models. The small zero-point variation implied a luminosity-weighted age difference of only ≈ 1 Gyr, with field galaxies being younger.
The authors stressed that the small differences in the ages and metallicities of galaxies in low and high-density environments could actually result from the age-metallicity degeneracy, with intrinsically larger changes in age and metallicity canceling each other out and leaving the observables unchanged.
Thomas et al. (2010) extended their previous work, presented in Thomas et al. (2005), by analyzing a larger catalog, and by adopting a visual classification criteria for selecting ellipticals.
Although confirming the correlations of luminosity weighted ages, metallicities and $[\alpha/Fe]$ ratios with mass, they found no dependence on environment for the age-, $[\alpha/Fe]$- and total metallicity-mass relations (see Fig. 2.10).

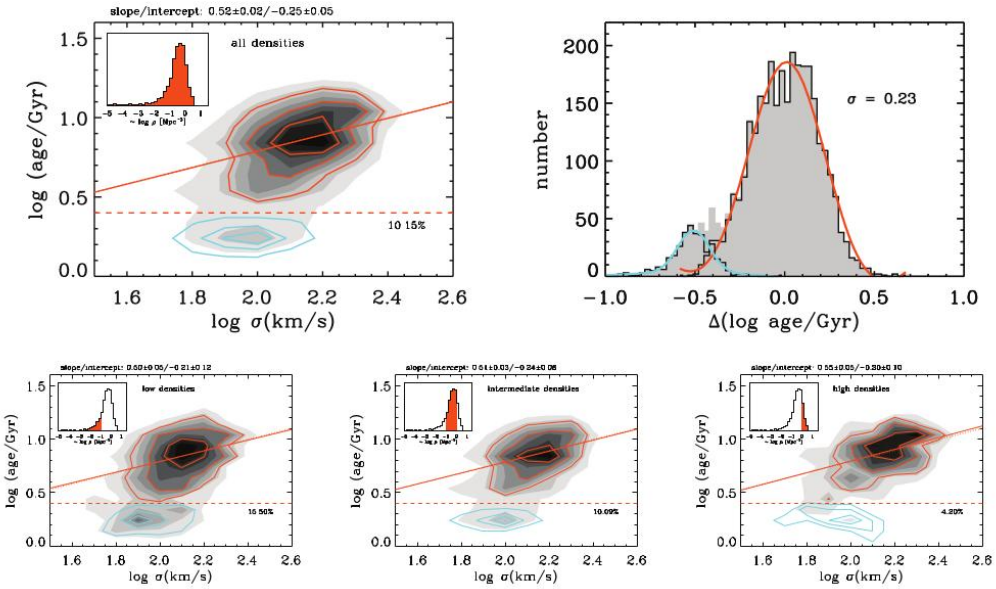

Figure 2.10: From Thomas et al. (2010) - Contour plots of the relationship between stellar velocity dispersion and luminosity-weighted age for various environmental densities, as indicated by the inset histograms. The environmental density is proportional to the number density per volume, but no precise physical units are associated to it. The lowest and highest density bins contain 658 and 571 out of 3360 galaxies, respectively. The dashed line separates an old red sequence population (orange contours) from rejuvenated objects in the blue cloud with light-averaged ages smaller than 2.5 Gyr (cyan contours). The fraction of this latter population is given by the label. The underlying grey contours include both populations. The solid line is a linear fit to the red sequence population, the parameters of the fit are given at the top of each panel. The dotted line is the fit for all environmental densities (parameters from top left-hand panel). Its distribution is shown by the top right-hand panel (same color coding). The label gives the standard deviation σ for the fit. The age-σ relationship for the red sequence population is independent of environment, while the rejuvenation fraction increases with decreasing density.

2.4 Initial Mass Function (IMF) in ellipticals

The Initial Mass Function (IMF) describes the mass distribution of stars at birth, so that for each event of star formation the number dN of stars produced with mass between m and $m + dm$ is given by:

$$dN = \varphi(m)\, dm \tag{2.4}$$

In the simplest approach, the IMF can be approximated by either a one or multi-slope power-law.
In the former case, it is given by:

$$\varphi(m) = A\, m^{-(1+x)} \tag{2.5}$$

where the value of the constant A is found by requiring the normalization of the function over the considered mass range (usually $0.1 - 100 M_{\odot}$):

$$\int_{0.1M_{\odot}}^{100M_{\odot}} m\, \varphi(m)\, dm = 1 \tag{2.6}$$

and where, in the commonly used parameterization by Salpeter, 1955, $x = 1.35$.
The IMF can be observationally derived by counting stars according to their magnitude only in the solar vicinity. As an example, Kroupa et al. (1993) suggested a multi-slope power law for the solar neighborhood:

$$\begin{cases} x_1 = 0.2 & m \leq 0.5 M_{\odot} \\ x_1 = 1.2 & 0.5 \leq M/M_{\odot} \leq 1.0 \\ x_3 = 1.7 & m \geq 1.0 M_{\odot} \end{cases} \tag{2.7}$$

Fig. 2.11 from Romano et al. (2005) shows various forms of IMFs, together with a comparison with the Salpeter (1955) form.

The IMF deeply affects the chemical evolution of a galaxy on many different levels, by determining the ratio between low and high mass stars.
As we already discussed in the previous sections, SNe Ia (originating from low and intermediate mass stars) produce the bulk of Fe in the galaxy over long time scales (Matteucci and Greggio, 1986; Matteucci and Recchi, 2001); additionally, even when not entering the cycle of production and recycling of elements due to their lifetime being larger than a Hubble time, low mass stars still affect chemical evolution by locking baryonic matter away from the ISM. On the other hand, massive stars are the main producers of α elements

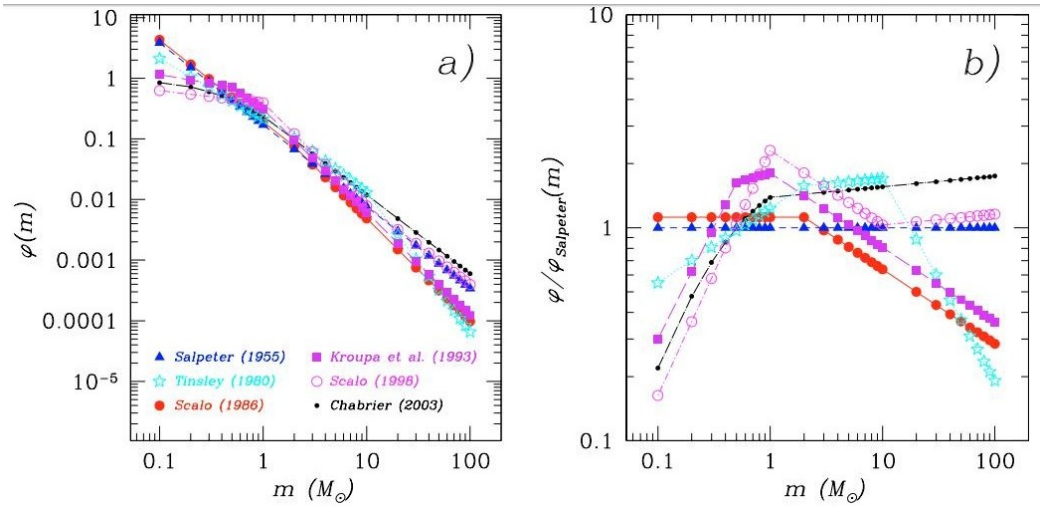

Figure 2.11: From Romano et al. (2005) - a) Stellar IMF according to Salpeter (1955) (triangles), Tinsley (1980) (stars), Scalo (1986) (full circles), Kroupa et al. (1993) (squares), Scalo (1997) (empty circles) and Chabrier (2003) (dots). Here, $\varphi(m)$ is the IMF by mass, and $\varphi(m) = m^{-x}$ (x = 1.35 in the case of Salpeter's IMF), except for Chabrier (2003), where a lognormal form for the low-mass domain ($m \leq 1M_{\odot}$) is suggested instead. The Chabrier IMF also has $x = 1.3$ as the exponent in the $m > 1M_{\odot}$ mass domain. b) Same as panel a), but with $\varphi(m)$ divided by the corresponding Salpeter value for each given mass. This allows a first-sight comparison of the various mass distributions expected according to the different IMFs with respect to the "standard" Salpeter choice.

(O, Mg, Si, Ca), via processes characterized by much shorter timescales than for Fe-peak elements. As previously mentioned, the time delay in the production of these two classes of elements is what allows us to use their abundance ratios to derive constraints on the history of star formation of the galaxy (Matteucci, 1994; Matteucci et al., 1998; Matteucci, 2012).
The implications of IMF variations, anyway, go well beyond chemical abundances, since they affect many other properties of a galaxy. Low mass stars are the main contributors to the total stellar mass budget at the present time (Kennicutt, 1998), while massive stars dominate the integrated light of galaxies (Conroy and van Dokkum, 2012b), and strongly influence the amount of energetic feedback produced by stellar winds and SNe after star formation episodes.
Different "portions" of the IMF have been found to affect different properties; Renzini and Greggio (2012), for instance, concluded that the M/L ratio in local early-types is mainly affected by the value of the IMF slope below $\approx 1\ M_{\odot}$, while the IMF values in the mass range between ≈ 1 and $\approx 1.4\ M_{\odot}$ affect the M/L evolution.

Since the IMF affects the properties of galaxies on so many different levels, a great number of works explored the topic in the past years, focusing either on providing models to explain its origin and properties, or on the challenge of its observational determination, especially in external galaxies where it cannot be estimated directly.
Concerning the theoretical aspect, a definite physical picture does not exist yet; to this regard, Silk (1995) and Krumholz (2011) analyzed the effect of molecular flows and protostellar winds, Larson (1998, 2005) tried to explain it in terms of the Jeans mass, while Bonnell et al. (2007), Hopkins (2013) and Chabrier et al. (2014) explored the effect of gravitational fragmentation and of the thermal physics.
As for the observational determination of the IMF, the task greatly differs between the Milky Way and other galaxies.
In our galaxy, direct star counts in star forming regions and clusters supported the adoption of a Kroupa/Chabrier-like invariant IMF, in the form of a power law for $m > 1M_{\odot}$, and a turn-off at lower masses (Scalo, 1986; Kroupa et al., 1993; Kroupa, 2001, 2002; Bastian et al., 2010; Kroupa et al., 2013). The invariance of the local IMF has been invoked for a long time to support claims for its universality, even though a direct confirmation of this claim through star counts in other galaxies is clearly precluded by the limitations of our observational capabilities at the present time (and, presumably, for some time to come).
For this reason, we need to employ indirect methods to obtain constraints on

the IMF of galaxies with unresolved stellar populations.
A powerful tool is the observation of features in the galaxy integrated spectra which are found to be sensitive to gravity; the NaI$\lambda\lambda$8183, 8195 doublet lines and the Wing-Ford FeH band at 9900 Å, for example, are only visible in presence of low-mass dwarfs, while the Ca triplet lines at λ8498, 8542, and 8662 Å are strong in the atmosphere of giants and almost undetectable in dwarfs (Wing and Ford, 1969; Faber and French, 1980; Diaz et al., 1989).
A number of works which investigated the topic, either by the use of the described spectral features or by other methods, agree in observing a trend of the IMF becoming skewed towards low-mass stars ("bottom-heavy" IMF) in more massive galaxies.
Saglia et al. (2002); Cenarro et al. (2003) for the first time proposed a trend implying an excess of low-mass stars in massive galaxies, from a study of the CaT region. Moreover, van Dokkum and Conroy (2010, 2011) came to a similar conclusion after analyzing a sample of eight massive ETGs in the Virgo and Coma clusters, and then confirmed this result by using stellar population models including variable element abundance ratios and using a full spectral fitting analysis on a set of 34 ETGs from the SAURON survey (Conroy and van Dokkum, 2012a,b). Ferreras et al. (2013), La Barbera et al. (2013), as well as Spiniello et al. (2014) showed that a systematic trend exists for the whole population of ETGs, with higher velocity dispersion (mass) galaxies showing a bottom-heavier IMF; A similar result was claimed by Auger et al. (2010), Grillo and Gobat (2010), Treu et al. (2010), Barnabè et al. (2011), Cappellari et al. (2012) and Spiniello et al. (2012) on the basis of kinematics and gravitational lensing studies, and by Dutton et al. (2011, 2012, 2013) from scaling relations and models of light and dark-matter distribution in galaxies.
However, on the other hand, Gunawardhana et al. (2011) observed a strong dependence of the IMF on star formation in a sample of low-to-moderate redshift star-forming galaxies from the GAMA survey, with the high mass slope of the IMF becoming flatter (hence providing a top-heavier IMF) in objects with higher formation activity, as it might be the case for the progenitors of more massive galaxies (Matteucci, 1994; Matteucci et al., 1998; Matteucci, 2012).
Smith et al., 2015, on the other hand, conduced a blind survey to identify strong gravitational lenses among low-redshift early-type galaxies, and derived total J-band mass-to-light ratios. Their results were in accordance with a Kroupa (2001) IMF ($\alpha = 1.00$), and strongly rejected IMFs with $\alpha \geq 2$. A Salpeter (1955) IMF ($\alpha = 1.55$), though inconsistent if the galaxies are old, could not be excluded.
Historically, galaxy formation models based on the hierarchical clustering

scenario failed in simultaneously reproducing two fundamental observational features of ellipticals, i.e. the increase of the $[\alpha/Fe]$ ratios for larger values of σ and the mass-metallicity relation (Pipino and Matteucci, 2008; Okamoto et al., 2017). In this sense, Pipino et al. (2009) tried to reproduce the mass- and $\sigma - [\alpha/Fe]$ relations in the stellar populations of early-type galaxies by a cosmologically motivated assembly history for spheroids within the semi-analytical model GalICS, which successfully reproduced basic low- and high-redshift galaxy properties, and included the contribution of both type Ia and II SNe. In spite of obtaining $[\alpha/Fe]$ ratios marginally consistent with the observed ones, thanks to the AGN quenching of star formation in massive haloes, they failed in reproducing the mass-metallicity relation.
Common solutions proposed to overcome this limit generally involved the introduction of AGN feedback and/or of variable IMFs, becoming top-heavier with mass.
In particular, Thomas (1999) calculated chemical enrichment and stellar abundance ratios of galaxies within a hierarchical clustering scheme, by adopting star formation histories (**SFH**) derived from semi-analytic models, and found that a $[Mg/Fe]$ overabundant population could only be obtained under the assumption of an initial mass function significantly flattened with respect to the Salpeter value during the starburst.
Thomas et al. (1999) proposed two scenarios for the formation of giant ellipticals, either via fast ($\approx 1Gyr$) collapse of smaller entities or via merging of spiral galaxies similar to the Milky Way; in the latter case, the expected $[\alpha/Fe]$ overabundance could be reproduced only by assuming an IMF flatter than a Salpeter one during the initial starburst triggered by the merging.

Similarly, an IMFs top-heavier than a Salpeter one was proposed by Calura and Menci (2009), who assumed a star-formation-dependent IMF - with a slope switching from a Salpeter (x=1.35) to a slightly flatter value (x=1) for SFR $>100 M_{\odot}\, yr^{-1}$ - together with interaction-triggered starbursts and AGN feedback. Arrigoni et al. (2010) used both a top-heavy IMF (with a slope x = 1.15) and a lower SNe Ia ratio. Gargiulo et al. (2015) implemented SFR-dependent IMF together with a radio-mode AGN feedback for quenching star formation.

Fontanot et al. (2017, 2018b,a) analyzed the implications of including the integrated galaxy-wide stellar initial mass function (IGIMF) in the semi-analytical model GAEA (GAlaxy Evolution and Assembly), and the effect of cosmic rays on its shape and evolution.
To conciliate the opposing indications as to whether the IMF in more massive ellipticals should be bottom or top-heavy, Weidner et al. (2013) and Ferreras et al. (2015) proposed a time dependent form of the IMF, switching from

a top-heavier form during the initial burst of star formation to a bottom-heavier one at later times; in particular, we investigated this last scenario in Chapter 6

Chapter 3

Chemical evolution models

The first application of the monolithic collapse scenario to the chemical evolution of elliptical galaxies is due to Larson (1974). As briefly described in section 2.2.4, these model are based on the following blueprint:

- unlike what is assumed in hierarchical formation models, the total mass budget is already in place at the beginning of the process, and undergoes a collapse through which the galaxy is formed;
- depending on the specific model, the collapse can be monolithic (closed box model), or the presence of gas flows can be accounted for;
- the increased density following the initial collapse leads to a phase of strong star formation;
- once the thermal energy produced by stellar winds and SN feedback ("galactic wind") overcomes the gas binding energy, the latter is driven away from the system, so that SF is quenched and the galaxy evolves passively.

Within this framework, Larson (1974) reproduced the MZR and the CMR by adopting what later came to be known as a "direct wind" model, namely assuming that the rate of star formation per unit mass of gas (*star formation efficiency*, see Sec. 3.1.1), was inversely proportional to the total mass.
The decreased thermal energy input resulting from the lower star formation activity, coupled with the higher potential energy barrier in more massive systems, causes a delay in the onset of the galactic wind, thus allowing a longer time to build up the total metallicity, with the resulting reddening of the galaxy.
The limit of the direct wind model is its inability to produce the observed supersolar values of the $[\alpha/Fe]$ ratios in the core of ellipticals, and their increase

with mass (see Sec. 2.2.4); as we discussed previously, both of these features result from a decrease of the star formation duration with mass ("downsizing" in star formation), which is exactly the opposite of what happens in direct wind models.
A solution to this problem, then, was the introduction by Matteucci (1994) of the "inverse" wind models, based on the assumption of a more efficient star formation in more massive galaxies, which provides enough thermal energy to overcome even the higher potential barrier, thus producing an earlier quenching of the star formation through the galactic wind. In these models, basically, the star formation is both intense enough to account for the increased metal content (mass-metallicity relation), and short enough to prevent the Fe-peak element pollution of the stellar population ($[\alpha/Fe]$-mass relation).
Conversely, other approaches, such as the ones followed in cosmological formation models, are not as successful in reproducing the effect of the downsizing star formation on chemical abundances, since they generally fail in providing the additional physical mechanisms needed to model the initial burst and the following quenching of star formation, and thus in reproducing both the MZR and the $[\alpha/Fe]$-mass relation. To name a few, Pipino and Matteucci (2008) included a detailed treatment for chemical evolution in a semi-analytical model, and relied on AGN feedback to quench star formation; while they found $[\alpha/Fe]$ ratios marginally consistent with data, they failed in reproducing the MZR. In the cosmological galaxy formation model by Calura and Menci (2009, 2011), fly-by triggered starbursts were combined with a late AGN feedback quenching, producing a better fit for the $[\alpha/Fe]$-mass relationship. Fontanot et al. (2017) was able to obtain the α-enhancement with stellar mass observed in data by replacing a canonical, universal IMF with the IGIMF (see later) in the semi-analytical model GAEA.

For the work presented in this Thesis, we adopted a modified version of the code for chemical evolution of elliptical galaxies originally presented in Pipino and Matteucci (2004), mainly extended to include the effects of different parameterizations for the IMF. The model follows the detailed evolution with time of 21 different chemical elements, and shares some of the properties we listed above, with a few additions or modifications:

- the infall episode of the initial gas cloud, from which the galaxy originates, can be modeled by an exponential law;
- the galaxy is modeled as formed by spherical, non-interacting shells with a radius equal to $0.1R_{eff}$. In the original work, this allowed for the study of abundance gradients, but since we were not interested in

the topic, in all the models presented in this Thesis we always assumed the galaxy to be formed by one shell, with radius $R = R_{eff}$;

- feedback effects by SNe, including both Type I (a, b, c) and II, are taken into account to determine the thermal balance of the galaxy;
- the model belongs to the "inverse wind" family, namely the star formation efficiency becomes higher with the total stellar mass, to obtain an earlier onset of the galactic wind and reproduce the $[\alpha/Fe]$-mass relation.

3.1 Basic ingredients of chemical evolution models

To compute a chemical evolution model, a few fundamental physical quantities need to be introduced (Matteucci, 2012):

- the initial chemical composition of the gas, namely whether the gas has a primordial composition, or if it has been pre-enriched by previous stellar generations;
- the presence of gas inflow/outflow, if we are not assuming a closed-box type of model;
- the stellar birthrate function, which in turn depends on the Initial Mass Function (IMF) and on the Star Formation Rate (SFR), describing the number of stars being born in the mass range $m - m + dm$ and in the time interval $t - t + dt$;
- the stellar yields, describing the quantity of each element which is returned into the ISM by dying stars.

All these quantities appear in the integro-differential equations of the model, whose solution provides the evolution with time of the abundance by mass of the various considered chemical elements in the ISM.

3.1.1 Birthrate function

The *birthrate function* provides the number of stars formed in the mass range $m - m + dm$ in the time interval $t + t + dt$. Mass and time can usually be factorized in this function, which then can be written as:

$$B(m,t) \equiv \psi(t) \times \varphi(m) \tag{3.1}$$

where the first term, $\psi(t)$, is the SFR, while $\varphi(m)$ is the IMF.

Star Formation Rate (SFR)

The SFR describes the gas mass quantity converted into stars in the time $t - t + dt$; as such, it is usually expressed in $M_{\odot}/yr$, or in some equivalent units.
A commonly assumed parameterization for the SFR has been provided by Kennicutt (1998), who expressed it as:

$$\psi(t) = \nu\, \rho_{gas}(t)^k \tag{3.2}$$

where $\rho_{gas}(t)$ is the surface mass density of the gas; Kennicutt (1998) studied this relation over a wide range gas of densities and star formation rates, by combining a sample of 61 spiral galaxies with 36 infrared-selected starburst galaxies, and found a good agreement with observations for $n \approx 1.4 \pm 0.15$.
Here, we adopt a linear law depending on the gas mass:

$$\psi(t) = \nu\, M_{gas}$$

according to Pipino and Matteucci (2004). The parameter ν, having the dimensions of the inverse of a time $[Gyr^{-1}]$, is the *star formation efficiency*; it can be seen as the SFR per unit mass of gas, and its inverse represents the time scale at which the total amount of gas is converted into stars.
As discussed at the beginning of this Chapter, the value of ν, and particularly its variation with the total galactic mass, has been a matter of discussion for a long time. While the first models of chemical evolution for elliptical galaxies assumed ν to be constant, or even a decreasing function of the galactic mass (Larson, 1974), more recent works seems to indicate that it should increase in more massive galaxies (Matteucci, 1994; Matteucci et al., 1998; Matteucci, 2012; Pipino and Matteucci, 2004; De Masi et al., 2018).

IMF

We provided a brief overview of the topic of the IMF in elliptical galaxies in Section 2.4. A detailed description of the functional forms adopted for the IMF in this work is provided in Sec. 5.3, 5.4, 6.2

3.1.2 Stellar Yields

Stellar yields provide the abundance of each element which is ejected into the ISM by dying stars of various masses, both as newly formed and pre-existing nuclei; as such, they are needed to correctly model nucleosynthesis.
In this Thesis, we adopted the set of yields already used in Pipino and Matteucci (2004):

- single low and intermediate-mass stars (LIMS: $0.8 < M/M_{\odot} < 8$): metallicity-dependent yields by van den Hoek and Groenewegen (1997);
- SNe Ia in the single degenerate scenario, i.e. originating from a C-O white dwarf in binary systems accreting material from a companion, and exploding via C-deflagration upon reaching the Chandrasekar mass: yields by Iwamoto et al. (1999);
- massive stars ($M > 8\,M_{\odot}$): yields by Thielemann et al. (1996).

3.2 Equations of chemical evolution

Once the general theoretical framework has been established, the chemical evolution model provides the variation in time (and, possibly, space) of the mass abundances of the various elements in the ISM, by solving a system of integro-differential equations, one for each element.

A complete analytical solution of this set of equations, however, is only possible when assuming a series of simplifying hypothesis.
The most famous example is probably the "simple model" (Tinsley, 1974; Pagel and Patchett, 1975; Tinsley, 1980), where the IMF is considered constant, inflows and outflows are neglected, the gas is assumed to be well-mixed at all time, and the so-called ***IRA (Instantaneous Recycling Approximation)*** holds, namely stellar lifetimes are neglected, by assuming that stars more massive than $1\,M_{\odot}$ die immediately, while less massive stars never die. Under these conditions, the total metallicity in the ISM of a galaxy as a function of time $Z(t)$ can be related to the gas mass fraction μ_{gas} through the well known relation:

$$Z(t) = y_Z\, ln\left(\frac{1}{\mu_{gas}}\right) \tag{3.3}$$

where

$$\mu_{gas} \equiv \frac{M_{\rm gas}}{M_{\rm tot}} \tag{3.4}$$

while the yield y_Z provides the fraction of newly produced and ejected metals by a stellar generation relative to the fraction of mass locked up in remnants and low-mass stars (Tinsley, 1980).
Albeit derived in these extremely simplified assumptions, this solution can still turn useful. For example, the relation between metallicity and gas mass fraction has been sometimes invoked to explain the existence of the MZR in active galaxies; this is achieved by assuming an "effective yield" depending on stellar mass, due to selective loss of metals from galaxies with low potential wells through galactic winds (Garnett, 2002; Tremonti et al., 2004), or is based on the observations of increasing gas mass fractions in smaller galaxies in the local universe (Roberts and Haynes, 1994; McGaugh and De Blok, 1997; Bell and De Jong, 2000; Geha et al., 2006).
Analytical solutions in more complex systems including gas flows (infall, outflow, galactic fountains) have been explored by Tinsley (1980); Pipino et al. (2014); Peng and Maiolino (2014); Spitoni (2015); Spitoni et al. (2017).
In general, analytical models are useful tools when studying the evolution of oxygen (which is an α-element, created on short time-scales) and of the total gas metallicity Z, which is actually dominated by the oxygen itself. However, they fail in reproducing a large number of observational constraints, such as the G-dwarf metallicity distribution (Matteucci, 2012), and they are not suitable to model the evolution of elements created on long time-scales, such as Fe, thus resulting in the inability to obtain the $[\alpha/Fe]$ increase with mass (see Sec. 2.2.4).

To overcome these shortcomings, and follow in detail the evolution of each chemical element, it is then necessary to drop the IRA, and to adopt numerical methods in order to solve the chemical evolution equations.
In this approach, the variation with time of the mass fraction G_i of the i-th

element in the gas of the galaxy is given by:

$$\begin{aligned}\frac{dG_i(t)}{dt} &= -\psi(t)\, X_i(t) + \\ &+ \underbrace{\int_{M_L}^{M_{Bm}} \psi(t-\tau_m) Q_{mi}(t-\tau_m)\, \varphi(m)\, dm}_{①} + \\ &+ \underbrace{A \int_{M_{B_m}}^{M_{B_M}} dm\, \varphi(m) \left[\int_{\mu_m}^{0.5} f(\mu_s)\, \psi(t-\tau_{m_2})\, Q_{mi}(t-\tau_{m_2}) d\mu_s \right]}_{②} + \\ &+ \underbrace{(1-A) \int_{M_{B_m}}^{B_M} \psi(t-\tau_m)\, Q_{mi}(t-\tau_m)\, \varphi(m)\, dm}_{③} + \\ &+ \underbrace{\int_{M_{B_M}}^{M_U} \psi(t-\tau_m)\, Q_{mi}(t-\tau_m)\, \varphi(m)\, dm}_{④} + \\ &+ \left[\frac{dG_i(t)}{dt} \right]_{infall}\end{aligned} \tag{3.5}$$

The physical meaning of the various terms appearing in this equations is straightforward.
The first term describes the decrease in the i-th element abundance due to gas being locked in stars, following star formation, while the last term indicates the abundance variation of the element due to the infall of the gas the galaxy is originating from.
As for the various integrals, each of them provides the restitution rate of the considered element from stars in a specific mass ranges; in other words, it is the quantity of that element which is emitted from the star at its death, either in the form of newly produced nuclei or as already existent ones.
The mass intervals relative to the integrals follow the following scheme:

1. single stars with mass between $M_L = 0.8\, M_\odot$ and $M_{B_m} = 3\, M_\odot$;

2. binary systems, with total mass comprised between $M_{B_m} = 3\, M_\odot$ and $M_{B_M} = 16\, M_\odot$. These systems are the progenitors of Type Ia SNe, so they are fundamental in the production of Fe; the meaning of the quantities appearing in this integral is better explored in Sec. 3.3;

3. this term represents single stars in the same mass range as the previous integral. These stars will end their life either as C-O dwarfs (up to $8\,M_{\odot}$), or will produce a type II SNe;

4. these are massive stars ($m > 16\,M_{\odot}$), producing core collapse (either type II or Ib/c) SNe.

As for the various terms appearing in the equation:

- as mentioned in Sec. 1.1, the abundance by mass of the i-th chemical species in the ISM $X_i(t)$ is:

$$X_i(t) \equiv \frac{M_i}{M_{gas}}$$

with the condition:

$$\sum_{i=1}^{N} X_i = 1$$

- $G_i(t)$ is the ratio between the mass density of the element i at the time t and its initial value

$$G_i(t) = X_i(t)\,\rho_{gas}(t) \tag{3.6}$$

- the function $\tau_m(m)$ describes the stellar lifetimes. Specifically, τ_{m_2} is the lifetime of the secondary star (the originally least massive one, see next Sec. 3.3) in binary systems originating SNe Ia, and represents the clock of the system.

- as mentioned in Sec. 3.1.1, until the onset of the galactic wind (**GW**), the star formation rate $\psi(t)$ is assumed to follow a Kennicut-like law, while it goes to zero when the wind starts:

$$\psi(t) = \begin{cases} \nu\,\rho_{gas}(t) & \text{before GW} \\ 0 & \text{after GW} \end{cases} \tag{3.7}$$

where we remember that the star formation efficiency ν is assumed to increase with the galactic mass, in accordance to the prescription of the "inverse wind model" (Matteucci, 1994; Matteucci et al., 1998).

- $\varphi(m)$ is the initial mass function (IMF); the different parameterizations used are detailed in the following sections.

- the meanings of the constant A, of the variable μ_s and of the function $f(\mu_s)$ are explained in the next Sec. 3.3;

- the quantity Q_{mi} is defined as:

$$Q_{mi}(t-\tau_m) \equiv \sum_j Q_{ij}(m)\, X_j(t-\tau_m) \tag{3.8}$$

  where $Q_{ij}(m)$ is the so-called **production matrix**, taking into account the restitution rate of element i, both as newly formed atoms of element i originating from the element j, and as already present in the star at birth (Talbot Jr and Arnett, 1971; Matteucci and Recchi, 2001). In this context, $X_j(t-\tau_m)$ is the abundance of the element j present in the star at its birth (again, τ_m is the lifetime of a star of mass m) and later transformed into the element i and ejected.

The method adopted to solve the main chemical evolution equation is taken from Talbot Jr and Arnett (1971), and is based on finding an analytical solution and then iterating on the same solution.
We are aware that chemical evolution models contain a certain number of free parameters, such as the efficiency of sar formation, the time-scale of gas accretion, and the ones characterizing the form of the IMF in external galaxies. For this reason, we try to constrain their values by comparing with as large as possible number of observational constraints (see Sec. 4).

3.3 Energetics

As previously mentioned, the code takes into account the feedback powered by both Type I and core-collapse (CC) SNe.
For the former, we assume a single degenerate scenario, as described in Whelan and Iben (1973). Specifically, the system is formed by a C-O white dwarf (WD) accreting material from a red giant companion, until the WD reaches the Chandrasekhar mass and Carbon deflagration is ignited.
The rate of this process can be expressed as (Greggio and Renzini, 1983; Matteucci and Greggio, 1986; Matteucci and Recchi, 2001):

$$R_{SNIa} = A \int_{M_{B_m}}^{M_{B_M}} dM_B\, \varphi(M_B) \int_{\mu_m}^{0.5} f(\mu_s)\, \psi(t-\tau_m)\, d\mu_s \tag{3.9}$$

where M_B is the total mass of the binary system, assuming values - as previously mentioned - in the range $M_{B_m} - M_{B_M}(3-16M_\odot)$.
The parameter $\mu_s \equiv M_2/M_B$ is the mass fraction of the secondary star (the

originally least massive one) with respect to the total mass of the binary system, which we assume to be distributed as:

$$f(\mu_s) = 2^{\gamma+1}(\gamma+1)\,\mu^{\gamma} \tag{3.10}$$

where the best-fitting value of the free parameter γ is found to be $\gamma = 2$.
Finally, A is a free parameter, representing the fraction in the IMF of binary systems with the right properties to give rise to Type Ia SNe; its value is constrained in order to reproduce the present-day observed value (Cappellaro et al., 1999).
The rate for core-collapse SNe (II, Ib, Ic) is given by:

$$\begin{aligned} R_{cc} = (1-A) &\int_{8}^{16} dm\,\varphi(m)\,\psi(t-\tau_m) + \\ &+ \int_{16}^{M_{WR}} dm\,\varphi(m)\,\psi(t-\tau_m) + \\ &+ \int_{M_{WR}}^{M_U} dm\,\varphi(m)\,\psi(t-\tau_m) + \\ &+ \alpha_{Ib/c} \int_{12}^{20} \varphi(m)\,\psi(t-\tau_m) \end{aligned} \tag{3.11}$$

It is apparent that the first integral in equation 3.11 refers to the upper mass end of the third integral in equation 3.5 (single stars in the mass range $8 - 16\,M_{\odot}$), while the second one refers to the lower mass end in the last integral of equation 3.5. M_{WR} is the lowest possible mass for a Wolf-Rayet star, i.e. the largest mass star resulting in a core collapse SN.
The last two integrals provide the Type Ib/c SNe rates, and account for single stars with masses larger than M_{WR} (corresponding to the upper mass end in the last integral of equation 3.5) and massive binary systems made of stars with masses in the range $12 \leq m/M_{\odot} \leq 20$, respectively.
M_U is the mass limit assumed for the IMF, while $\alpha_{Ib/c}$ is a free parameter, representing the fraction of stars in the considered mass range which can actually produce Type Ib/c SNe.

Following the prescription by Cioffi et al. (1988), only a few percent of the initial energy ($\approx 10^{51} erg$) provided by core collapse SNe is actually injected into the ISM, due to the high cooling efficiency provided by metal ions. The same does not hold for Type Ia SNe, because of the delay in their appearance; once the peak of their contribution is reached, the ISM has already been heated by CC SNe (Recchi et al., 2001), so Type Ia contribute with their whole energy output.

Averaging over the two types provides an overall energy release efficiency of $\approx 20\%$, as described in Pipino et al. (2002).

Aside from the thermal energy, the other critical ingredient to be determined in order to evaluate the energetics of the system is the potential binding energy in the gas in each considered shell. This quantity can be obtained by integrating the equation:

$$E^i_{bin}(t) = \int_{R_i}^{R_{i+1}} dL(R) \tag{3.12}$$

where $L(R)$ is the work required to bring a mass $dm = 4\,\pi\,R^2\,\rho_{gas}\,dR$ from the shell radius R_i to infinity (Martinelli et al., 1998).
In order to calculate this integral, a model providing the baryonic and dark matter within a radius R is needed. For the baryonic (stars plus gas) matter, a Jaffe (1983) profile is assumed:

$$F_{bar} \propto \frac{r/r_0}{1 + r/r_0} \tag{3.13}$$

where $r_0 = R_{eff}/0.763$.
The Dark Matter (DM) is assumed to be distributed in a diffuse halo, with a characteristic scale length ten times larger than the effective radius ($R_{DM} = 10\,R_{eff}$- Matteucci, 1992), and with a profile taken from Bertin et al. (1992).

The code computes the evolution with time of these quantities, and the galactic wind starts at the time t_{GW} for which the following equality holds:

$$E^i_{th}(t_{GW}) = E^i_{bin}(t_{GW}) \tag{3.14}$$

3.4 Comparison with data

In active galaxies, present time chemical abundances in the ISM can be directly estimated through the observation of emission lines in the galactic spectra (Pilyugin, 2001; Kewley and Dopita, 2002; Pettini and Pagel, 2004; Stasinska, 2004; Tremonti et al., 2004; Pilyugin and Thuan, 2005; Kewley and Ellison, 2008).
As discussed in Sec. 2.2, the lack of gas and star formation in elliptical galaxies complicates the task of abundance determination, which have to be determined in the stellar population.
The chemical composition of the latter, however, is the result of the contribution by all the previous stellar generations. On the other hand, our

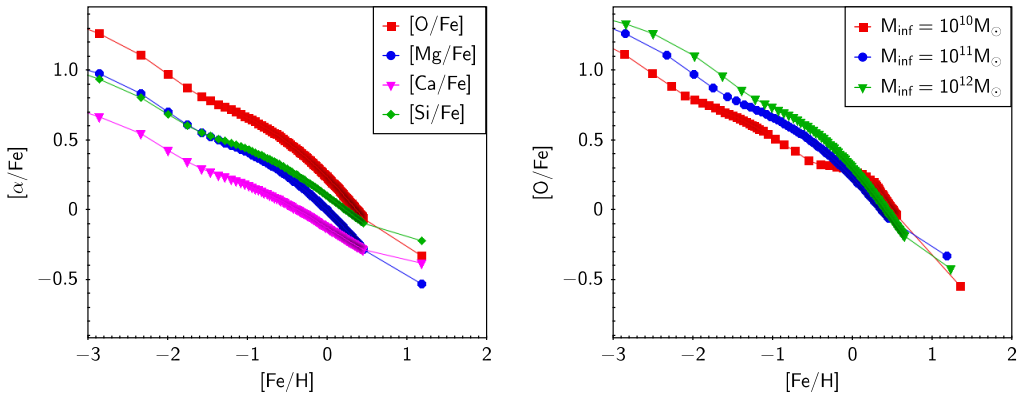

Figure 3.1: Output of the chemical evolution code. Left: theoretical abundance ratios in the ISM of [O/Fe] (line with overlying squares), [Mg/Fe] (line with overlying circles), [Si/Fe] (line with overlying rhombus), [Ca/Fe] (line with overlying triangles) as functions of [Fe/H] in the core of a $10^{11}\,M_{\odot}$ galaxy. Right: theoretical [O/Fe] abundance ratio in the ISM as functions of [Fe/H] for the core of galaxies with $10^{10}M_{\odot}$ (squares), $10^{11}M_{\odot}$ (circles) and $10^{12}M_{\odot}$ (triangles) initial infall masses. The parameters used to obtain this output are the same as in Model 01a (see Table 5.1).

chemical evolution code provides the abundance in the ISM as a function of time for the 21 different chemical elements; for reference, Fig. 3.1 shows the abundances of different α-elements in the core $(0 - 0.1\,R_{eff})$ of a galaxy with a $10^{11}\,M_{Sun}$ stellar mass (left panel), and the [O/Fe] ratio in the cores of galaxies of different total masses (right panel).
In order to compare the outputs of our models with the observed averaged stellar abundances of the galaxies in the dataset, we first computed for each model the average stellar abundances at the present time.

To this regard, this can be done by averaging either on luminosity or mass (Matteucci et al., 1998). Since indices are usually obtained by weighting on the V-band luminosity (Arimoto and Yoshii, 1987; Matteucci et al., 1998), the more physically correct way to proceed is by using luminosity-weighted abundances; however, Gibson (1997) and Matteucci et al. (1998) showed that there is no significant difference for massive galaxies ($M > 10^9\,M_{\odot}$) between light and mass weighted abundances.
As described in Sec 4, for the works presented in this Thesis we produced series of models and compared them with two different datasets.
Model galaxies analyzed in the first part of the work (Chapter 5) are all characterized by masses higher than this value, so that the matter of the difference between the two averaging methods does not hold.
As for the second dataset, although some of our models produce final stellar

masses as low as $\approx 10^8\ M_\odot$, the stellar mass in the data never gets lower than $\approx 10^{9.8}\ M_\odot$ (see Fig. 4.2), so that when matching models and data, only models with stellar masses higher than this value have been retained.
For this reason, when analyzing abundances for models matching the observed data through out all the Thesis, we always applied mass-weighted estimates, which are a natural outcome of the chemical evolution code, according to the relation (Pagel and Patchett, 1975; Matteucci, 2012):

$$< X/H >_{mass} \equiv \frac{1}{M_0} \int_0^{M_0} Z(M)\, dM \tag{3.15}$$

where M_0 is the total mass of stars ever born contributing to light at the present time; an alternative, equivalent formulation is given in Pagel (1997)

$$< X/H >_{mass} (t) \equiv \frac{\int_0^t dt'\, (X/H)(t')\, \psi(t')}{\int_0^{t'}\ dt'\, \psi(t')} \tag{3.16}$$

where $\psi(t)$ is, as usual, the SFR.
Moreover, we further tested the validity of this approach, by computing the light-averaged metallicities for some of the models presented in Chapter 6 (specifically, for the Models 01, created by assuming a Salpeter IMF). The results, summarized in Appendix A, show that the light-averaged metallicities are slightly higher than the mass-weighted ones. The difference is almost constant, and always lower than 0.1 dex. It is worth noting that our conclusions cannot be significantly affected by this shift, since we are not interested in absolute abundances, but in abundance trends.
As mentioned in Sec. 2.2, once the average has been determined, it can be converted to spectral indices to compare with observations, either i) by performing a fitting procedure between the observed absorption features and libraries of spectro-photometric models (Bruzual A., 1983; Renzini and Buzzoni, 1986; Chiosi et al., 1988; Buzzoni, 1989; Charlot and Bruzual, 1991; Bruzual A. and Charlot, 1993; Worthey et al., 1994; Tantalo et al., 1996; Maraston, 1998; Brocato et al., 2000; Bruzual and Charlot, 2003; Maraston, 2003; Thomas et al., 2003; Peletier, 2013) ii) or by using calibration relations (Tantalo et al., 1998), which however are an approximation of the use of stellar population models, hence less accurate.
In this work, we followed the simplified approach, and adopted the calibration relations from Tantalo et al. (1998), taking into account the $[Mg/Fe]$

enhancement:

$$\begin{cases} Mg_2 & = 0.233 + 0.217\,[\text{Mg/Fe}] + \\ & + (0.153{+}0.120[\text{Mg/Fe}])[\text{Fe/H}] \\ < Fe > & = 3.078 + 0.341\,[\text{Mg/Fe}] + \\ & + (1.654\text{-}0.307[\text{Mg/Fe}])[\text{Fe/H}] \end{cases} \tag{3.17a}$$

(3.17b)

Chapter 4

Datasets

In this chapter, we describe the two catalogs we used in the Thesis.

4.1 MOSES dataset

The first dataset we tested our models against is the one originally presented in Thomas et al. (2010).
It consists of 3360 early-type galaxies in the redshift range $0.05 < z < 0.06$, extracted from the MOSES (Morphologically Selected Early types in SDSS) catalog, which have been morphologically inspected and classified as early-types out of an initial sample extracted from the Data Release 4 (DR4) of the Sloan Digital Sky Survey (SDSS).
The use of a morphological selection criteria had the aim of removing any bias against recent star formation; as a result, the dataset has been further divided into two separate subsets:

- a subset of objects with ages peaked at old values, analogous to the "red sequence" observed in the color-magnitude of populations including both late and early-type galaxies (see Sec. 2.2.2, and de Vaucouleurs, 1961; Strateva et al., 2001; Bell et al., 2004);

- a small ($\approx 10\%$) fraction of galaxies with ages peaking at $\approx 2.5\,Gyr$, analogous to the so-called "blue cloud". The lower ages, lower $[\alpha/Fe]$ ratio values and the presence of signs of star formation suggest these galaxies have been rejuvenated by means of recent, minor star formation events.

For the comparisons with our models, we always only used the galaxies in the "red sequence" subset of the catalog.

Objects in the catalog had their stellar population parameters (luminosity-weighted ages, total metallicities, $[\alpha/Fe]$ ratios) derived from the fitting of the 25 Lick absorption line indices to spectro-photometric models (Thomas et al., 2003); moreover, an estimate of the dynamical mass is provided, which should also provide a good approximation of the galactic baryonic mass inside the effective radius (Cappellari et al., 2006; Thomas et al., 2007).
As for the $[\alpha/Fe]$ ratio, in Thomas et al. (2003) the following relationship between total metallicity [Z/H], $[\alpha/Fe]$ and iron abundance [Fe/H] is assumed to hold:

$$[Z/H] = [Fe/H] + A[\alpha/Fe] \tag{4.1}$$

with $A = 0.94$.
To account for possible differences in the α-elements assumed to contribute to the total $[\alpha/Fe]$ ratio in the models and in the data, throughout the text we compared the $[\alpha/Fe]$ ratio provided in the dataset both to our predicted $[Mg/Fe]$ and to an $[\alpha/Fe]$ estimate derived from our model by inverting equation 4.1.
Other than the total metallicity $[Z/H]$ and the $[\alpha/Fe]$ ratio, the catalog reports both the $< Fe >$ and the Mg_2 index for the various galaxies, providing us with a further constraint for our models. For the comparison involving these indices, we adopted the following procedure:

1. from the time-dependent gas abundances provided by the chemical evolution model, we derived the average abundances $[< Z/H >]$ and $[< \alpha/Fe >]$ in the stellar population by applying the mass-averaging process described by equation 3.15;

2. after determining these quantities, we converted them into the required spectral indices by adopting the Tantalo et al. (1998) calibration relations 3.17a and 3.17b.

4.2 SPIDER Dataset

The second dataset we adopted is a subsample of the catalogue of ETGs presented in La Barbera et al. (2010).
Details on the selection of the general dataset can be found in La Barbera et al. (2013), and the final state of the dataset used in this work can be found in Rosani et al. (2018). Briefly, we analyze stellar galaxy properties inferred from spectra stacked in central velocity dispersion from 20996 ($0.05 < z < 0.095$) early-type galaxies, extracted from the 12th Data Release of the SDSS.

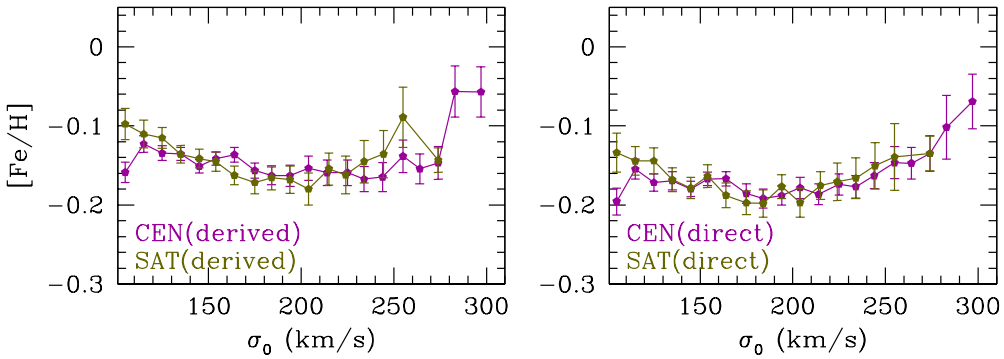

Figure 4.1: Comparison of $[Fe/H]$ values obtained using the "direct" method (fit of Fe5270 and Fe5335 iron lines) and the "derived" method using the values presented in this paper. The "CEN" and "SAT" labels refer to the division of the dataset in central and satellite galaxies,respectively, as described in Rosani et al. (2018).

The stacked spectra were collected to ensure a S/N ratio of the order of a few hundreds, needed to obtain constraints on the IMF from gravity-sensitive features (Conroy and van Dokkum, 2012a).
The environment information for the galaxies in the dataset are derived from the catalog of Wang et al. (2014). As detailed in Rosani et al. (2018), stellar population properties and chemical abundances for various elements have been derived from the stacked spectra by fitting the equivalent widths of a set of line indices to the equivalent widths predicted by synthetic stellar population (SSP) models. The models used for the fitting are the EMILES SSPs of Vazdekis et al. (2016), with variable IMF slope, age, and total metallicity. Two approaches have been explored in the fitting by Rosani et al. (2018): i) the case in which only age, metallicity and IMF-sensitive indices were used; ii) the case in which, additionally to the ones of the previous case, indices sensitive to abundance pattern of different elements (among which $[Mg/Fe]$) were used. In this work, the values of IMF slope, age and total metallicity $[Z/H]$ used are those derived by Rosani et al. (2018) for case i).
Since ETGs are found to be not solar-scaled in abundance pattern, but the EMILES models are, the abundances obtained in the fit for each stacked spectrum had to be corrected to reflect the α-enhancement of ETGs. The method used to derive $[Mg/Fe]$ in Rosani et al. (2018) is the same as in La Barbera et al. (2013). First, one estimates a proxy for $[Mg/Fe]$, defined as the difference between the metallicity derived from the $Mgb5177$ index and the metallicity derived using the Fe_3 index at fixed age (see Trager et al., 1998 and Kuntschner, 2000, respectively, for index definition). Then, the proxy is converted into $[Mg/Fe]$. The conversion factor is established by comparing

the proxy to $[Mg/Fe]$ estimates obtained with the "direct method", based on Thomas et al. (2010) stellar population models with varying $[\alpha/Fe]$ (see Fig.6 of La Barbera et al. (2013)). For the sample analyzed in La Barbera et al. (2013) (and thus in Rosani et al. (2018)), the conversion is very accurate, with an rms of ≈ 0.025 dex, i.e. well within the differences arising in a direct estimate of $[Mg/Fe]$ when adopting different stellar population models (see, e.g., Fig. 18 of Conroy et al., 2014). The comparison of $[Mg/Fe]$ estimates based on the proxy and the direct method has been discussed in La Barbera et al. (2013) and Vazdekis et al. (2015).
Finally, to obtain $[Fe/H]$ for each of the stacked spectra, we invert the relation linking $[Mg/Fe]$, $[Fe/H]$ and total metallicity:

$$[Z/H] = [Fe/H] + 0.75 \times [Mg/Fe]. \tag{4.2}$$

The factor of 0.75 is the same as for the α-enhanced MILES models of Vazdekis et al. (2015). For this set of models, theoretical α-enhanced stellar spectra are produced by a uniform enhancement of $[X/Fe] = +0.4$, for elements O, Ne, Mg, Si, S, Ca and Ti, assuming the solar mixture from Grevesse and Sauval (1998). The above factor refers to these calculations (and is mostly driven by O and Mg). The factor varies for different studies in the literature, depending on the adopted partition table of enhanced vs. depressed elements in the theoretical calculations. For instance, in the case of Thomas et al. (2003) stellar population models, the conversion factor is as high as 0.94, most likely because the authors also include C, N, and Na, besides O, Mg, Si, Ca, Ti, in the α enhanced group. Since we estimate $[\alpha/Fe]$ from Mgb and Fe lines, our abundance estimates mostly reflect the behaviour of $[Mg/Fe]$ and other elements that (closely) track Mg. Hence, the scaling factor adopted in Vazdekis et al. (2015) should suffice our purposes. As a test, we have also computed $[Fe/H]$ directly, as the metallicity estimate obtained when fitting only Fe line strengths. Figure 4.1 shows the fit obtained using the "direct" method (by fitting the mean value of equivalent width of the Fe5270 and Fe5335 iron lines) and the "derived" method using the values presented in this Thesis (the "CEN" and "SAT" labels refer to the division of the galaxies in the dataset in central and satellites, respectively - see Rosani et al., 2018). The comparison shows good agreement between the "direct" values and the estimate of $[Fe/H]$ obtained with our adopted scaling factor. Both the [Fe/H] and the [Mg/Fe] abundances are compared to the analogous ratios as directly predicted by our chemical evolution code. Specifically, we use these values to test the mass-metallicity and $[Mg/Fe]$-mass relation predicted by our chemical evolution model.
In Figure 4.2, we show the variation of $[Fe/H]$ and $[Mg/Fe]$ as a function of galaxy mass in the SDSS stacked spectra, with their 1-σ uncertainties. Since

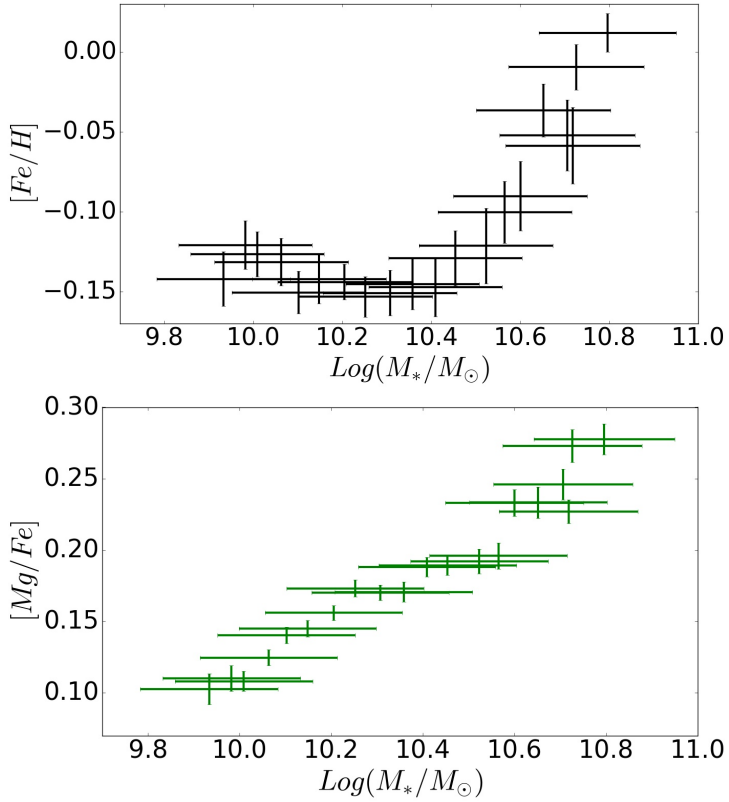

Figure 4.2: $[Fe/H]$ and $[Mg/Fe]$ ratios variation with stellar mass in the 20 mass bins provided in the dataset.

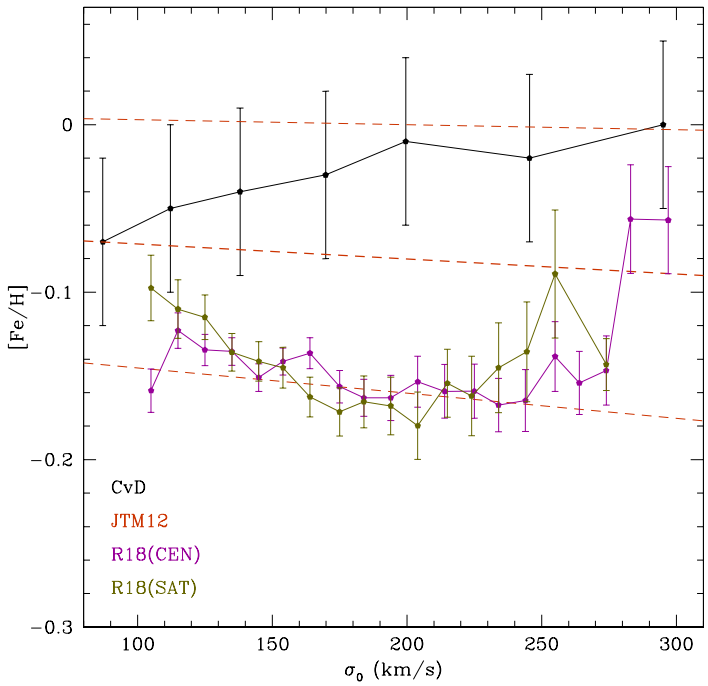

Figure 4.3: Comparison of the $[Fe/H]$-mass relation for the CEN and SAT samples (central and satellites, respectively - see Rosani et al., 2018) with the ones presented in Conroy et al. (2014), in black, and Johansson et al. (2012), in red.

the stacking in Rosani et al. (2018) is originally performed in central velocity dispersion (σ_0) bins, we derived the stellar mass associated to a given stacked spectrum. Specifically, we took the stellar masses listed in the group catalog of Wang et al. (2014); as described by Yang et al. (2007), stellar masses are derived from the relation between stellar mass- to-light ratio and color of Bell et al. (2003).

The resulting relation shows a slight turnover at $LogM = 10.3$, with a rise of iron abundance toward lower masses. Figure 4.3 shows a comparison of the $[Fe/H]$-mass relation for the R18 CEN and SAT samples, with two literature relations by Conroy et al. (2014), in black, and Johansson et al. (2012), in red. While trends presented in literature do not show an upturn at low masses, one should also notice that our error bars on $[Fe/H]$ are far smaller than those from previous works. Therefore, the upturn might be just seen because of the very large number of spectra that we stack together in each sigma bin, and the corresponding very high S/N ratio (as discussed in Rosani et al. (2018)) of our stacked spectra, compared to previous studies. However, notice that for the sample of CENs (compared to SATs), the upturn

is far less evident (almost absent at all). Still, our matching procedure does not provide significant differences between CENs and SATs, implying that the detailed shape of the $[Fe/H]$-mass relation at low mass is not affecting the main conclusions of our work.

Chapter 5

Testing the downsizing scenario

5.1 Introduction

In this Chapter, we review our attempts to reproduce the observed abundance patterns in the MOSES catalog described in Chapter 4, by adopting a revised version of the code for chemical evolution of ellipticals by Pipino and Matteucci (2004).
As stated in Section 4.1, the available observables for this dataset that we analyzed are the total metallicity $[Z/H]$, the $[\alpha/Fe]$ ratio, and the indices $< Fe >$ and Mg_2.
At first, following the results derived by Pipino and Matteucci (2004), we tested the downsizing scenario. Namely, we created a series of model galaxies of increasing total mass, and fine-tuned the model parameters by assuming a shorter time-scale for the initial infall episode and a higher star formation efficiency in more massive galaxies, as described in Section 5.2.
Given the poor match we obtained with this approach, we extended our analysis by testing the effect of a variable IMF, becoming top-heavier (characterized by more massive stars) in more massive galaxies, and of the Integrated Galactic IMF (IGIMF). The parameterizations we tested, and the results of the matching procedure are detailed in Sections 5.3 and 5.4.

5.2 Star formation efficiency variation

As mentioned in the introduction of this Chapter, we compared data to different Models, namely sets of a few ($\approx 5 - 6$) model galaxies, obtained by increasing the value of the initial infall mass and by choosing the other parameters accordingly.
Specifically, galaxies in each Model are characterized by:

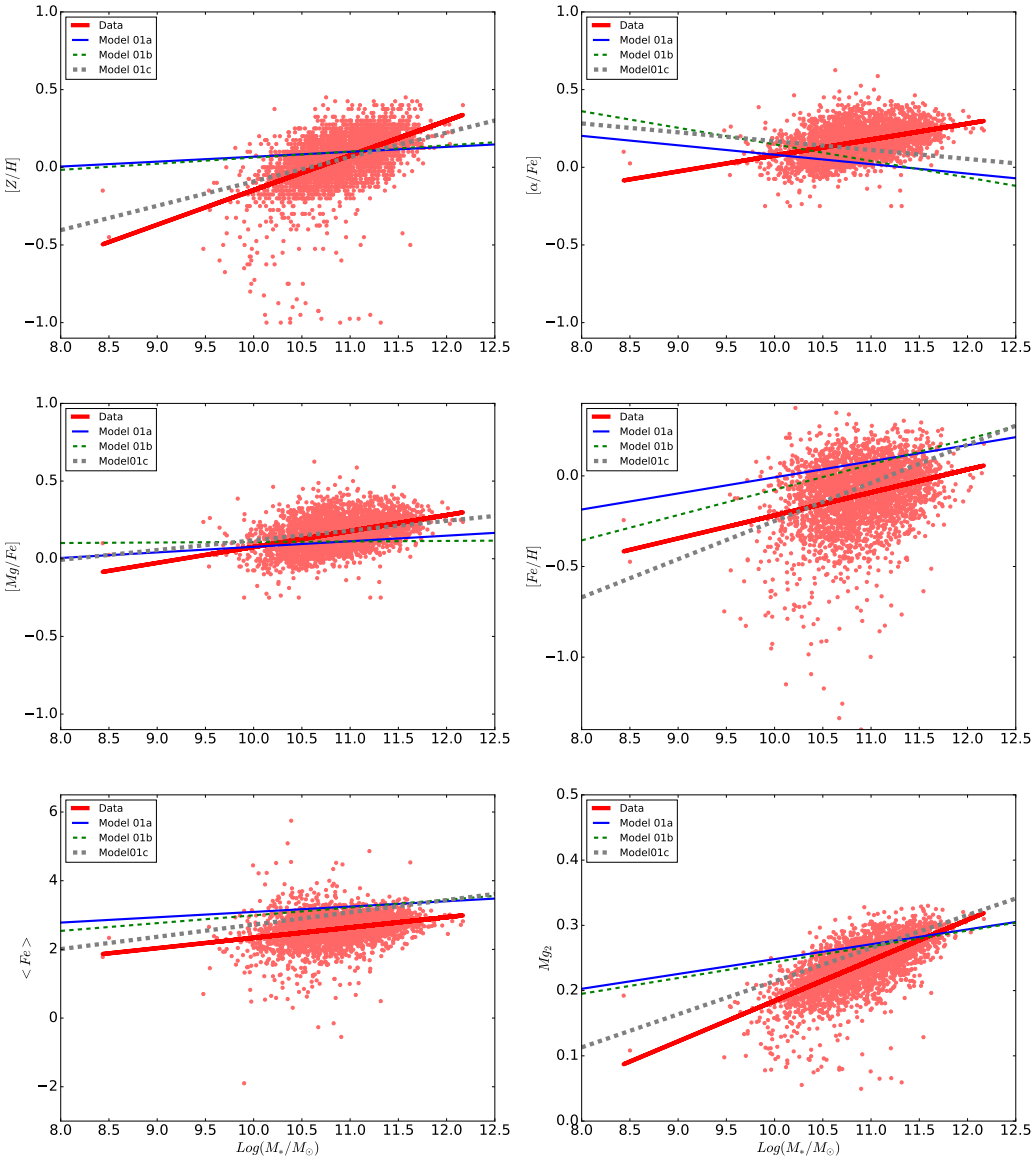

Figure 5.1: Comparison between the observed abundance patterns and the ones derived from Models 01. The models are described in Section 5.2, and their features summarized in Table 5.1. The red dots represent galaxies in the catalog, while the lines indicate linear fits to data (thick solid line) and to Models 01a (thin solid line), 01b (thin dashed line) and 01c (thick dashed line) respectively.

- initial infall masses in the $5 \times 10^9 - 10^{12}\, M_{Sun}$ range;
- effective radius increasing with the galactic mass;
- increasing star formation efficiency ν and decreasing infall timescale τ for more massive galaxies, in agreement with the"inverse wind" model by Matteucci (1994).

Table 5.1 summarizes the parameters values used in creating the model galaxies; column 1 indicates the number identifying the Model, while columns 2 to 7 report the initial infall mass, the effective radius (the final radius achieved once the collapse is over), the star formation efficiency, the infall timescale, the time of the galactic wind onset predicted by the code and the assumed IMF for the different model galaxies, respectively. Notice that, in agreement with the downsizing formation scenario, the galactic wind appears earlier as the total mass increases, as due to the steep increase in star formation efficiency.
As a starting point, in Model 01a we adopted the same parameters as in the best model of Pipino and Matteucci (2004). We included a slightly larger number of model galaxies in this set than in P04, so that for galaxies with masses different from the ones analyzed in that work, we obtained R_{eff}, ν and τ by interpolating between the known values. Figure 5.1 presents the comparison between the catalog (red points) and the predictions of our models.
In the plots, we show the linear fit between the values of the abundance ratios for the 6 galaxies considered in Model01a, to highlight the trend of the ratios with mass; this comparison shows that, in general, the chemical abundance patterns in Model 01a provide a poor agreement with the ones observed in the data.
The increase of both total metallicity $[Z/H]$ and Mg_2 index with mass are considerably flatter than what reported in the dataset.
Regarding the $[\alpha/Fe]$ ratio, a distinction needs to be made, since we compared two different quantities derived from our models against the one provided for the galaxies in the MOSES catalog.
In the plot with the $[\alpha/Fe]$ label (top right panel in Fig. 5.1), we show the variation with mass of the $[\alpha/Fe]$ ratio as obtained by considering our $[Z/H]$ and $[Fe/H]$ values, and by inverting equation 4.1; in this case, even a negative trend is observed, contrary to what is evident in the data and expected theoretically.
On the other hand, the third panel (middle row, left) of Fig. 5.1 shows our $[Mg/Fe]$ ratio, adopted as a proxy, against the $[\alpha/Fe]$ of the catalog; in this case, the positive trend with galactic stellar mass is preserved, even if the

Table 5.1: Parameters used to create the three sets of models described in Section 5.2. Within each set of models (column 1), we modified the effective radius R_{eff}, the star formation efficiency ν and the infall timescale τ (columns 3, 4 and 5, respectively) for different values of the initial infall mass M_{inf} (column 2), and we always assumed a Salpeter IMF (column 7). Column 6 reports the time of the onset of the galactic wind in the model galaxies calculated by the code.

Model	M_{inf}/M_{Sun}	$R_{eff}\,(kpc)$	$\nu\,(Gyr^{-1})$	$\tau\,(Gyr)$	$t_{GW}\,(Gyr)$	IMF
	5×10^9	0.44	2.61	0.50	1.63	Salp
	1×10^{10}	1.00	3.00	0.50	1.49	Salp
	5×10^{10}	1.90	6.11	0.46	0.92	Salp
01a	1×10^{11}	3.00	10.00	0.40	0.56	Salp
	5×10^{11}	6.11	15.33	0.31	0.58	Salp
	1×10^{12}	10.00	22.00	0.20	0.45	Salp
	5×10^9	0.44	0.89	0.50	3.72	Salp
	1×10^{10}	1.00	1.00	0.50	3.34	Salp
	5×10^{10}	1.90	1.89	0.46	2.17	Salp
01b	1×10^{11}	3.00	3.00	0.40	1.52	Salp
	5×10^{11}	6.11	11.44	0.31	0.67	Salp
	1×10^{12}	10.00	22.00	0.20	0.45	Salp
	1×10^{10}	1.00	0.10	0.50	13.64	Salp
	5×10^{10}	1.90	4.50	0.46	1.15	Salp
	1×10^{11}	3.00	10.00	0.40	0.56	Salp
01c	5×10^{11}	6.11	50.00	0.31	0.33	Salp
	1×10^{12}	10.00	100.00	0.20	0.24	Salp

slope is generally still too shallow with respect to the data.
Finally, in the fourth panel (middle row, right) of Fig. 5.1, we compare the $[Fe/H]$-mass relationship as predicted from our model with the one derived from the data by inverting equation 4.1. A small positive trend of the $[Fe/H]$ ratio with mass is apparent in the data, and its slope is reproduced by the model with reasonable agreement, although the predicted $[Fe/H]$ values are slightly overestimated. Taken all of this into account, it appears that the flatness of the $[\alpha/Fe]$ trend with mass in the model can be attributed to the α-elements abundance not increasing enough in massive galaxies.

Given the discrepancies between models and data, we tested a few other parameter configurations, still within the prescriptions of the "inverse wind" model.
Specifically, in an attempt to increase the slope of the $[Z/H]$ and Mg_2 curves, in Model 01b we decreased the star formation efficiency for the less massive galaxies in the set; however, as shown in figure 5.1, this modification proved to be almost ineffective, producing little to no impact.
Finally, in Model 01c we further increased the difference in star formation efficiency between low and high mass galaxies, as again summarized in Table 5.1. Though slightly improving the agreement with data for the total metallicity [Z/H] and the Mg_2 index derived by adopting the Tantalo calibration, this variation generally provided even worse results for the $[\alpha/Fe]$ ratio.

5.3 IMF variation

The results described in the previous section show how the attempts of reproducing the data trends by modifying only the star formation efficiency and the infall timescale in the models proved to be unsuccessful; for this reason, we decided to test the effect of varying the IMF used in the models.
The topic of the IMF in elliptical galaxies, and specifically of whether this function should become bottom or top-heavier (more skewed towards less or more massive stars, respectively), has been discussed in Sec. 2.4. In our case, the shallowness of the obtained mass-metallicity and $[\alpha/Fe]$-mass relations clearly indicated that the effect of (a reasonable) downsizing was not sufficient to quench the star formation early enough to produce the required increase of $[\alpha/Fe]$ with galactic mass.
To solve this problem by operating on the IMF, it was necessary to assume a transition from a bottom to a top-heavy IMF as the galaxy mass increased, in order to produce an effect similar to the increasing star formation efficiency. To this aim, we created two new sets of model galaxies, Model02a and 02b,

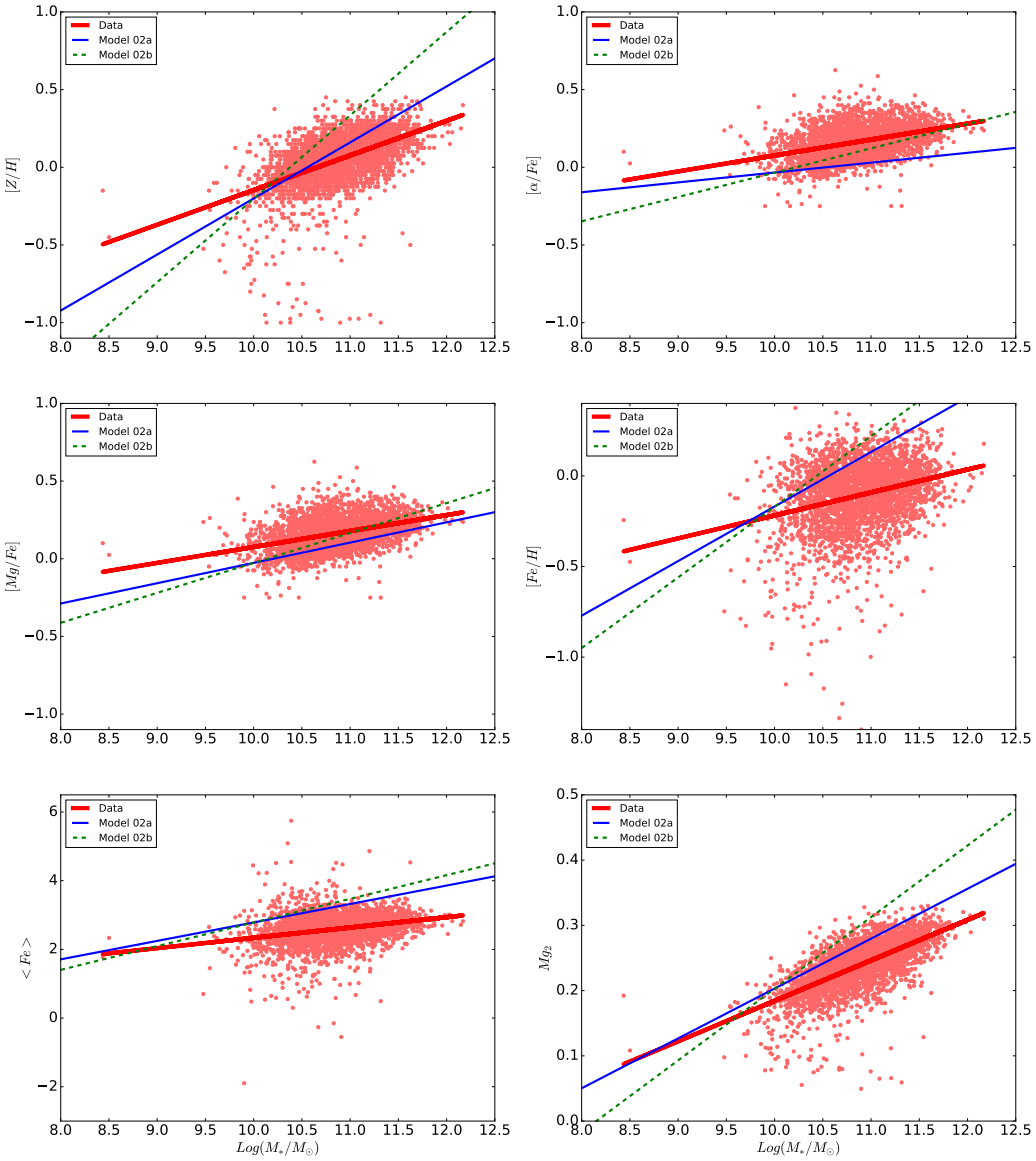

Figure 5.2: Comparison between the observed abundance patterns and the ones derived from Models 02. The models are described in Section 5.3, and their features summarized in Table 5.2. The red dots represent galaxies in the catalog, while the lines indicate the linear fit to data (thick solid line) and to Models 02a (thin solid line) and 02b (thin dashed line) respectively.

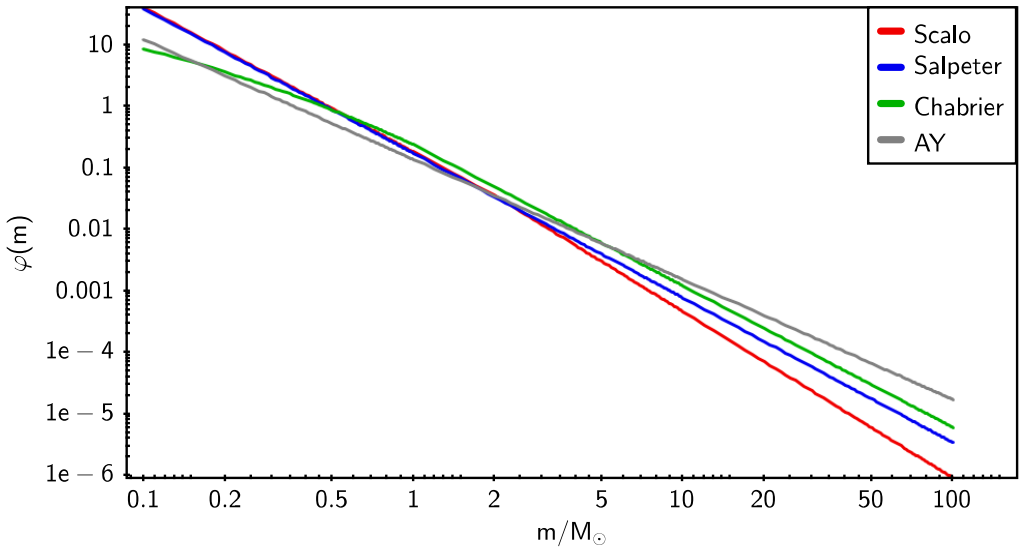

Figure 5.3: Comparison of the different IMFs used for the Models 02.

by adopting the following parameterizations for the IMF:

- **Scalo (1986) IMF**: we used the approximate expression adopted in Chiappini et al. (1997):

$$\varphi(m) \propto \begin{cases} m^{-2.35} & 0.1 \leq m/M_{\odot} < 6 \\ m^{-2.7} & 6 \leq m/M_{\odot} \leq 100 \end{cases} \tag{5.1}$$

- **Salpeter (1955) IMF**, which is a simple power-law:

$$\varphi(m) \propto m^{-2.35} \qquad 0.1 \leq m/M_{\odot} < 100 \tag{5.2}$$

- **Chabrier (2003) IMF**:

$$\varphi(m) \propto \begin{cases} e^{-\frac{(Log(m)-Log(0.079))^2}{2(0.69)^2}} & 0.1 \leq m/M_{\odot} < 1 \\ m^{-2.2} & 1 \leq m/M_{\odot} \leq 100 \end{cases} \tag{5.3}$$

- **Arimoto & Yoshii (1987) IMF**:

$$\varphi(m) \propto m^{-1.95} \qquad 0.1 \leq m/M_{\odot} < 100 \tag{5.4}$$

The specific IMFs we assumed for galaxy models of various masses in the two sets are reported in table 5.2. The results obtained with the IMF varying

Table 5.2: Parameters used to create the sets of models described in Section 5.3. The effective radius R_{eff}, the star formation efficiency ν and the infall timescale τ (columns 3, 4 and 5, respectively) are the same as used in Models 01a, but the assumed IMF (column 7) varies for different values of the initial infall mass M_{inf} (column 2). Column 6 reports the time of the onset of the galactic wind in the model galaxies calculated by the code.

Model	M_{inf}/M_{Sun}	$R_{eff}\,(kpc)$	$\nu\,(Gyr^{-1})$	$\tau\,(Gyr)$	$t_{GW}\,(Gyr)$	IMF
	5×10^9	0.44	2.61	0.50	1.59	Scalo
	1×10^{10}	1.00	3.00	0.50	1.37	Scalo
	5×10^{10}	1.90	6.11	0.46	0.92	Salp
02a	1×10^{11}	3.00	10.00	0.40	0.56	Salp
	5×10^{11}	6.11	15.33	0.31	0.52	Chabrier
	1×10^{12}	10.00	22.00	0.20	0.41	Chabrier
	5×10^9	0.44	2.61	0.50	1.59	Salp
	1×10^{10}	1.00	3.00	0.50	1.37	Salp
	5×10^{10}	1.90	6.11	0.46	0.92	Salp
02b	1×10^{11}	3.00	10.00	0.40	0.56	Salp
	5×10^{11}	6.11	15.33	0.31	0.51	AY
	1×10^{12}	10.00	22.00	0.20	0.41	AY

from the Scalo (1986) to the Chabrier (2003) form has greatly improved the agreement between model predictions and data.
In particular, Model 02a provided the best results, being able to simultaneously reproduce the observed trends for all the considered quantities. On the other hand, Model 02b, which contains the same IMF variation adopted in Matteucci (1994), has provided overestimated values for all the chemical properties in high mass galaxies, which can be attributed to the excessive numbers of massive stars produced by assuming the Arimoto and Yoshii (1987) IMF.
Figure 5.2 shows how, in this case, the slope of the $[Fe/H]$-mass relationship predicted by our models is steeper than the one derived from equation 4.1 for the data; in spite of this, the top-heavier IMF, and therefore the larger number of produced massive stars, leads to an increased production of α-elements, thus yielding a positive trend of the $[\alpha/Fe]$ ratio with mass.

5.4 IGIMF

As a last step, we decided to test the effect of the Integrated Galactic IMF (IGIMF - see Kroupa and Weidner, 2003; Weidner and Kroupa, 2005; Recchi et al., 2009, 2014; Weidner et al., 2010; Vincenzo et al., 2015) on the predicted abundance patterns.

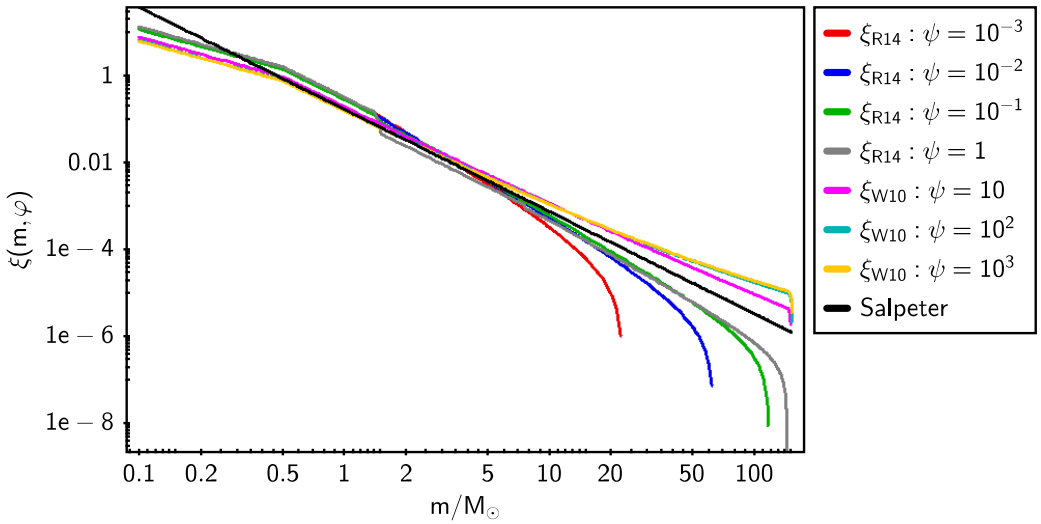

Figure 5.4: Comparison between the IGIMF for different SFRs ($M_\odot\, yr^{-1}$) and a canonical Salpeter IMF.

The IGIMF theory is based on the idea that star formation is expected to take place mostly in embedded clusters, namely the place of a correlated star formation event, where interstellar gaseous matter gets converted into stars following a gravitationally-driven collective process on a spatial scale of about 1 pc and within about 1 Myr (Lada and Lada, 2003; Kroupa et al., 2013; Yan et al., 2017).
Within each cluster, masses of new-born stars are indeed distributed following a canonical IMF $\varphi(m) \propto m^{-\alpha}$, while young embedded star clusters themselves are assumed to follow a mass function (embedded cluster mass function; ECMF).
The ECMF has been found to be (Zhang and Fall, 1999; Hunter et al., 2003; Lada and Lada, 2003; Recchi et al., 2009) a simple power-law:

$$\xi_{ecl} \propto M_{ecl}^{-\beta} \tag{5.5}$$

where M_{ecl} is the mass of all the stars formed in the embedded cluster, and the index β generally assumes values ≈ 2.
This influences the resulting stellar IMF due to two concurring main factors:

1. the upper mass limit of the ECMF, i.e. the most massive star forming embedded cluster, has been found to depend on the SFR of the galaxy, in the sense that it increases in more star-forming environments (Weidner and Kroupa, 2004; Bastian, 2008; Weidner et al., 2011);

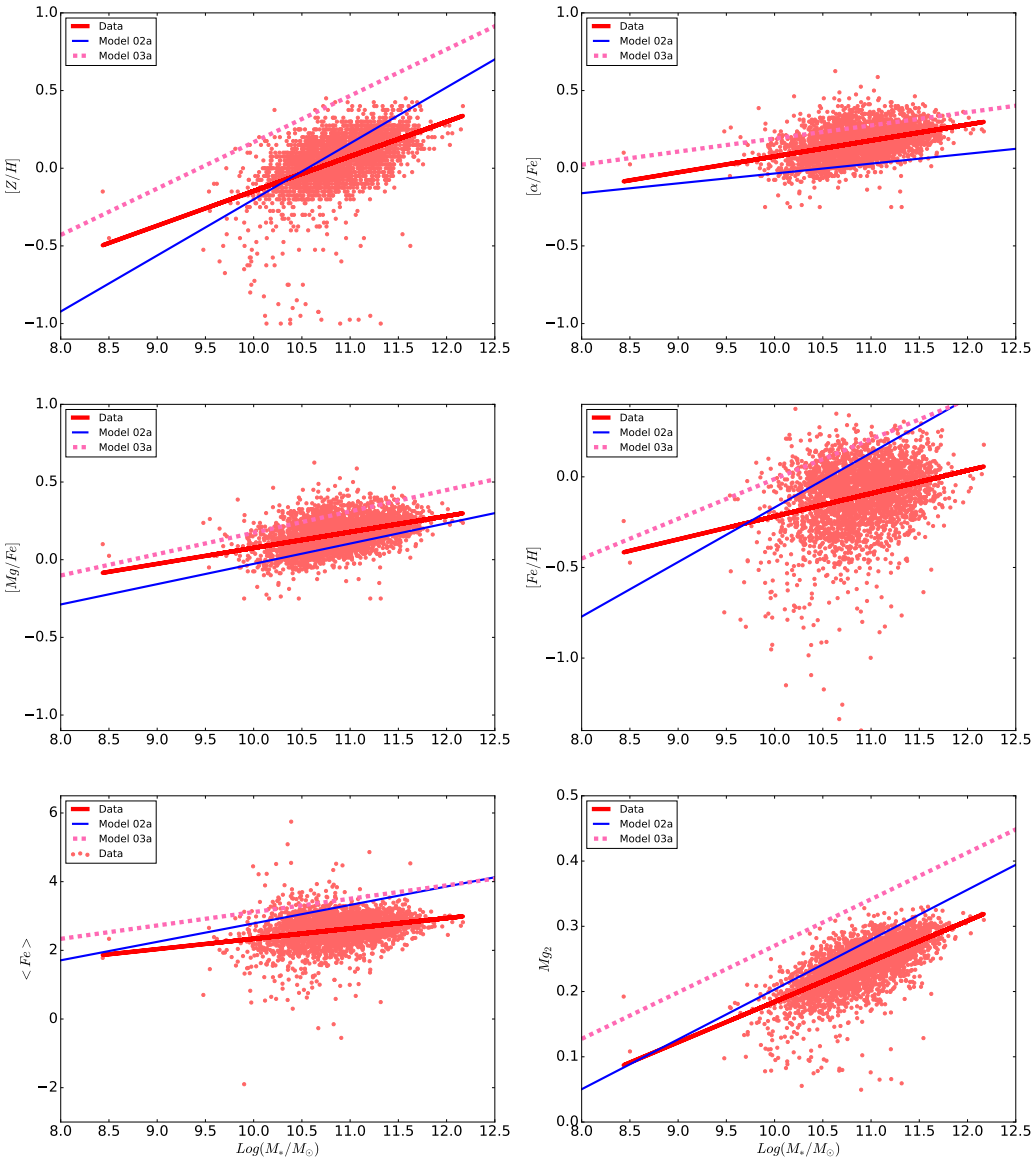

Figure 5.5: Comparison between the observed abundance patterns and the ones derived from Models 02a and Model 03a, which assumes an IGIMF. The red dots represent galaxies in the catalog, while the lines indicate the linear fit to data (thick solid line) and to Models 02a (thin solid line) and 03a (thick dashed line) respectively.

Table 5.3: Parameters used to create the sets of models described in Section 5.4. The effective radius R_{eff}, the star formation efficiency ν and the infall timescale τ (columns 3, 4 and 5, 3 respectively) are the same as used in Models 01a and 02a, but we are assuming an IGIMF. Column 6 reports the time of the onset of the galactic wind in the model galaxies calculated by the model.

Model	M_{inf}/M_{Sun}	$R_{eff}\,(kpc)$	$\nu\,(Gyr^{-1})$	$\tau\,(Gyr)$	$t_{GW}\,(Gyr)$	IMF
	5×10^9	0.44	2.61	0.50	1.60	IGIMF
	1×10^{10}	1.00	3.00	0.50	1.43	IGIMF
	5×10^{10}	1.90	6.11	0.46	0.96	IGIMF
03a	1×10^{11}	3.00	10.00	0.40	0.53	IGIMF
	5×10^{11}	6.11	15.33	0.31	0.55	IGIMF
	1×10^{12}	10.00	22.00	0.20	0.44	IGIMF

2. the maximum stellar mass which can be formed within each embedded star cluster increases with the mass of the cluster itself (Weidner et al., 2010, 2011).

Therefore, more massive clusters are formed in galaxies with higher SFRs, and within these clusters stars with larger masses are produced.

The resulting IGIMF is then obtained by considering all the IMFs in all of the embedded clusters, i.e. it is defined as (Weidner et al., 2011; Vincenzo et al., 2015):

$$\begin{aligned} &\xi_{IGIMF}(m,t) \equiv \\ &\equiv \int_{M_{ecl}^{min}}^{M_{ecl}^{max}(\psi(t))} \varphi(m < m_{max}(M_{ecl}))\, \xi_{ecl}(M_{ecl})\, dM_{ecl} \end{aligned} \tag{5.6}$$

The IGIMF is usually normalized based on the total mass forming during a considered time interval, generally $\delta t \approx 10 Myr$ (Weidner and Kroupa, 2005; Weidner et al., 2011); in our case, on the other hand, we do not follow this approach, but require the IGIMF to be normalized according to (Vincenzo et al., 2015):

$$\int_{m_{min}}^{m_{max}} dm\, m\, \xi_{IGIMF}(m) = 1 \tag{5.7}$$

The IGIMF theory has been applied, with different prescriptions, both to systems with low star formation rates, like dwarf galaxies (Vincenzo et al., 2015), and to starbursts (Weidner et al., 2011); to account for the variation of the SFR, going from low values in the first time steps up to higher values throughout the evolution of the galaxies in our models, we decided to combine the two prescriptions.

In particular:

- in the low star formation regime ($\lesssim 10\, M_{Sun}/yr$), we have followed the approach by Recchi et al. (2009); in this case, the maximum mass limit of the embedded clusters is given by:

$$Log(M_{ecl}^{max}) = 4.83 + 0.75\, Log\,(\psi(t)) \tag{5.8}$$

and the stellar IMF within each cluster is a two slope power law:

$$\varphi(m) = \begin{cases} A\, m^{-\alpha_1} & 0.08 \leq m/M_{Sun} \leq 0.5 \\ B\, m^{-\alpha_2} & 0.5 \leq m/M_{Sun} \leq m_{max} \end{cases} \tag{5.9}$$

where $\alpha_1 = 1.30$ and $\alpha_2 = 2.35$ (in the formulation by Recchi et al., 2014, α_2 depends on the [Fe/H] abundance as well, but this is neglected in Weidner and Kroupa, 2005)

- when the systems reached higher SFR values, we referred to the Weidner et al. (2011) formulation. In this case, the dependence of the maximum cluster mass on the SFR is given by:

$$M_{ecl}^{max} = 8.5 \times 10^4\, (\psi(t))^{0.75} \tag{5.10}$$

while the assumed stellar IMF is

$$\varphi(m) = k \begin{cases} \left(\frac{m}{m_H}\right)^{-\alpha_0} \\ \left(\frac{m}{m_H}\right)^{-\alpha_1} \\ \left(\frac{m_0}{m_H}\right)^{-\alpha_1} \left(\frac{m}{m_1}\right)^{-\alpha_2} \\ \left(\frac{m_0}{m_H}\right)^{-\alpha_1} \left(\frac{m_1}{m_0}\right)^{-\alpha_2} \left(\frac{m}{m_1}\right)^{-\alpha_3} \end{cases} \tag{5.11}$$

with

$$\begin{aligned} \alpha_0 &= 0.30 \qquad 0.01 \leq m/M_\odot \leq 0.08 \\ \alpha_1 &= 1.30 \qquad 0.08 \leq m/M_\odot \leq 0.50 \\ \alpha_2 &= 2.35 \qquad 0.50 \leq m/M_\odot \leq 1.00 \end{aligned}$$

and, for $1.00 \leq m/M_\odot \leq m_{max}$

$$\alpha_3 = \begin{cases} 2.35 & M_{ecl} < 2 \times 10^5\, M_\odot \\ -1.67 \times Log\left(\frac{M_{ecl}}{10^6\, M_\odot}\right) & M_{ecl} > 2 \times 10^5\, M_\odot \\ 1 & M_{ecl} > 1 \times 10^6\, M_\odot \end{cases}$$

Figure 5.4 shows the IGIMF resulting from the combination of the two prescriptions for different values of the SFR, compared to a canonical Salpeter IMF.
The adopted parameters are summarized in Table 5.3, and Figure 5.5 shows the comparison between the results obtained with the IGIMF and the ones provided by Model 02a, which so far proved to be the best one.
Consistently with what we observed with the increasingly top-heavy IMF we presented in the previous section, the inclusion of the IGIMF had the effect of steepening the trends with mass produced by our models; as a matter of fact, the Models 03 were the ones with the best fitting slopes. On the other hand, however, the chemical abundances predicted by all of these models were always higher, to some extent, than what observed in the data, which is particularly noticeable when comparing the total metallicity $[Z/H]$ and the Mg_2 spectral index (as for the latter, it is worth stressing that, as for all spectral indices measurements, its value is greatly influenced by the assumed calibration relation).
Table 5.4 summarizes the linear fit coefficients obtained for data and all the models presented in the work.

Table 5.4: Coefficients of the linear fits ($y = mx + q$) for data and all the models.

	[Z/H]		$[\alpha/Fe]$		$[Mg/Fe]$		$< Fe >$		Mg_2	
	m	q	m	q	m	q	m	q	m	q
Data	0,223	-2,377	0,103	-0,95	0,103	-0,950	0,301	-0,671	0,062	-0,436
Model01a	0,032	-0,248	0,061	0,688	0,036	-0,282	0,155	1,537	0,023	0,020
Model01b	0,039	-0,332	-0,107	1,215	0,003	0,074	0,227	0,722	0,024	0,001
Model01c	0,157	-1,660	-0,057	0,739	0,063	-0,509	0,357	-0,849	0,050	-0,293
Model02a	0,361	-3,808	0,064	-0,669	0,131	-1,333	0,537	-2,588	0,076	-0,561
Model02b	0,537	-5,573	0,157	-1,600	0,193	-1,954	0,689	-4,110	0,110	-0,895
Model03a	0,299	-2,819	0,084	-0,652	0,138	-1,202	0,389	-0,781	0,071	-0,443

Chapter 6

The "bimodal" IMF, and the time-dependent scenario

6.1 Introduction

In the work presented in the previous Chapter, we analyzed the chemical properties of elliptical galaxies in the MOSES catalog (see Sec. 4.1) by using a modified version of the chemical evolution code by Pipino and Matteucci (2004).
To do so, we generated sets of model galaxies by manually fine-tuning the values of the various initial parameters of the model (star formation efficiency, infall time scale, effective radius and IMF) for different values of the mass, which yielded constraints on the formation and evolution of elliptical galaxies.
In accordance to the "inverse wind scenario" (Matteucci, 1994), we found that the best fitting models were those with higher star formation efficiency, larger effective radius and shorter infall time scale in more massive galaxies. Moreover, at variance with what was concluded in Pipino and Matteucci (2004), we observed the necessity for a variation in the IMF as well, becoming top-heavier in more massive galaxies, in order to reproduce the observed $[\alpha/Fe]$ VS mass trend.
As we will further discuss in Chapter 7, we identified the reasons for this discrepancy - aside from the obvious consideration of using different data - in the operational definition of the quantities in play. In the dataset we used, the $[\alpha/Fe]$ ratio is related to the difference between the total metallicity $[Z/H]$ and the Fe abundance $[Fe/H]$. In order to be consistent, and to account for possible differences in the elements included in the α-mixture between us and the authors of the catalog, we derived for our models a value

of the $[\alpha/Fe]$ ratio obtained following the same relation assumed to hold in the dataset, and compared it to the data. This quantity, although being consistent with observations, does not well represent the actual $[\alpha/Fe]$ ratio, since it also includes in the mixture of a α-elements other elements, such as C and N, which have a different behavior. In Pipino and Matteucci (2004), on the other hand, the comparison with observations was made by using the $[Mg/Fe]$ ratio directly predicted from the code, which is representative of the "true" α-element behavior. As a matter of fact, in De Masi et al. (2018), when using the $[Mg/Fe]$ we obtain a better agreement with data (positive correlation with mass, although with a slightly flatter slope).

Following this work, we performed a further analysis, characterized by three main differences:

1. we adopted a new dataset for the comparison (see Sec. 4.2);

2. we followed a different approach in generating the models, with the aim of better exploring the available parameter space;

3. we extended our investigation to other parameterizations of the IMF; specifically, we tested the effect of a low-tapered ("bimodal") IMF (see Sec. 6.2);

6.2 Bimodal IMF

In this work, together with the forms for the IMF described in Sec. 5.2, 5.3 and 5.4, we tested a new parameterization, specifically a low-mass tapered ("bimodal") IMF, as defined in Vazdekis et al. (1997, 2003).
In this formulation, the IMF is defined as

$$\xi(m) = \beta \begin{cases} m_1^{-\mu} & 0.1 \quad < m/M_\odot < 0.2 \\ p(m) & 0.2 \quad < m/M_\odot < 0.6 \\ m^{-\mu} & 0.6 \quad < m/M_\odot < 100 \end{cases} \tag{6.1}$$

where $m_1 = 0.4$, and $p(m)$ is a third degree spline, i.e.

$$p(m) = (A + B\,m + C\,m^2 + D\,m^3) \tag{6.2}$$

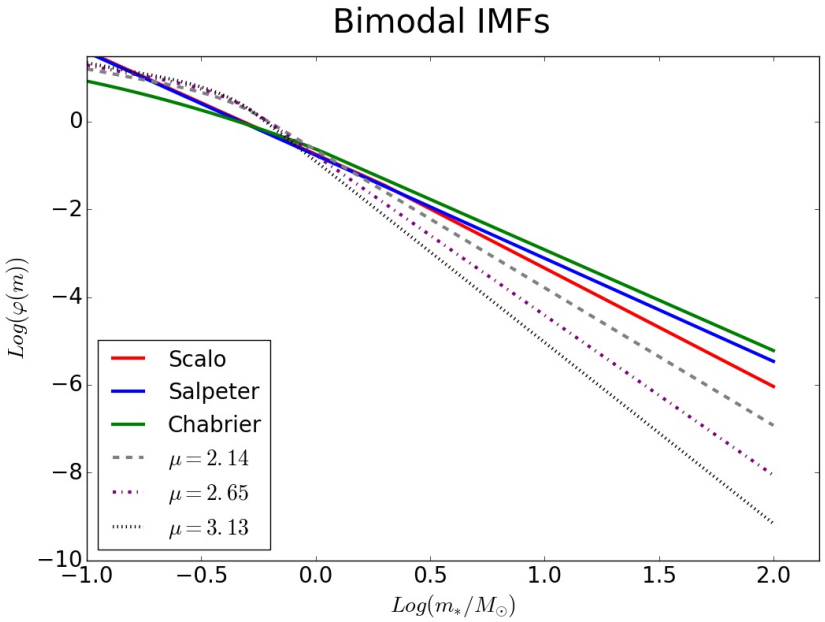

Figure 6.1: Comparison between bimodal IMF with different slope values μ, and the IMFs used in our previous work (i.e. Scalo, 1986, Salpeter, 1955, and Chabrier, 2003 IMF; see the inset panel).

whose normalization constants are determined by solving the following boundary conditions:

$$\begin{cases} p(0.2) = m_1^{-\mu} \\ p'(0.2) = 0 \\ p(0.6) = 0.6^{-\mu} \\ p'(0.6) = -\mu\ 0.6^{(-\mu-1)} \end{cases}$$

Notice that, defined this way, the bimodal IMF is completely characterized by the value of the slope μ.
For $\mu = 1.3$, the bimodal IMF closely matches a Kroupa (2001) distribution. For $\mu > 1.3$, this IMF becomes more and more bottom-heavy, while for $\mu < 1.3$ the IMF is top-heavy.
So, overall, in the remainder we use the following classifications for the models

- **Models 01:** same as in the previous Chapter, these Models have a constant Salpeter (1955) IMF;
- **Models 02:** variable IMF, as described in Sec. 5.3;
- **Models 03:** IGIMF, as in Sec. 5.4;

- **Models 04**: we obtained these models with the bimodal IMF, by assuming an increasing value for the slope μ (namely, a bottom heavier IMF) in more massive galaxies. Figure 6.1 compares the bimodal IMFs with those described in the previous Chapter (i.e. Models 01 and 02; see above);

- **Models 05**:
  In this final set of models, we tested an explicitly time dependent form for the bimodal IMF, as described in Weidner et al. (2013) and Ferreras et al. (2015), where the slope value μ changes from an initial value μ_1 to a final value μ_2 after a time interval t_{switch} (the IMF switches from top to bottom-heavy, so that by construction $\mu_2 > \mu_1$).

6.3 Models creation

As previously mentioned, in this work we modified the approach we followed to create the models, with respect to what previously described in Chapter 5.
Once we assumed one of the IMF parameterizations described above, we generated a number of model galaxies (far larger than what done in the previous Chapter) by varying all the initial parameters over a grid of values, and considering all their possible combinations. This allowed us to fully explore the available parameter space, and to avoid biases or mistakes deriving from the manual selection of the parameter values.
Table 6.1 details this process, by reporting the values of the parameters we used in the time-independent case (Models01 to 04). Table 6.2, only valid for Models05 (with the explicitly time-dependent bimodal IMF), differs from the previous one in that it also reports the values of the IMF slope before and after the switch (μ_1 and μ_2, respectively), together with the time when the switch itself takes place ($t_{\rm switch}$).
The results of this procedure are shown in Figures 6.2 to 6.7, where we plot the variation of the $[Fe/H]$ and $[Mg/Fe]$ abundance ratios with stellar mass, as calculated by the chemical evolution code for all model galaxies. For each ratio, we provide various versions of the same plot, color-coded to show the dependency on the other various parameters as follows:

- for Models 01 to 04, we show the dependency on:
  - the star formation efficiency ν, defined as in equation 3.2 as the proportionality constant between the SFR and the gas density;

Table 6.1: Possible values of the initial parameters used to generate the model galaxies in the time-independent cases (Models 01-04). For each choice of the IMF, we generated model galaxies using all the possible combinations of values reported in this table.

Parameter	Value
Infall mass ($M_\odot$)	5×10^9, 9×10^9, 1.62×10^{10}, 2.92×10^{10}, 5.25×10^{10}, 9.45×10^{10}, 1.70×10^{11}, 3.06×10^{11}, 5.51×10^{11}, 9.92×10^{11}, 1.79×10^{12}
Effective radius (kpc)	1, 2, 3, 4, 5, 6, 7, 8, 9, 10
Star formation efficiency ν (Gyr^{-1})	5, 10, 15, 20, 25, 30, 35, 40, 45, 50
Infall time-scale τ (Gyr)	0.2, 0.3, 0.4, 0.5

Table 6.2: Possible values of the initial parameters used to generate the model galaxies in the time-dependent case (Model 05; see text). We generated model galaxies using all the possible combinations of values reported in this table.

Parameter	Value
Infall mass ($M_\odot$)	5×10^9, 1×10^{10}, 2×10^{10}, 4×10^{10}, 8×10^{10}, 1.6×10^{11}, 3.2×10^{11}, 6.4×10^{11}, 1.3×10^{12}
Effective radius (kpc)	1, 3, 5, 7, 9
Star formation efficiency ν (Gyr^{-1})	5, 10, 30, 50, 70, 100
Infall time-scale τ (Gyr)	0.2, 0.5
μ_1	$0.4, 0.7, 1.0, 1.3$
μ_2	$1.3, 1.6, 1.9, 2.3, 2.6, 2.9$
t_{switch} (Gyr)	0.1, 0.3, 0.5, 0.8, 1.0

  - the infall time scale τ, describing the time-scale of the initial infall, according to:

$$\left(\frac{dG_i(t)}{dt}\right)_{infall} = X_{i,infall}\, C\, e^{-t/\tau}$$

    where the term on the LHS of the equation is the abundance variation of the i-th element in the gas due to infall alone, $X_{i,infall}$ is the abundance of the i-th element in the infalling gas and C is a normalization constant;
  - the effective radius R_{eff} achieved after the collapse is over.

- for Model 05, we produced additional plots (Fig 6.7), showing the dependency of the $[Fe/H]$-mass and $[Mg/Fe]$-mass relations on three additional parameters:
  - μ_1 and μ_2, i.e. the value of the bimodal IMF slope before and after the switch, respectively;
  - $t_{\rm switch}$, i.e. the time when the switch from the bottom to the top-heavy form of the bimodal IMF occurs.

A look at Figures 6.2 - 6.6 shows that the $[Mg/Fe]$ ratio in galaxies of the same stellar mass are higher in models with increasing ν, where the larger thermal energy output by stellar winds and SNe into the ISM results in an earlier onset of a galactic wind, resulting in the faster quenching of star formation by driving the gas away from the galaxy.
The effect of decreasing the infall time scale τ, which is similar to increasing ν and R_{eff}, appears to be less significant.
The opposite result is obtained, as shown in Fig. 6.7, by increasing μ_1 (i.e., galaxies whose IMF was bottom-heavier before the switch), which results in galaxies having lower $[Mg/Fe]$ for a given mass, accordingly to theoretical expectations (no significant trend with μ_2 and $t_{\rm switch}$ is noticeable from the plot).

It should be stressed that the presented grids of models have been produced by simply considering all the possible combinations of the values for the initial input parameters of the code. As a result, some of these parameter configurations end up being physically less plausible, and some degeneracies in the model galaxies are present. In spite of this, here we chose to present the whole grids without any selection on the model galaxies, in order to highlight the response of our model to the change of parameters. A complete discussion will be presented in later sections, only considering models actually matching the data.

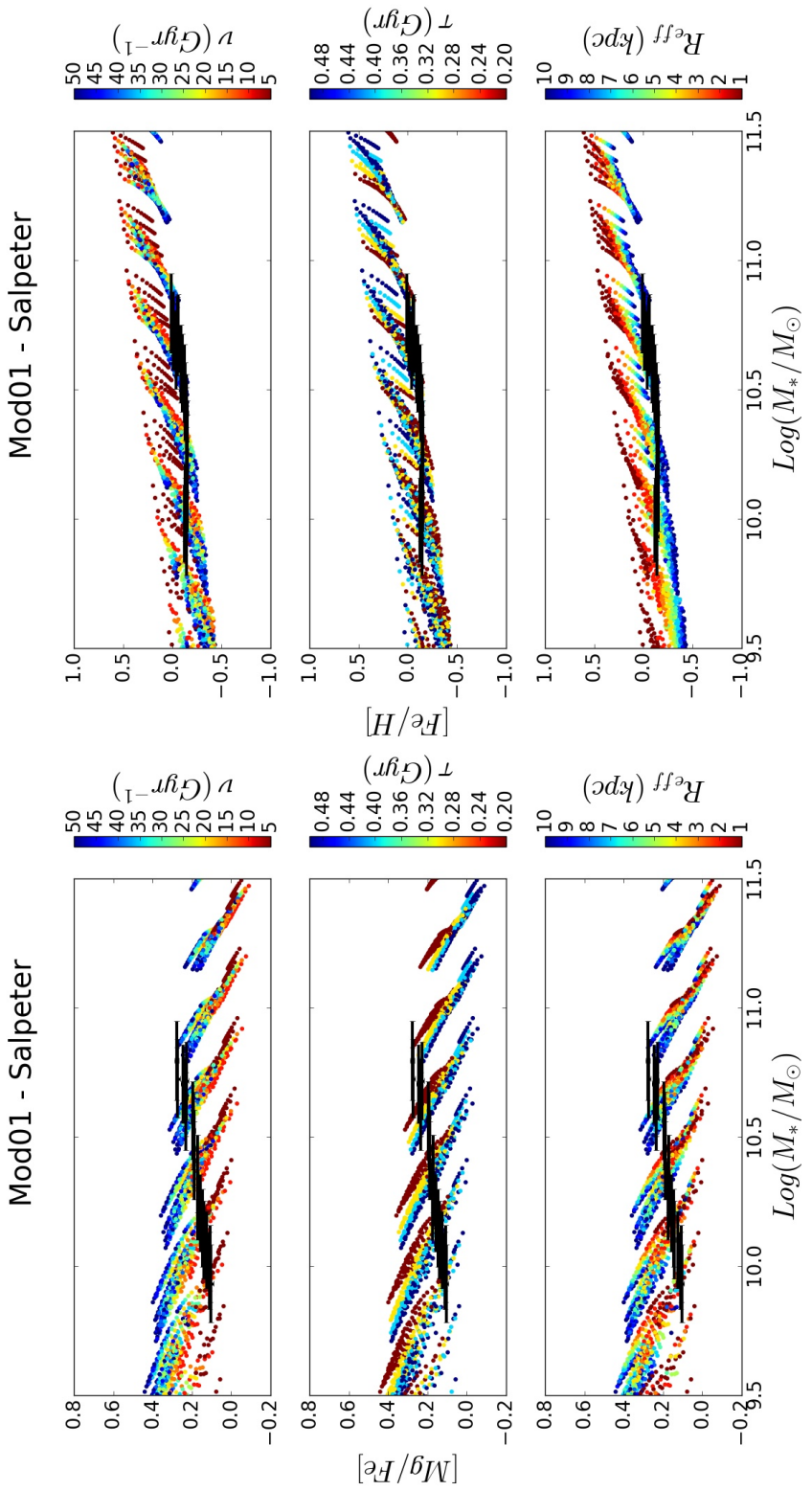

Figure 6.2: $[Fe/H]$ and $[Mg/Fe]$ ratios (top and bottom 3 panels, respectively) for 4400 model galaxies, obtained by varying the model initial parameters over the grid of values reported in table 6.1, and assuming a constant Salpeter IMF (Models 01). The black crosses represent abundances in the dataset, with the respective errors. The points show the variation of chemical abundances with total stellar mass, and are color coded to further show the dependance on the star formation efficiency ν (top panel of each group of three), infall time-scale τ (central panel) and effective radius R_{eff} (bottom panel).

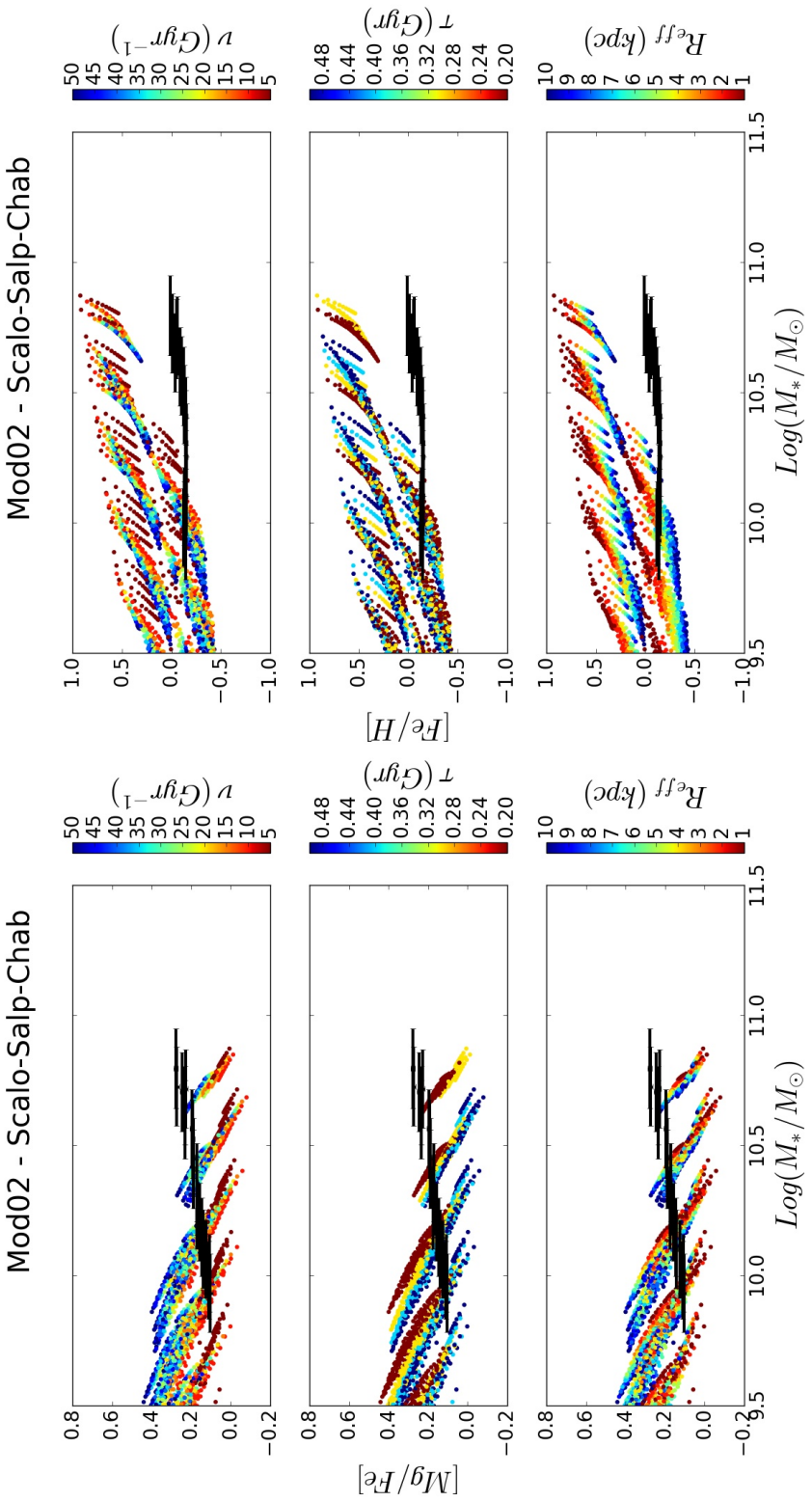

Figure 6.3: Same as figure 6.2, but for Model 02, where we assume an IMF that varies with galaxy mass, becoming top-heavier in more massive galaxies (see sec. 5.3).

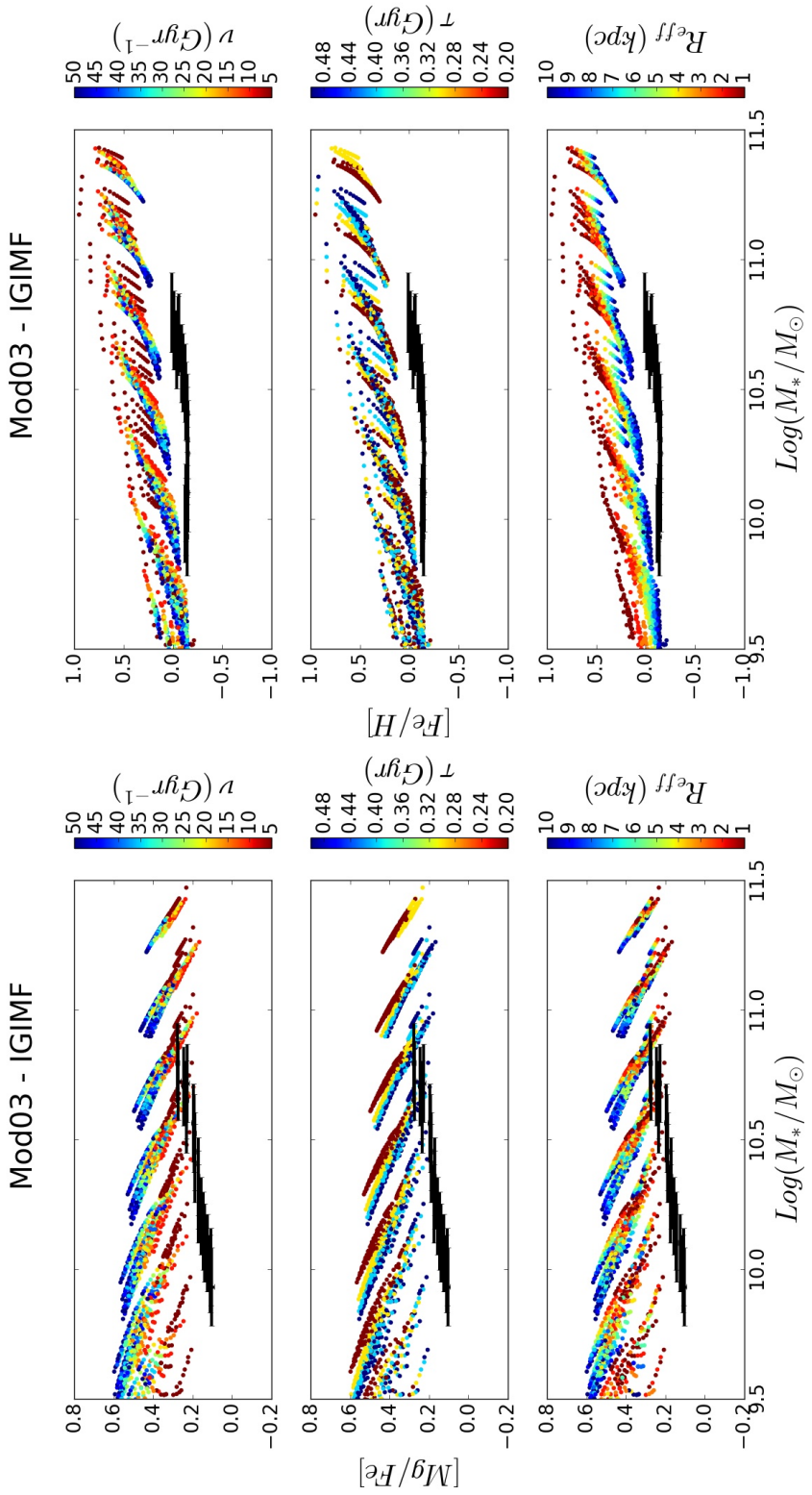

Figure 6.4: Same as figures 6.2 - 6.3, for Models 03 assuming an IGIMF, becoming top-heavier for higher SFR values in more massive galaxies (see sec. 5.4).

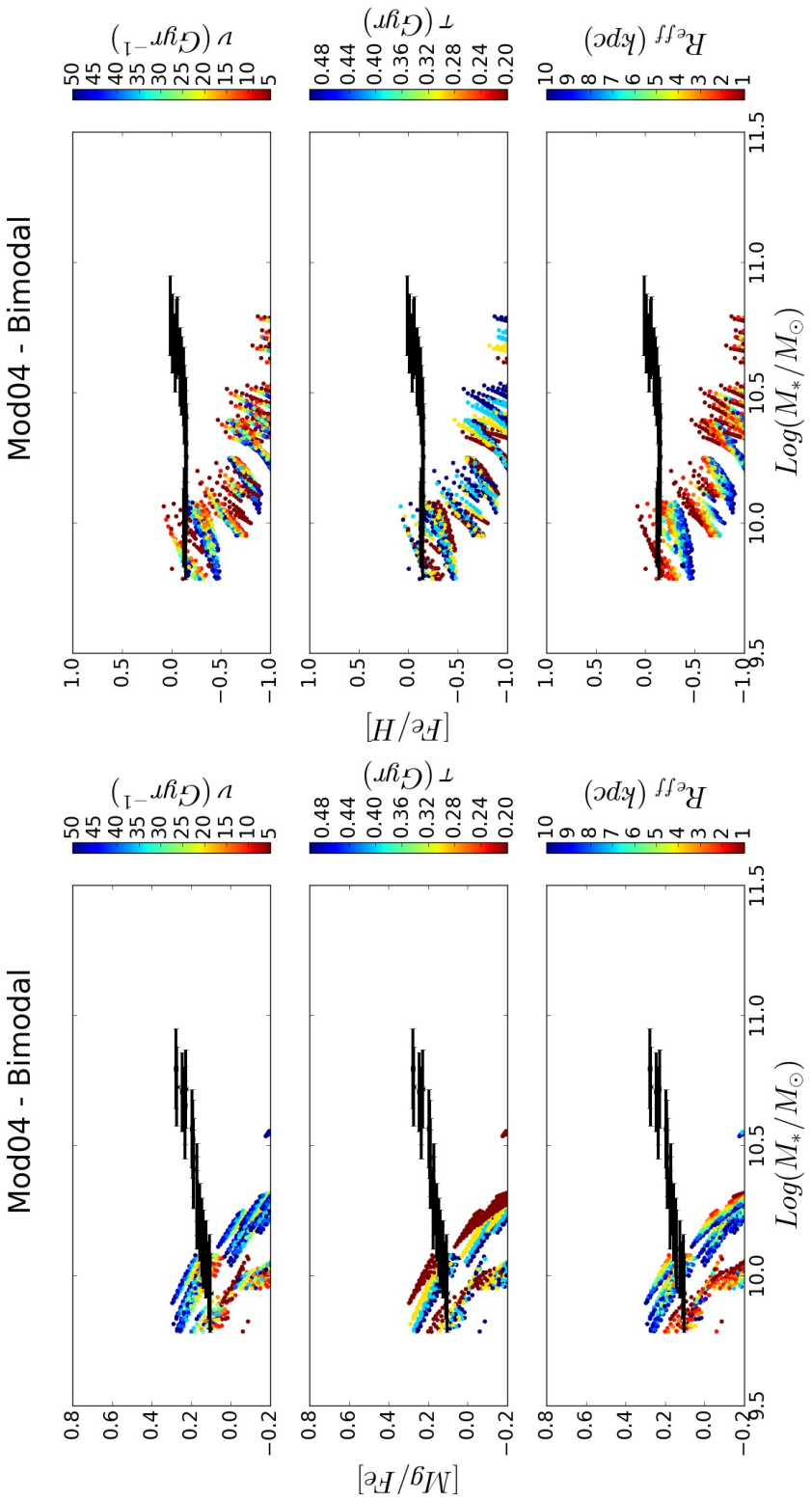

Figure 6.5: Same as figures 6.2 - 6.4 for Model 04, obtained by assuming a bimodal IMF, becoming bottom-heavier in more massive galaxies (see sec. 6.2).

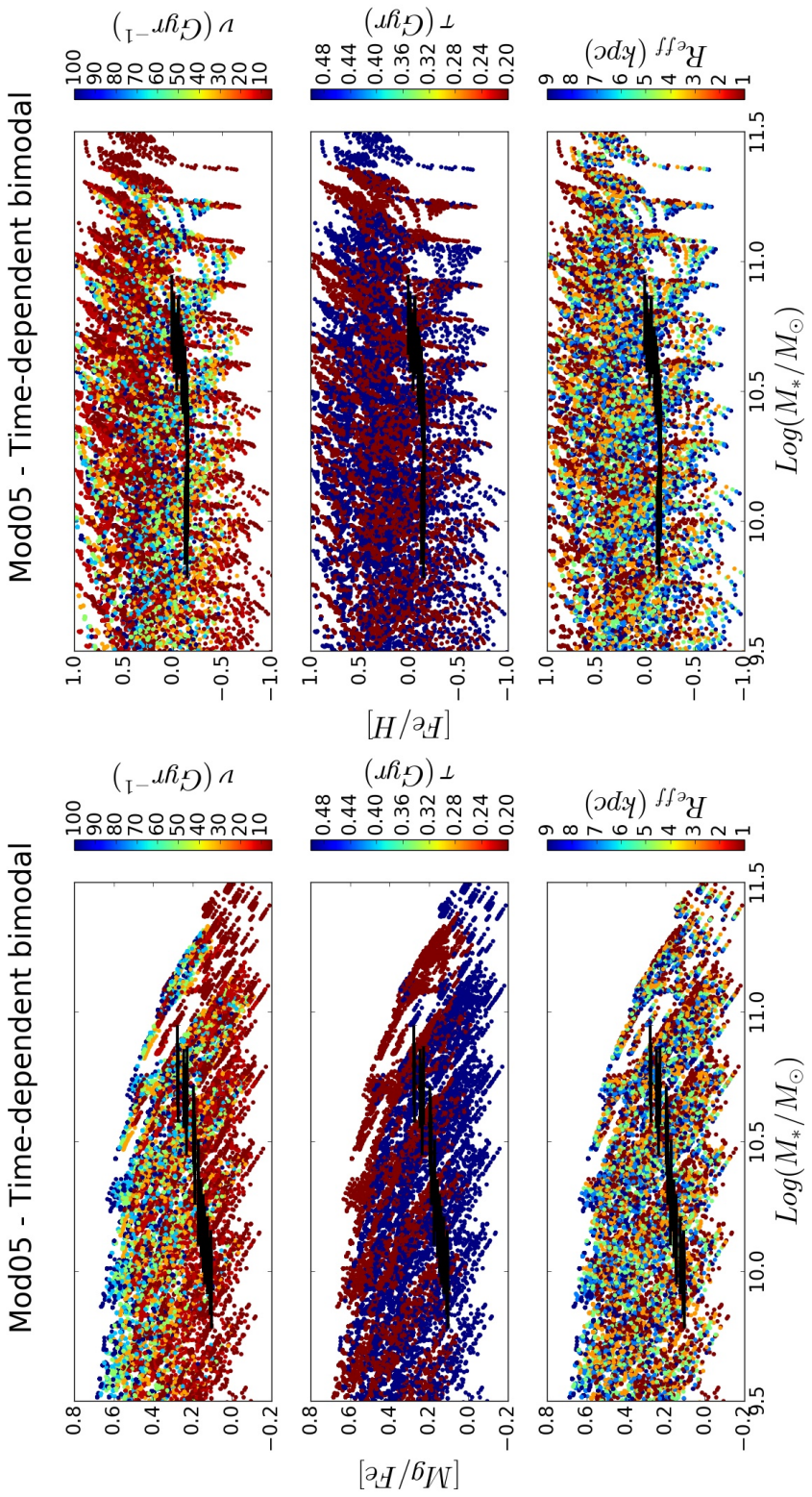

Figure 6.6: Same as figures 6.2 - 6.5, this time for models with an explicitly time-dependent bimodal IMF, switching from a bottom-heavy (slope μ_1) to a top-heavy (slope μ_2) form after a time $t_{\rm switch}$ (see sec. 6.2). Here, the color coding is analogous to the ones in previous pictures.

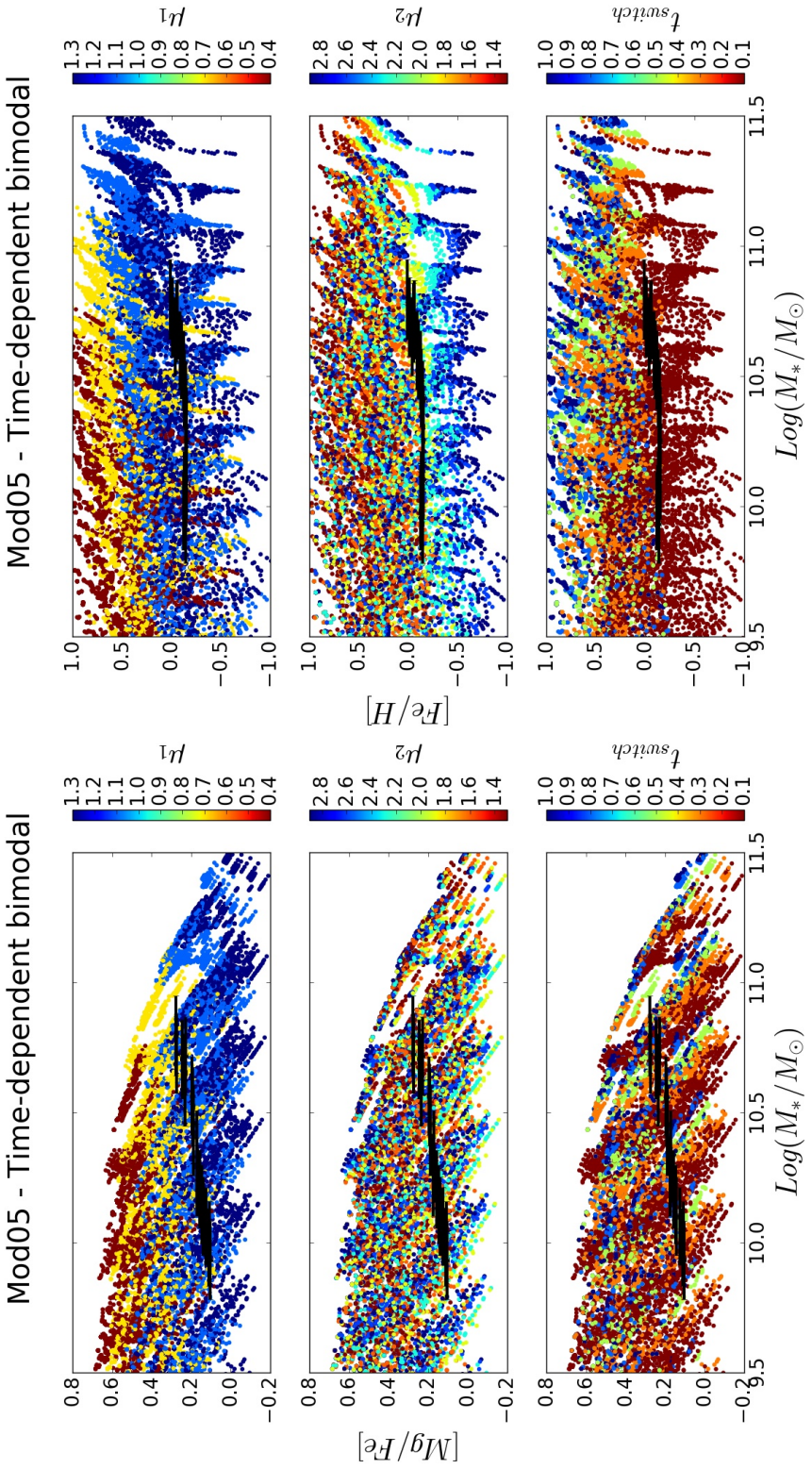

Figure 6.7: Same as figures 6.2 - 6.6, for models with an explicitly time-dependent bimodal IMF, switching from a bottom-heavy to a top-heavy form after a time $t_{\rm switch}$. In this case, plots are color coded to show the dependency on the slope values μ_1 and μ_2 (before and after the switch, respectively), and on the value of $t_{\rm switch}$

6.4 Results

In this section, we describe the results of the comparison between predictions from different models and observations.
Such a comparison has been performed by selecting, for every choice of the IMF, the model galaxies matching the observed mass-$[Fe/H]$ and mass-$[Mg/Fe]$ relations within the observational errors.

The results of the matching procedure are summarized in figures 6.8 to 6.13 and in table 6.3.
Specifically, in figures 6.8 and 6.9 the black crosses represent abundances in the dataset, with the respective errors. Galaxy models matching one of the analyzed relations (either the $[Fe/H]$-mass or the $[Mg/Fe]$-mass relation) are shown as gray points, while we highlight and color-code the models matching the two relations simultaneously; the color-coding shows the dependence of these matching models on the other free parameters (star formation efficiency ν, infall time-scale τ, effective radius R_{eff} for Models 01-04, and μ_1, μ_2 and t_{switch} for Model05).
For each IMF, the number of model galaxies matching the data is reported in table 6.3, for three different mass ranges and in total, for the $[Fe/H]$ ratio (columns 2-5), the $[Mg/Fe]$ ratio (columns 6-9) and for both these quantities simultaneously (columns 10-13).
In the lower mass bin, model galaxies matching the abundance ratios of the data can be produced by using any of all the considered IMFs aside from the IGIMF, for which the predicted abundances are always slightly too high (consistently with what observed in the previous Chapter). The number of matches, however, decreases in the other sets of Models, particularly when considering the $[Fe/H]$ ratio. The only Models where this does not happen are the ones with a Salpeter (Models 01) or time-dependent bimodal IMFs (Models 05); moreover, these are the only two choices for the IMF producing a significant number of matches for both the abundance ratios simultaneously. For this reason, we select from Models 01 and 05 the ones matching both $[Fe/H]$ and $[Mg/Fe]$, and analyze their properties.

The analysis of both the classes of Models confirms the downsizing scenario presented in Matteucci (1994) and Pipino and Matteucci (2004), as the best matching models are obtained by imposing a higher star formation efficiency in more massive galaxies (see Fig. 6.14 and 6.15).
It is significant to stress that, to generate the grid of models with the time-dependent bimodal IMF, we tested a range of values for the time $t_{\rm switch}$ when the switch from top to bottom-heavy form takes place. In spite of this, all the model galaxies reproducing the two abundance ratios simultaneously switch

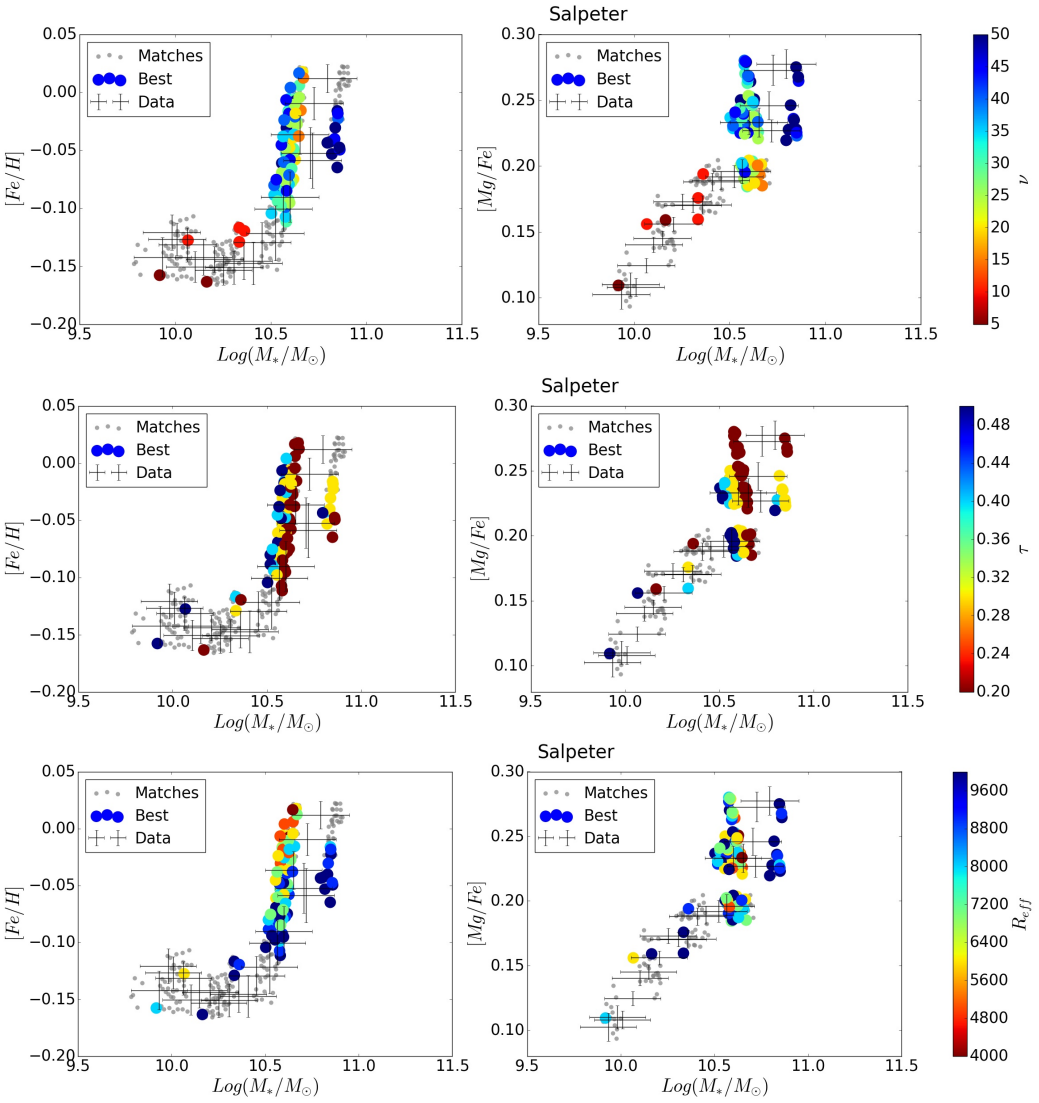

Figure 6.8: Comparison between data and Models01 for the $[Fe/H]$ and $[Mg/Fe]$ abundance ratios. The black crosses represent abundances in the dataset, with the respective errors. Models matching the $[Fe/H]$-mass and the $[Mg/Fe]$-mass relations simultaneously are color-coded according to their star formation efficiency ν (top row), infall time-scale τ (middle row) and effective radius R_{eff} (bottom row), while the ones matching only one of the two relations are shown with fading, smaller markers.

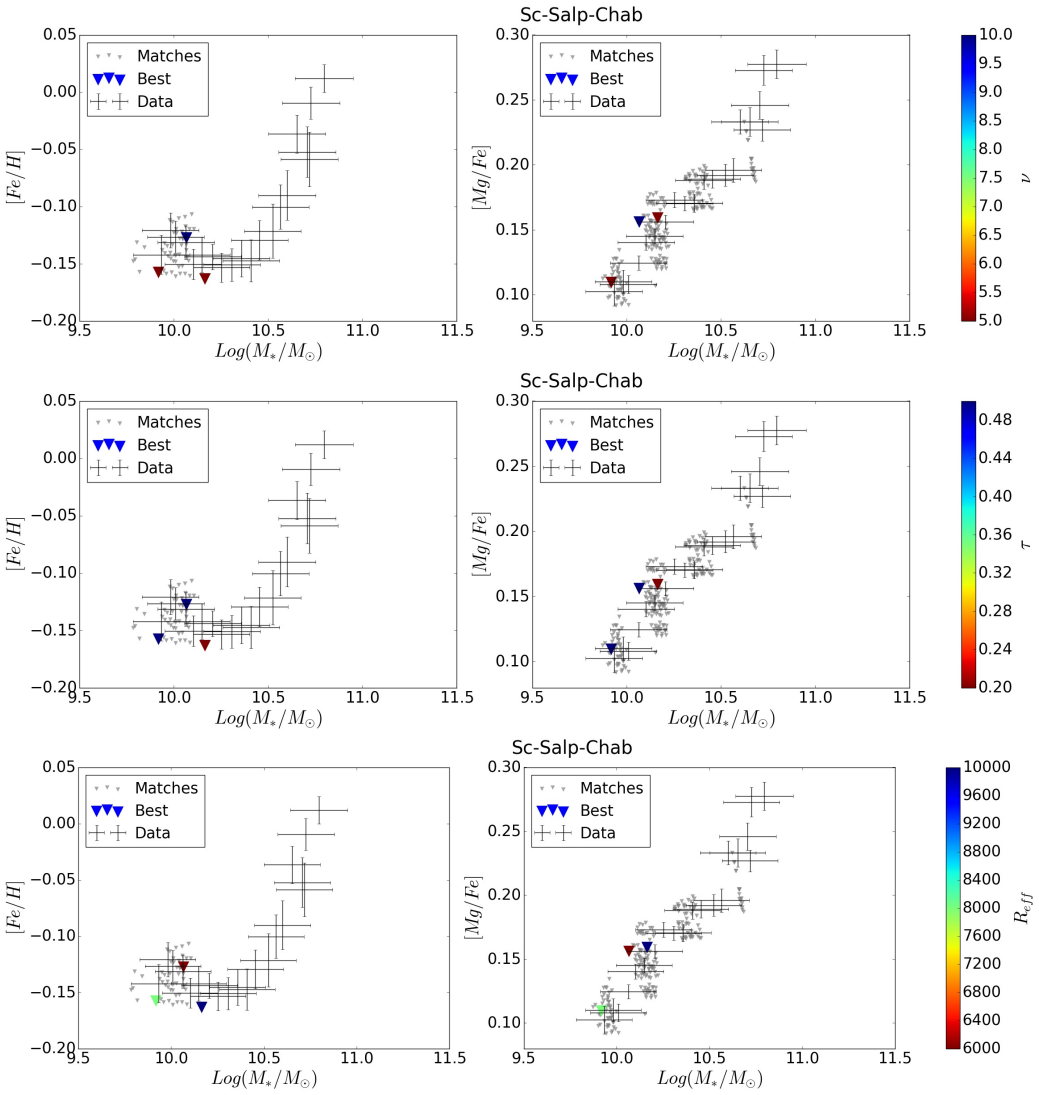

Figure 6.9: As Figure 6.8, but for Model02

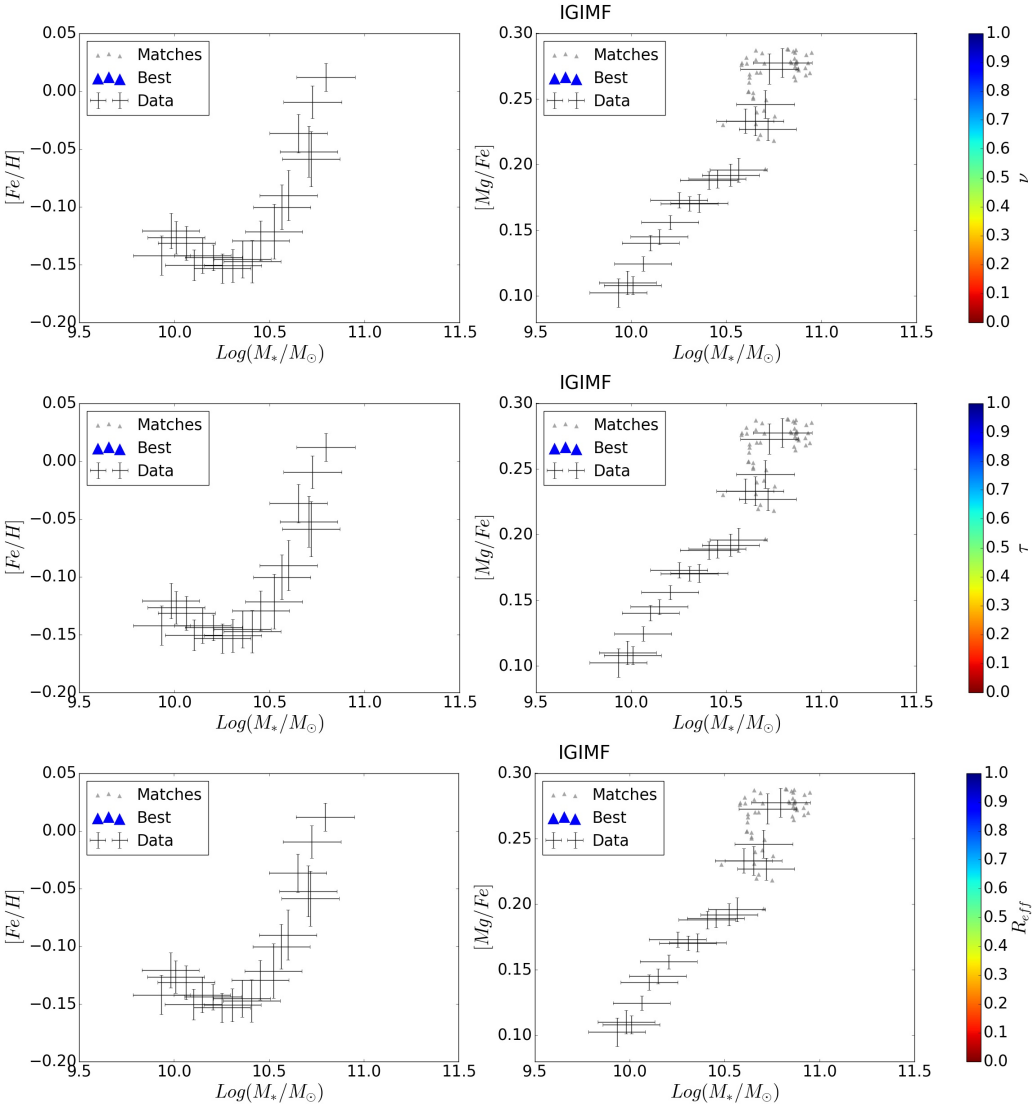

Figure 6.10: As Figures 6.8 and 6.9, but for Model02

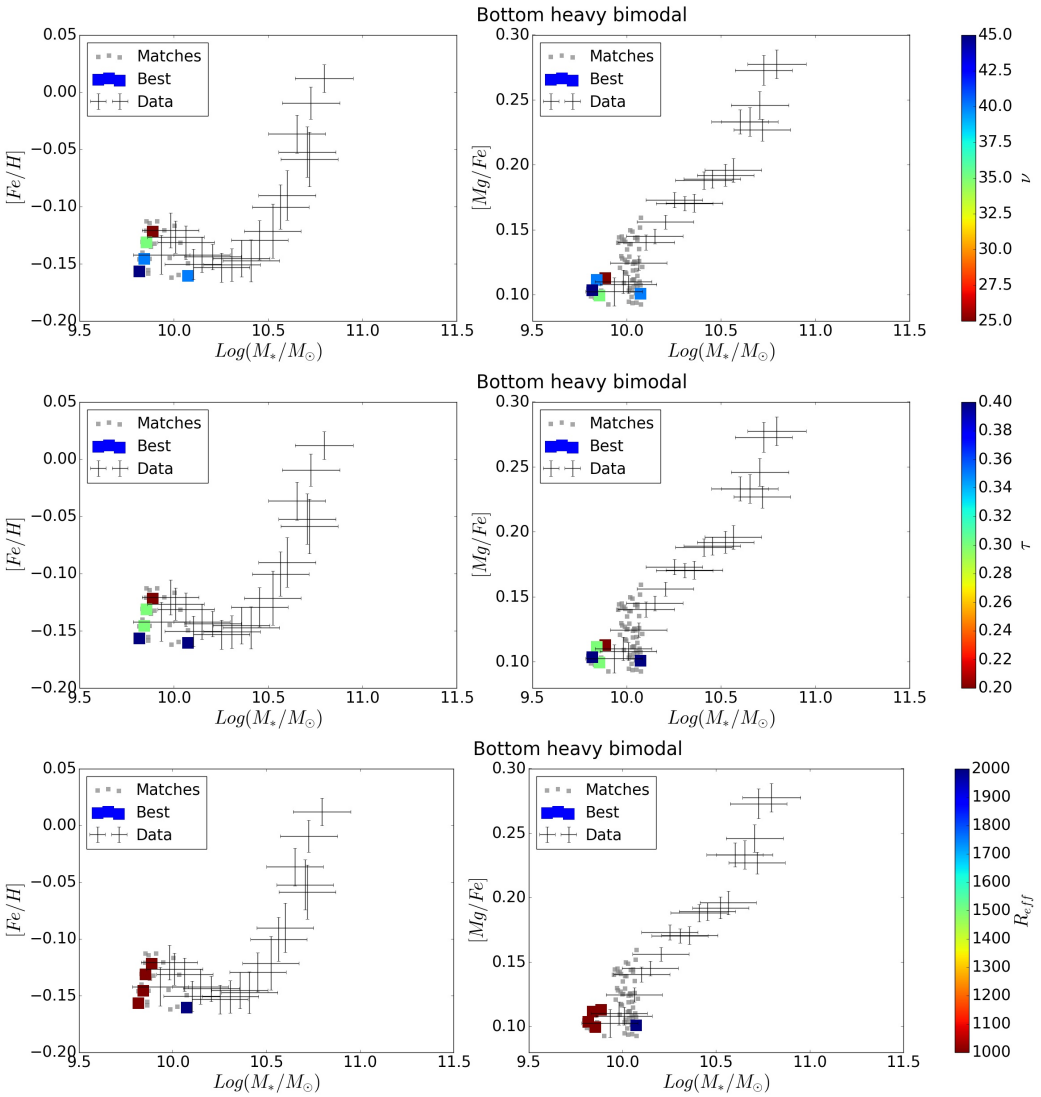

Figure 6.11: As Figures 6.8 - 6.10, but for Model04

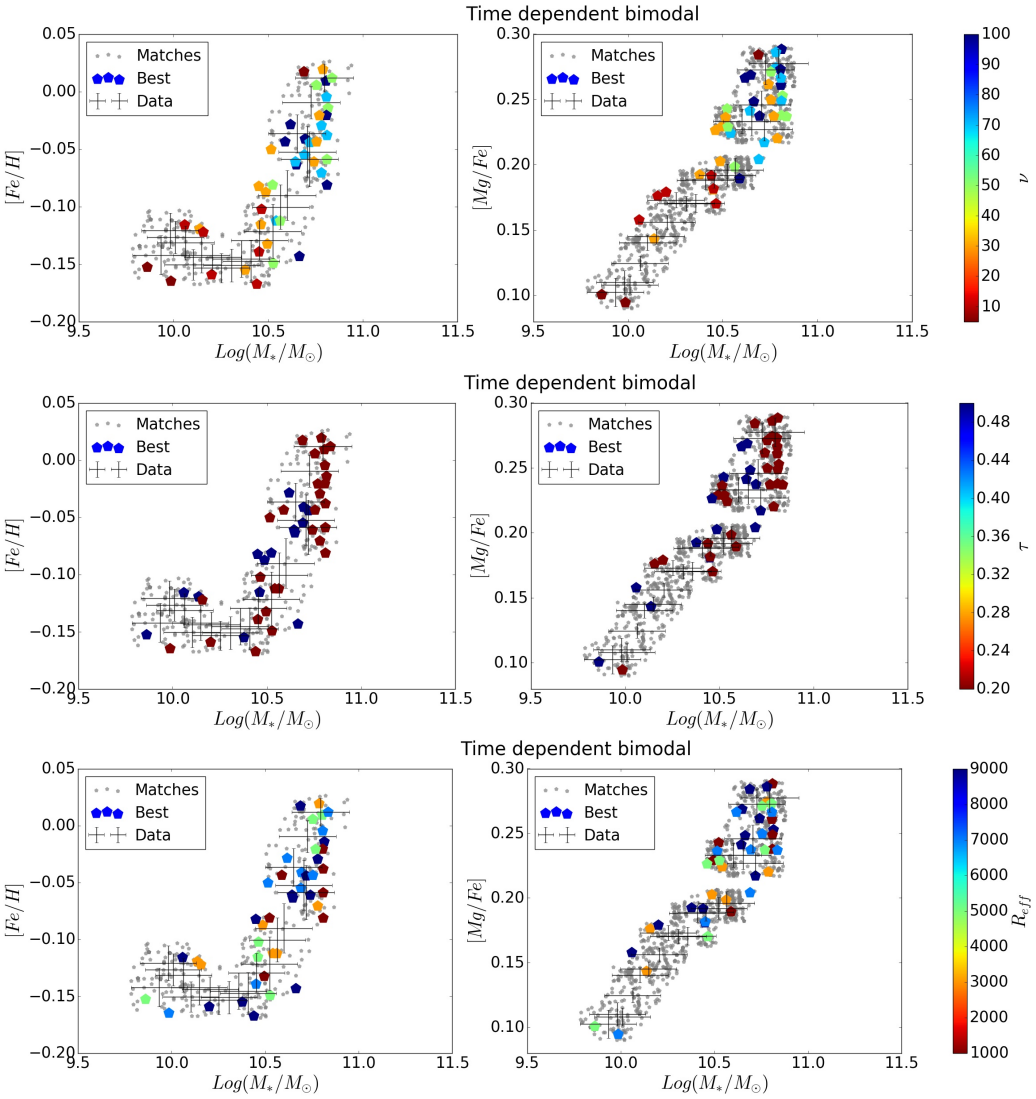

Figure 6.12: As Figures 6.8 - 6.11, but for Model05

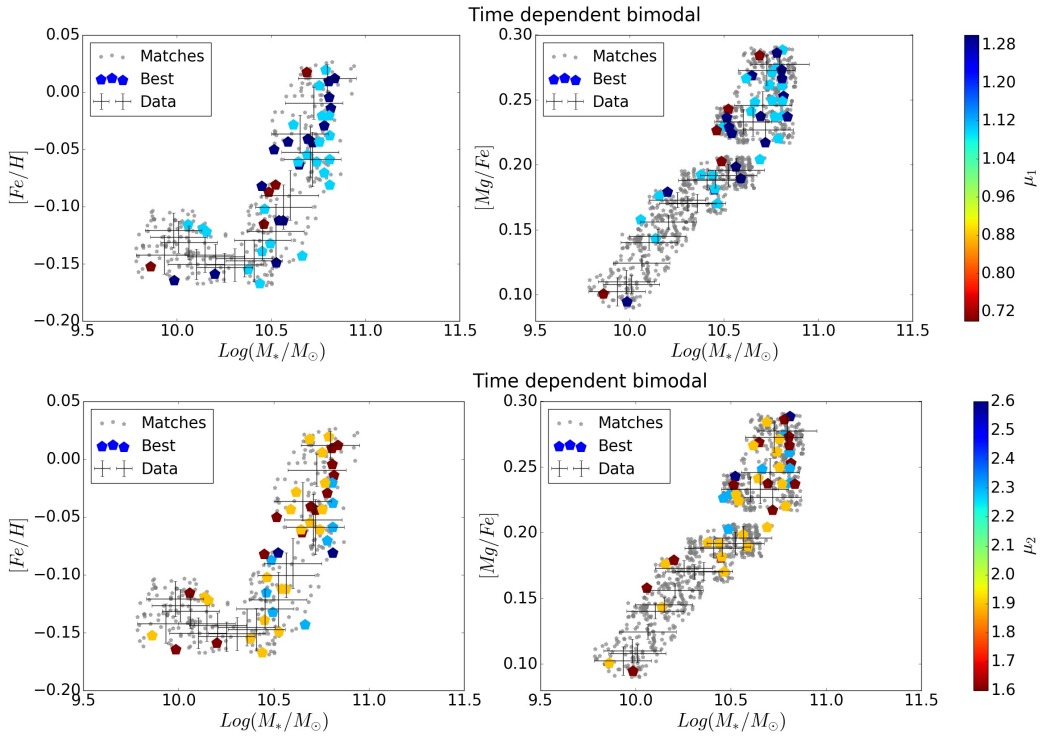

Figure 6.13: Comparison between data and Models05 for the $[Fe/H]$ and $[Mg/Fe]$ abundance ratios. Models matching the $[Fe/H]$-mass and the $[Mg/Fe]$-mass relations simultaneously are color-coded according to the slope of the bimodal IMF before (μ_1, top row) and after (μ_2, bottom row) the switch (all these models switch IMF at $t_{\rm switch} = 0.1$ Gyr). Models matching only one of the two relations are shown with fading, smaller markers.

slope at the same time; specifically, at $t_{switch} = 0.1$ Gyr, the lowest value we tested (for reference, Weidner et al. 2013 found the optimal time for the switch to be $t_{switch} \geq 0.3$ Gyr). In a standard ΛCDM scenario, this corresponds to a $z_{switch} \approx 8.33$. So, data trends are reproduced only if the passage between the two forms happens in the early stages of the chemical evolution. To make a comparison, in Fig. 6.16 (upper panel) we plot the distribution of the galactic wind onset time for the 20 best-matching Model05 galaxies. In all of them, the wind starts (and so star formation is quenched) some time after the slope switch in the IMF. The percentage of stellar mass created before the switch (so, under a top-heavy IMF regime) is always smaller than 50% (see Fig. 6.16, lower panel). The values of the slope before and after the switch present a weak positive trend with mass, as can be seen in Fig. 6.17. For the low-mass best matching models, the values of μ_1 and μ_2 are in the range from 1 to 2, i.e. not so different from the Kroupa-like slope (1.3). For more massive galaxies this range is wider, with the slope before the switch μ_1 becoming as low as 0.5 (top-heavier), while the slope after the switch μ_2 gets as high as 2.6 (bottom-heavier).

6.5 M/L ratios

We find two classes of models providing a good match to the observed stacked spectra:

1. Models with a constant, Salpeter (1955) IMF;
2. Models with the bimodal IMF by Vazdekis et al. (1997, 2003), with a slope switching from an initial μ_1 value (top-heavy) to a different one (bottom heavy) after a time $t_{\rm switch} = 0.1\,{\rm Gyr}$.

As stressed throughout this Thesis, the IMF has a powerful effect on the properties of a galaxy, especially on its M/L ratio, by determining the ratio between low and high-mass stars.
To place a further constraint on these two best-fitting sets of models, we examined their M/L ratios by combining luminosities derived from the population synthesis model by Vincenzo et al. (2016) with the stellar masses provided by our chemical evolution code.

The resulting $(M/L)_B$ ratios span between $11.4 - 13.5$ for Model01 (Salpeter IMF), and assume the values $7.8 - 12.9$ for Model05 (time-dependent form of the bimodal IMF) depending on the total stellar mass.
These ratios turn out to be slightly higher than modern M/L ratios estimates. For comparison, La Barbera et al. (2016) showed the stellar r-band

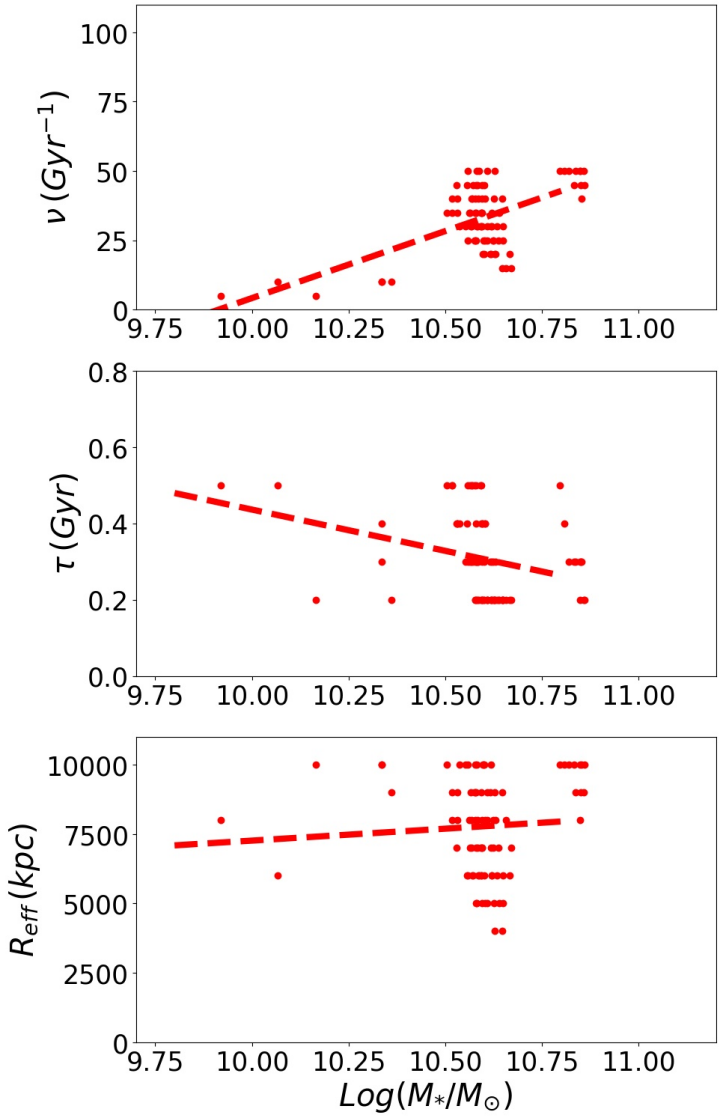

Figure 6.14: Variation with stellar mass of the star formation efficiency (top panel), infall time scale (middle panel) and effective radius (bottom panel) for the models matching the $[Fe/H]$-mass and the $[Mg/Fe]$-mass relations observed in data simultaneously, for a Salpeter IMF. Dotted lines show linear fits to the models.

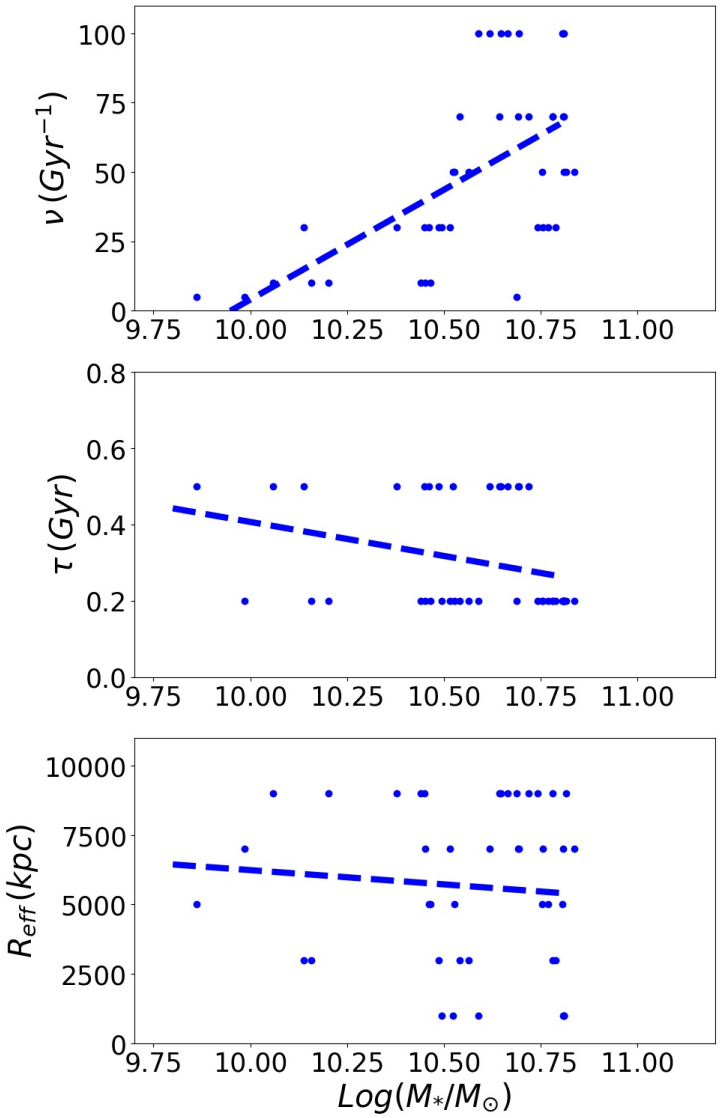

Figure 6.15: Same as previous Fig. 6.14, for a time-dependent bimodal IMF (Model05).

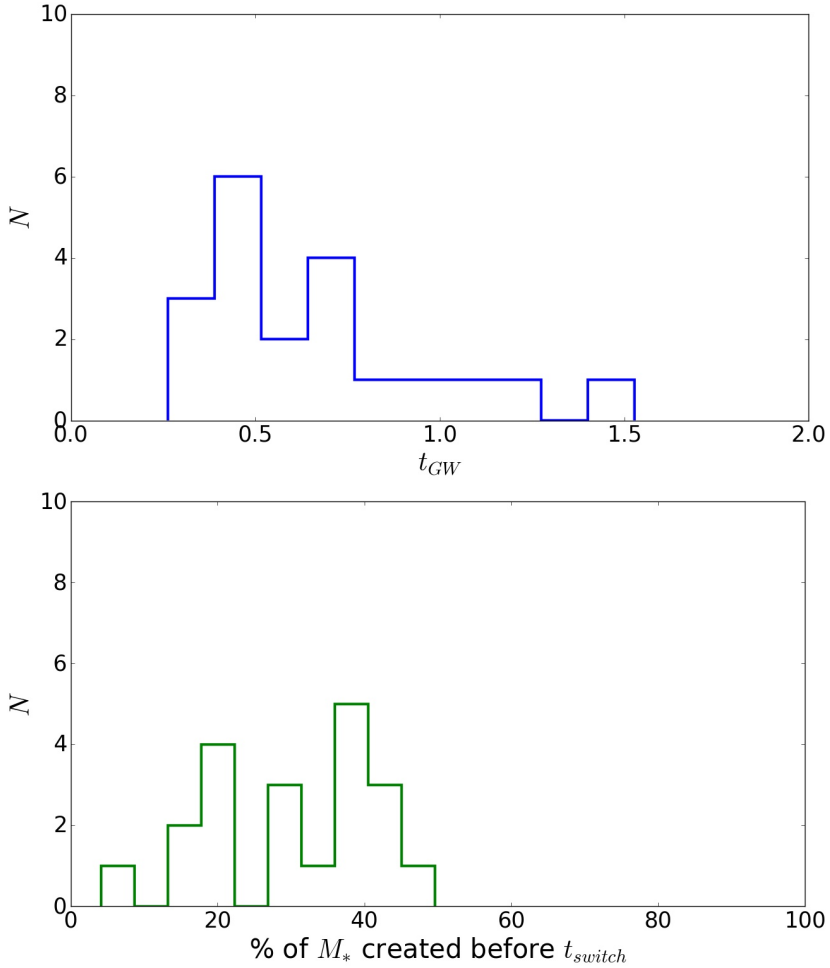

Figure 6.16: Upper panel: Distribution of the onset time of the galactic wind (t_{GW}) for the Model05 galaxies matching the observed $[Fe/H]$-mass and the $[Mg/Fe]$-mass relations simultaneously. For comparison, all of these galaxies switch from a top to a bottom-heavy bimodal IMF for $t_{switch} = 0.1$ Gyr. So, *the switch always takes place before the onset of galactic wind* and the following quenching of star formation. Lower panel: Distribution of the percentage of stellar mass created before the IMF switching from top to bottom-heavy in the same galaxies.

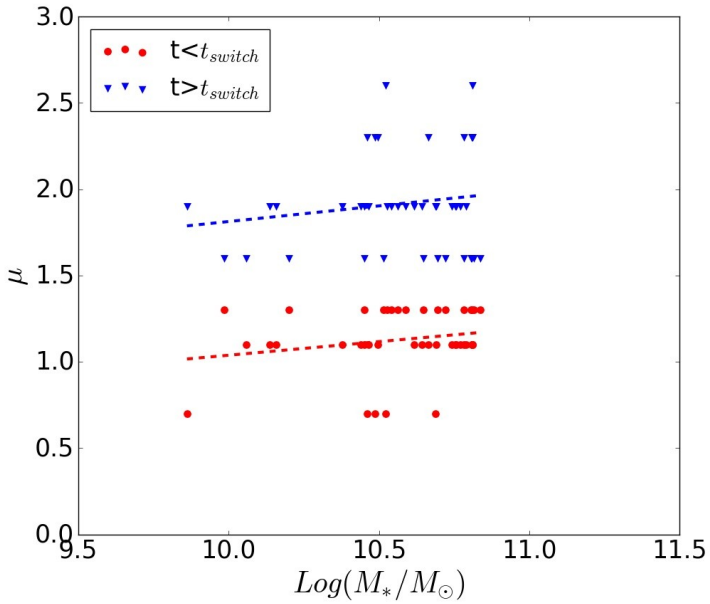

Figure 6.17: Variation with mass of the IMF slope before and after the switch for the time-dependent bimodal models matching the observed $[Fe/H]$-mass and the $[Mg/Fe]$-mass relations simultaneously.

(M/L) variation with σ for a local sample of elliptical galaxies extracted from the $ATLAS^{3D}$ survey (Cappellari et al., 2013). These ratios were computed from the SDSS r-band luminosities, and were converted into the analogous for the B band by using EMILES SSP models (Vazdekis et al., 2015, 2016); the resulting conversion factor varies between 1.45 and 1.7, according to the mass of the galaxy (it does not depend on the IMF). After such a conversion, their estimated $(M/L)_B$ ratios are in the range (4.9-12.9).
These values match ours extremely well for massive galaxies, but our M/L are larger for less massive objects; in other words, since the trend of M/L with M is related to the tilt of the fundamental plane (FP), our models would imply a shallower tilt than observations suggest.
These differences could be mainly ascribed to the use of different prescriptions in the adopted population synthesis models (i.e., different evolutionary tracks, assumed metallicity).
However, it should be stressed that changing the IMF can lead to M/L ratios even order of magnitudes in disagreement with observations (Padovani and Matteucci, 1993). Since the discrepancies we observe do not go to this extent, and since our main focus is to reproduce the chemical trends of the observed galaxies, specifically the mass-metallicity and the $[Mg/Fe]$-mass relations, we considered the comparison between our models and the dataset

satisfying, leaving further investigation to future works.

6.6 Environment dependence

As mentioned in the introduction, the topic of the environment dependence of ellipticals is of great interest.
In this sense, Rosani et al. (2018) analyzed the environmental dependence of the IMF -mass relation for the SPIDER sample.
To quantitatively define the environmental properties of their galaxies, they separated their sample according to the following criteria:

- a first division has been based on hierarchy, namely the dataset has been divided in centrals and satellites (5425 objects), regardless of the mass of the host halo;
- within the same hierarchical group, galaxies were further separated on the basis of the mass of the dark matter host halo where galaxies reside; the limiting values of the host halo mass have been set to $10^{12.5} M_{\odot}/h$ and $10^{14} M_{\odot}/h$ for centrals and satellites, respectively.

They concluded that while age, $[Z/H]$ and $[Mg/Fe]$ do show a dependence on environment, the IMF slope is not influenced either by hierarchy or by host halo mass, showing a constant trend of increasing (bottom-heavier IMF) in more massive galaxies.

We tested this result, by repeating the matching procedure between models and observed galaxies, after adopting the same hierarchy-based division of the dataset as in Rosani et al. (2018).
Similarly to what concluded by Thomas et al. (2010), we do not find any dependence on the environment, since the results of the new matching appear to be mostly independent of hierarchy. This is shown in table 6.4 where, in analogy with table 6.3, the number of matching models for galaxies in the two different groups are reported. In Appendix B, Figures B.1 to B.4 (in analogy with Figures 6.8 to 6.13) show the matching for centrals and satellites separately.

Table 6.3: Number of models matching the data, either for $[Fe/H]$ or $[Mg/Fe]$ separately, or for both of them simultaneously. In each case, the number of matches are reported in three different mass ranges referred to as "low", "middle", and "high", respectively, and for all masses ("tot").

Model	$[Fe/H]$				$[Mg/Fe]$				both			
	low	middle	high	tot	low	middle	high	tot	low	middle	high	tot
01	73	188	44	305	44	137	12	193	3	72	11	86
02	50	0	0	50	155	71	0	226	3	0	0	3
03	0	0	0	0	0	27	25	52	0	0	0	0
04	24	0	0	24	66	0	0	66	5	0	0	5
05	218	181	54	453	372	1004	437	1813	6	23	14	43

Table 6.4: Number of models matching the data, either for $[Fe/H]$ or $[Mg/Fe]$ separately, or for both of them simultaneously. We show the number matches between models and galaxies, for the whole dataset (columns 1-3), for central galaxies only (4-6) and satellites (7-9), respectively.

Model	All			Central			Satellites		
	$[Fe/H]$	$[Mg/Fe]$	both	$[Fe/H]$	$[Mg/Fe]$	both	$[Fe/H]$	$[Mg/Fe]$	both
01	305	193	86	309	193	76	342	204	93
02	50	226	3	62	194	1	67	284	9
03	0	52	0	0	61	0	0	14	0
04	24	66	5	30	43	8	23	82	7
05	453	1813	43	373	1713	38	639	1526	40

Chapter 7

Summary and conclusions

In this Thesis, we present our work on the chemical evolution of elliptical galaxies, with a particular focus on the impact on the IMF.
The main tool adopted for this study is a modified version of the chemical evolution code presented by Pipino and Matteucci (2004), taking into account SNe feedback and an initial fast infall episode leading to the formation of galaxies, and modified to include different parameterizations of the IMF.

Our first efforts have been dedicated to the study of the dataset by Thomas et al. (2010), containing information on the chemical abundance patterns for ≈ 3000 galaxies, which have been visually inspected and classified as ellipticals from a starting sample of SDSS DR4 galaxies. From the complete sample, we only considered the objects which did not show signs of recent star formation activity (the "red sequence" subset).
We tried to reproduce the observed mass-metallicity and the $[\alpha/Fe]$-mass relations, expressed through the total metallicity $[Z/H]$, the $[\alpha/Fe]$ ratio, and the Lick spectral indices $< Fe >$ and Mg_2, the latter two derived by applying the Tantalo et al. (1998) calibration to the chemical abundances predicted by our model.
Theoretically, the process of downsizing in star formation alone could be able to account for both the mass-metallicity and $[\alpha/Fe]$-mass relationships, by intensifying the production of heavy elements and by hastening the onset time of the galactic wind with consequent earlier quenching of star formation in more massive galaxies, as concluded in Matteucci (1994) and Pipino and Matteucci (2004). The earlier wind onset prevents SNe Ia, which are the major Fe producers, to pollute the gas with Fe, which will be mostly produced only after star formation has stopped and will eventually end up in the intracluster medium.
Theoretically, this should be achieved by assuming an increase of star for-

mation efficiency with mass, steep enough to overcome the deeper potential well, and this assumption actually allowed Pipino and Matteucci (2004) to find a good agreement with the data available at that time.
Our attempts to match data by only assuming the downsizing scenario, however, turned out to be unsuccessful, since the trends we obtained for the models with a constant Salpeter IMF and downsizing in star formation were always considerably flatter than the observed ones.
Particularly, the flatness of the $[\alpha/Fe]$-mass relationship in our models, considering that we obtained a good fit for the $[Fe/H]$ increase with mass (see Fig. 5.1), indicated that the problem was mainly due to an insufficient production of α-elements when only assuming the downsizing scenario.
The fit to the data remained poor, regardless of our attempts to stress the variation of the various parameters (star formation efficiency ν, infall timescale τ, SNe feedback) with mass and the downsizing effect.

However, some configurations actually allowed to partially improve the fit.
The extreme star formation efficiency variation tested in Model 01c (see table 5.1), for example, provided good agreement with most of the observed trends, at the cost of assuming, for low mass galaxies, values even smaller than the ones usually assumed for dwarf galaxies (Vincenzo et al., 2014), which is difficult to explain from a physical point of view.
Moreover, when analyzing the trend of the $[\alpha/Fe]$ ratio as obtained by deriving $[Z/H]$ and $[Fe/H]$ from our models and by adopting equation 4.1, the trend with mass was negative, contrary to the theoretical expectations of higher $[\alpha/Fe]$ ratios in more massive galaxies, due to the shorter period of star formation.
To this regard, the ratio defined this way probably does not provide a good proxy for the real behavior of α-elements, since in the global metal content, Z, there are other abundant metals such as C and N, for example, which do not behave as α-elements. As a confirmation, when plotting just the [Mg/Fe] ratios versus mass the agreement with the data is more reasonable.

Considering the inability to fit the data in the case of the fixed IMF, we tested models with different variable IMFs.
In spite of the claims for the need of a bottom heavy IMF in more massive galaxies (Cenarro et al., 2003; Auger et al., 2010; Grillo and Gobat, 2010; Treu et al., 2010; van Dokkum and Conroy, 2010; Barnabè et al., 2011; Dutton et al., 2011; van Dokkum and Conroy, 2011; Cappellari et al., 2012; Conroy and van Dokkum, 2012a,b; Dutton et al., 2012; Spiniello et al., 2012; Dutton et al., 2013; Ferreras et al., 2013; La Barbera et al., 2013; Spiniello et al., 2014), the results obtained with the Salpeter (1955) IMF suggested

the need for more massive stars in larger galaxies, hence a top-heavier IMF. A variation with mass of the IMF, switching from a (Scalo, 1986) for the less massive ellipticals, to a Salpeter (Salpeter, 1955) for the intermediate mass ones and then to a Chabrier (Chabrier, 2003) in more massive ones, together with the downsizing formation scenario (increasing efficiency of star formation with mass) allowed us to successfully obtain the desired trends.
The transition from bottom to top-heavier IMFs with the increasing total mass has been found to be the dominant one, with the variation of the other parameters providing a smoothing effect between the different mass ranges. In other words, the IMF is the most effective parameter influencing the chemical evolution of galaxies.
Although with some discrepancies with data, mainly consisting in a slight underestimate of the $[\alpha/Fe]$ and $[Mg/Fe]$ ratios, this variable IMF was the only one producing the best simultaneous agreement for all the considered chemical properties ($[Z/H]$, $[\alpha/Fe]$, $[Mg/Fe]$, $< Fe >$ and Mg_2).
Another test, where we adopted an Arimoto-Yoshii IMF (Arimoto and Yoshii, 1987) in more massive galaxies (e.g. an IMF even flatter than the Chabrier one), showed that this IMF generally overestimate the metals in these galaxies.

Finally, we tested the effect of introducing the Integrated Galactic IMF (IGIMF), obtained by integrating the canonic stellar IMF over the mass function of embedded clusters, within which star formation is assumed to take place (Recchi et al., 2009; Weidner et al., 2010). This IMF is naturally top-heavier in galaxies with a higher star formation activity, since they are found to host more massive clusters, where larger masses are produced. Specifically, given the range of star formation rates experienced by our model galaxies during their evolution, we combined the two prescriptions of Recchi et al. (2009) and Weidner et al. (2010), each of which is valid under a certain star formation rate regime.
The IGIMF produced the models with the best fitting slopes, but a slight offset was always present, with the chemical abundances predicted by these models always being too high, probably due to calibration effects.

As a general consideration about this exercise, it is worth to stress the role played by intrinsic uncertainties in the derivation of abundances through the use of indices in elliptical galaxies. As shown in Pipino and Matteucci (2004), different calibration can produce different results, so that we do not expect to reproduce the exact values of the abundances and of the abundance ratios in these galaxies, but rather the trends shown by such abundances.
Aside from this, the first work presented in the Thesis provides strong indi-

cations against the use of IMFs privileging low mass stars (bottom-heavier IMF); moreover, the only way to reproduce the slopes of the mass-metallicy and the mass-$[\alpha/Fe]$ relations at the same time is to combine downsizing and an IMF having the opposite behavior, namely becoming top-heavier with increasing galactic mass.

These conclusions were, to different degrees, generally confirmed in the work described in the second part of the Thesis.
We extended our analysis by considering a new dataset (see Sec. 4.2), and we tested the same implementations of the initial mass function used in De Masi et al. (2018), plus two forms of the bimodal IMF by Vazdekis et al. (1997, 2003). Specifically, a form becoming bottom-heavier in more massive galaxies, as suggested in Ferreras et al. (2013), La Barbera et al. (2013), and an explicitly time-dependent bimodal IMF, switching from top-heavy to bottom-heavy after a time t_{switch} (Ferreras et al., 2015; Weidner et al., 2013).
Another important difference was in the approach followed to generate the models.
Instead of manually choosing the parameters values for every model in the various sets (i.e., for the various IMFs), as done previously, we created for every considered IMF a grid of models by varying all the parameters of the code over a grid of value, thus making sure to explore a much larger volume in the parameter space.
Each of the IMFs we tested provided matches with data, at least in some limited mass bins, but only in two cases we were able to fit the mass-metallicy and the mass-$[\alpha/Fe]$ relations simultaneously: (1) with a Salpeter (1955) IMF, and (2) with the time-dependent form of the bimodal IMF, always combined with the effect of downsizing in star formation.

The success of the fit by models with a Salpeter (1955) IMF provided a significant difference with the previous work, where we needed to invoke a change in the IMF.
We identified the following points as the reasons to this difference:

- simply, the use of a different dataset, characterized by a different slope of the mass-metallicity and $[\alpha/Fe]$ relations;

- in De Masi et al. (2018), the main indication for the need of a IMF variation came from the analysis of the spectral indices Mg_2 and $< Fe >$, which we derived from the average abundances of the stellar population by applying the calibration relations by Tantalo et al. (1998). Since different calibrations generally yield different results (Pipino and

Matteucci, 2004), this procedure is always plagued by uncertainties, so that results based on such a comparison should be taken with care.

- one of the main problems one has to deal with when comparing models with data lies in the operational definition of the various considered quantities. Our model directly provides us with the abundances of single chemical elements, whereas the abundance ratios reported for the objects in the catalog are often resulting from other quantities (see section 4.2 for the definitions of $[Fe/H]$ and $[Mg/Fe]$ adopted in this case). We always tried to be consistent in the comparison, and derived similar quantities from our models by adopting the same definitions as in the observed data. However, this means that the comparison of a given abundance ratio performed on two different catalogs may lead to a discrepancy in the resulting trends.

In spite of this difference, we confirmed the result that, as far as the chemical properties of ellipticals are concerned, scenarios involving IMFs which are bottom-heavier through the whole evolution of more massive galaxies should be discarded, since they invariably lead to drastic underestimation of the values of $[\alpha/Fe]$ ratios, (in agreement, for example, with Martín-Navarro, 2016).

Concerning this point, the second successful scenario we described, i.e. a time-dependent bimodal IMF, allows us to reconcile the indications obtained from chemical abundances (i.e., higher $[\alpha/Fe]$ ratios in more massive galaxies) with the suggestions derived from the spectra of stellar population of ellipticals, favoring bottom-heavier IMFs.
This IMF is top-heavy in the first period of the chemical evolution of galaxies, thus accounting for the characteristic $[\alpha/Fe]$ trends with mass, and then switches to a different, bottom-heavy form after a given time ($0.1\ Gyr$). This bottom-heavy phase would account for observations, as IMF-sensitive features in the integrated spectra of ETGs at $z \approx 0$ are dominated by stars still alive at the present time, i.e. less massive stars, whereas the more massive ones, born during the initial top-heavier phase, do not contribute to the spectra since they died a long time ago.
We tested different possible values for the switching time, but in all of the matching models the switching was always found to take place at the same time, specifically at the earliest possible one ($\approx$ 0.1Gyr). This, again, is in accordance with observations, since ellipticals are old objects, and consequently the IMF constraints we observe at the present time are related to old stellar populations.
Although the bimodal IMFs in lower mass galaxies mostly present slopes similar to a canonical Kroupa (2001) IMF ($\gamma \approx 1.3$), more massive ones span

a wider range of values, ranging from $\mu_1 = 0.5$ (top-heavier) before the switch to $\mu_2 = 2.6$ (bottom-heavier) after the switch.
We also decided to investigate the M/L ratios of these two sets of models, which are very sensitive to the IMF, to obtain another, independent constraint for the IMF, by combining our masses with luminosities from the population synthesis model of Vincenzo et al. (2016). Our M/L ratio estimates are generally slightly higher than recent observations (Cappellari et al., 2013; La Barbera et al., 2016), particularly at lower masses, whereas we obtain a good agreement for more massive galaxies. The discrepancies we find are not large enough to provide indication able to discard these models, and we reserve a further analysis of the topic for future works.
Finally, we repeated all the tests with a different version of the dataset, where the mass stacking was performed by separating central and satellites galaxies; the obtained results, however, do not show any significant difference, thus reinforcing the idea that the IMF is an intrinsic galaxy property, and is not affected by other "external" effects, such as the environment where galaxies reside.

In summary, our main conclusion is that:

- we confirm the need for a downsizing in star formation, i.e. a shorter star formation in more massive galaxies, powered by an increasing star formation efficiency with total stellar mass, in order to reproduce the observed trends;

- a bottom-heavy IMF for the whole galactic life-time should be rejected, since produces results at variance with the main chemical features of elliptical galaxies;

- on the other hand, and in relation to the inspected dataset and the assumed calibrations, we find indications for the need of a constant IMF, or even for an increasingly top-heavier one in more massive ellipticals;

- one possible way to reconcile the need for a top-heavy IMF in our model with the observational claims for a bottom-heavy IMF in massive ellipticals is to assume an IMF having an explicit dependence on time, acting as top-heavy in the early evolutionary phases, and transitioning to bottom-heavy at later times.

7.1 Developments an future prospects

In the course of the works presented in this Thesis, we focused our analysis on certain parameters of the model, whose influence on the chemical properties we deemed to be dominant, and did not investigate the results obtained by acting on other quantities.
Specifically:

- as described in Sec. 3.3, following Matteucci (1992), in our model we always assumed Dark Matter to be distributed in a diffuse halo, with a characteristic scale length $R_{DM} = 10\,R_{eff}$, and with a profile taken from Bertin et al. (1992).
  Different possibilities could be explored, and their effect on the outcome of the model (especially on the potential energy and hence the energetic) could be studied;

- when testing the time-dependent bimodal IMF in Sec. 6.2, we considered a range of values for the time t_{switch} when said IMF switches from a top- to a bottom-heavy form. We chose for t_{switch} a lower limit of $0.1\,Gyr$, with the expectation that even lower values, i.e. shorter periods of evolution under a top-heavy regime, could result to be negligible (as a matter of fact, we showed how models characterized by this minimum value of t_{switch} always formed a percentage of their total stellar mass lower than $\approx 50\%$ under the top-heavy IMF). However, as described in Sec. 6.4, all the Models with the time-dependent bimodal IMF turned out to be characterized by this minimum value for t_{switch}. In the wake of this result, new grids of models with even lower values for t_{switch} could be analyzed, in order to verify whether they could match observed data;

- we did not test whether variations in the SNIa rate could alleviate the tension between some models and observations (consider, for example, the steepness of the $[Fe/H]$-mass relation produced by MOdels with a varying IMF in Sec. 5.3). This possibility, however, has not been taken into account because the SNIa rate currently considered in the model has been tuned to match observations (Cappellaro et al., 1999).

- Lian et al. (2017) investigated the origin of the MZR for the stellar population and gas of local star-forming galaxies, by using a chemical evolution model that included both IMF variations and variable inflow strength and outflow fraction f_{out} (defined as the mass fraction of stellar ejecta that are expelled from the galaxy). They found evidence that

the two relations can be simultaneously reproduced with models with a strong time dependence of either the metal outflow fraction or the IMF slope (specifically, enhanced metal outflows or steeper IMF slopes at early times) match the observations very well.
A possible extension of our model could analogously include the possibility of testing (i) variable compositions for the infall (which we always assumed to be primordial) or (ii) different solutions for the galactic wind, or selective loss of metals. This could be a possibility, for example, to fix the issue of the IGIMF always predicting abundance ratios too high with respect with observations (Sec. 5.4 and 6.4);

Most of these modification, however, would lead to an increase of the number of free parameters of the model, and hence should be applied with care, and only after imposing further observational constraints.
Regarding the future prospects for our work, we plan to focus on two main points:

Extension of the IGIMF theory

Weidner et al. (2013); Jerabkova et al. (2018) presented an extension of the IGIMF theory that, unlike the form used in this Thesis, also presents a dependence o metallicity.
In general, the main challenge regarding the inclusion of these type of IMF in our theoretical framework lays in the necessity to normalize the IMF.
Within our chemical evolution model, we require the adopted IMFs to be normalized to unity, i.e. (see Sec. 2.4):

$$\int_{m_{min}}^{m_{max}} m\,\varphi(m)\,dm = 1 \tag{7.1}$$

which also applies to the IGIMF.
However, while this normalization is straightforward to calculate for IMF with known analytical forms, the procedure is more challenging for the IGIMF. In order to overcome this issue, we adopted the following procedure:

1. by using the publicly available GalIMF code (Jerabkova et al., 2018), we calculated grid of values for the IGIMF for different combinations of the SFR and the metallicity $[Fe/H]$ (see Fig. 7.1)

2. we used previously generated grid as input for our chemical evolution model, and interpolated between the IGIMF values reported in the grid for the different SFR and $[Fe/H]$ required every time (see Fig. 7.2)

	$[Fe/H]_1$	$[Fe/H]_2$	...	$[Fe/H]_m$
ψ_1	ξ_{11}	ξ_{12}	...	ξ_{1m}
ψ_2	ξ_{21}	...	...	ξ_{2m}
...	...	...	...	...
ψ_n	ξ_{n1}	...	...	ξ_{nm}

Figure 7.1: Grid of IGIMF values calculated by using the GalIMF code (Jerabkova et al., 2018) for different combinations of the SFR and the metallicity $[Fe/H]$.

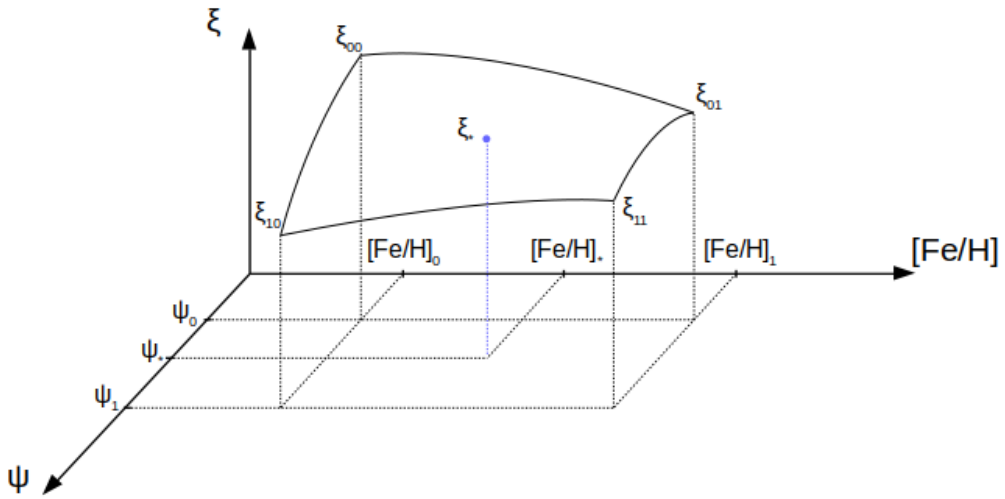

Figure 7.2: Interpolation from the Grid of IGIMF values calculated by using the GalIMF code, using the values of SFR and $[Fe/H]$ required by the chemical evolution code every time.

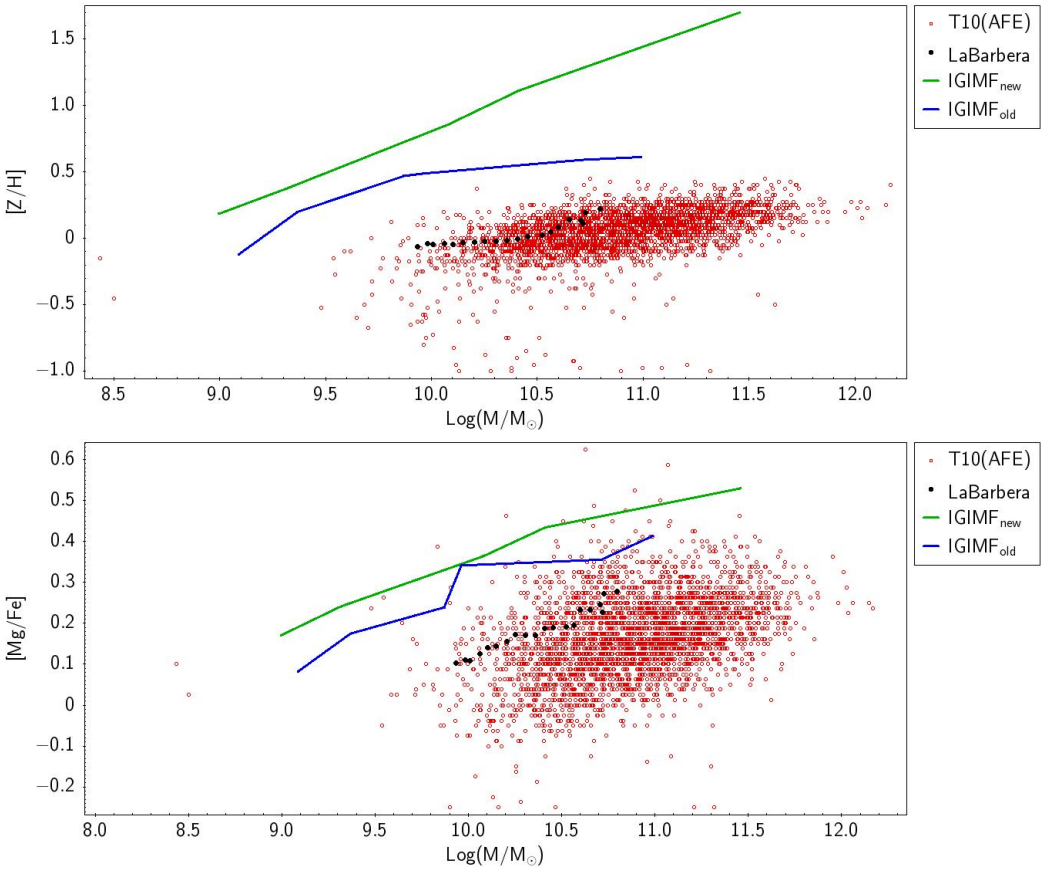

Figure 7.3: Interpolation from the Grid of IGIMF values calculated by using the GalIMF code, using the values of SFR and $[Fe/H]$ required by the chemical evolution code every time.

The preliminary results of a test we ran with this new form of the IGIMF are shown in Fig. 7.3, where we compare the output of our chemical evolution model with both the datasets used in the Thesis. Notice that in the bottom plot, we plotted the $[\alpha/Fe]$ ratio for the MOSES dataset, and the $[Mg/Fe]$the SPIDER one (Sec. 4).
From both of these plots, it is evident that the problems we encountered when adopting the IGIMF are still present; as a matter of fact, the offset with data, due to the prediction of too high values of $[Z/H]$ and $[Mg/Fe]$, is even larger than with the previous prescription for the IGIMF.

AGN feedback

Finally, we plan to include the effect of accretion on a massive black hole (MBH) at the center of the galaxy, and studying its contribution to the

overall feedback and to chemical evolution.
In a simple approach, the energy released by the central black hole could be modeled as:

$$L_{bol} = \eta \, \dot{M}_* \, c^2 \tag{7.2}$$

where

$$\begin{cases} \eta \rightarrow \text{efficiency of mass to energy conversion} \\ \dot{M}_* \rightarrow \text{rate of mass accretion into the central black hole} \end{cases}$$

For the determination of η and $\dot{M}_*$, we plan to follow the prescription by (Ciotti and Pellegrini, 2018).

Bibliography

Arabsalmani, M., Møller, P., Perley, D. A., Freudling, W., Fynbo, J. P. U., Le Floc'h, E., Zwaan, M. A., Schulze, S., Tanvir, N. R., Christensen, L., Levan, A. J., Jakobsson, P., Malesani, D., Cano, Z., Covino, S., D'Elia, V., Goldoni, P., Gomboc, A., Heintz, K. E., Sparre, M., de Ugarte Postigo, A., and Vergani, S. D. (2018). Mass and metallicity scaling relations of high-redshift star-forming galaxies selected by GRBs. *MNRAS*, 473:3312–3324.

Aragon-Salamanca, A., Ellis, R. S., Couch, W. J., and Carter, D. (1993). Evidence for systematic evolution in the properties of galaxies in distant clusters. *Monthly Notices of the Royal Astronomical Society*, 262(3):764–794.

Arimoto, N. and Kobayashi, C. (1999). Metallicity distributions of elliptical galaxies and globular cluster systems. *Astrophysics and Space Science*, 265(1):513–521.

Arimoto, N. and Yoshii, Y. (1987). Chemical and photometric properties of a galactic wind model for elliptical galaxies. *A&A*, 173:23–38.

Arrigoni, M., Trager, S. C., Somerville, R. S., and Gibson, B. K. (2010). Galactic chemical evolution in hierarchical formation models - I. Early-type galaxies in the local Universe. *MNRAS*, 402:173–190.

Asplund, M., Grevesse, N., Sauval, A. J., and Scott, P. (2009). The Chemical Composition of the Sun. *ARA&A*, 47:481–522.

Auger, M. W., Treu, T., Gavazzi, R., Bolton, A. S., Koopmans, L. V. E., and Marshall, P. J. (2010). Dark Matter Contraction and the Stellar Content of Massive Early-type Galaxies: Disfavoring "Light" Initial Mass Functions. *ApJ*, 721:L163–L167.

Balogh, M., Eke, V., Miller, C., Lewis, I., Bower, R., Couch, W., Nichol, R., Bland-Hawthorn, J., Baldry, I. K., Baugh, C., et al. (2004). Galaxy ecol-

ogy: groups and low-density environments in the sdss and 2dfgrs. *Monthly Notices of the Royal Astronomical Society*, 348(4):1355–1372.

Bamford, S. P., Nichol, R. C., Baldry, I. K., Land, K., Lintott, C. J., Schawinski, K., Slosar, A., Szalay, A. S., Thomas, D., Torki, M., et al. (2009). Galaxy zoo: the dependence of morphology and colour on environment. *Monthly Notices of the Royal Astronomical Society*, 393(4):1324–1352.

Barnabè, M., Czoske, O., Koopmans, L. V., Treu, T., and Bolton, A. S. (2011). Two-dimensional kinematics of slacs lenses–iii. mass structure and dynamics of early-type lens galaxies beyond zâL'Č 0.1. *Monthly Notices of the Royal Astronomical Society*, 415(3):2215–2232.

Bastian, N. (2008). On the star formation rate - brightest cluster relation: estimating the peak star formation rate in post-merger galaxies. *MNRAS*, 390:759–768.

Bastian, N., Covey, K. R., and Meyer, M. R. (2010). A Universal Stellar Initial Mass Function? A Critical Look at Variations. *ARA&A*, 48:339–389.

Baugh, C., Cole, S., and Frenk, C. (1996). Evolution of the hubble sequence in hierarchical models for galaxy formation. *Monthly Notices of the Royal Astronomical Society*, 283(4):1361–1378.

Baugh, C. M. (2006). A primer on hierarchical galaxy formation: the semi-analytical approach. *Reports on Progress in Physics*, 69:3101–3156.

Baum, W. (1959). Population inferences from star counts, surface brightness and colors. *Publications of the Astronomical Society of the Pacific*, 71:106–117.

Bell, E. F. and De Jong, R. S. (2000). The stellar populations of spiral galaxies. *Monthly Notices of the Royal Astronomical Society*, 312(3):497–520.

Bell, E. F., McIntosh, D. H., Katz, N., and Weinberg, M. D. (2003). The Optical and Near-Infrared Properties of Galaxies. I. Luminosity and Stellar Mass Functions. *ApJS*, 149:289–312.

Bell, E. F., Wolf, C., Meisenheimer, K., Rix, H.-W., Borch, A., Dye, S., Kleinheinrich, M., Wisotzki, L., and McIntosh, D. H. (2004). Nearly 5000 Distant Early-Type Galaxies in COMBO-17: A Red Sequence and Its Evolution since z˜1. *ApJ*, 608:752–767.

Bender, R., Burstein, D., and Faber, S. M. (1992). Dynamically hot galaxies. I - Structural properties. *ApJ*, 399:462–477.

Benson, A. J., Cole, S., Frenk, C. S., Baugh, C. M., and Lacey, C. G. (2000). The nature of galaxy bias and clustering. *MNRAS*, 311:793–808.

Berlind, A. A. and Weinberg, D. H. (2002). The Halo Occupation Distribution: Toward an Empirical Determination of the Relation between Galaxies and Mass. *ApJ*, 575:587–616.

Bernardi, M., Nichol, R. C., Sheth, R. K., Miller, C. J., and Brinkmann, J. (2006). Evolution and Environment of Early-Type Galaxies. *AJ*, 131:1288–1317.

Bernardi, M., Renzini, A., da Costa, L. N., Wegner, G., Alonso, M. V., Pellegrini, P. S., Rité, C., and Willmer, C. N. (1998). Cluster versus field elliptical galaxies and clues on their formation. *The Astrophysical Journal Letters*, 508(2):L143.

Bernardi, M., Sheth, R. K., Annis, J., Burles, S., Eisenstein, D. J., Finkbeiner, D. P., Hogg, D. W., Lupton, R. H., Schlegel, D. J., SubbaRao, M., Bahcall, N. A., Blakeslee, J. P., Brinkmann, J., Castander, F. J., Connolly, A. J., Csabai, I., Doi, M., Fukugita, M., Frieman, J., Heckman, T., Hennessy, G. S., Ivezić, Ž., Knapp, G. R., Lamb, D. Q., McKay, T., Munn, J. A., Nichol, R., Okamura, S., Schneider, D. P., Thakar, A. R., and York, D. G. (2003). Early-Type Galaxies in the Sloan Digital Sky Survey. III. The Fundamental Plane. *AJ*, 125:1866–1881.

Bertin, G., Saglia, R. P., and Stiavelli, M. (1992). Elliptical galaxies with dark matter. I - Self-consistent models. II - Optimal luminous-dark matter decomposition for a sample of bright objects. *ApJ*, 384:423–447.

Blumenthal, G. R., Faber, S., Primack, J. R., and Rees, M. J. (1984). Formation of galaxies and large-scale structure with cold dark matter. *Nature*, 311(5986):517.

Bodansky, D., Clayton, D. D., and Fowler, W. A. (1968). Nucleosynthesis during silicon burning. *Physical Review Letters*, 20(4):161.

Bonnell, I. A., Larson, R. B., and Zinnecker, H. (2007). The Origin of the Initial Mass Function. *Protostars and Planets V*, pages 149–164.

Bower, R. G., Lucey, J. R., and Ellis, R. S. (1992). Precision Photometry of Early Type Galaxies in the Coma and Virgo Clusters - a Test of the

Universality of the Colour / Magnitude Relation - Part Two - Analysis. *MNRAS*, 254:601.

Bressan, A., Chiosi, C., and Fagotto, F. (1994). Spectrophotometric evolution of elliptical galaxies. 1: Ultraviolet excess and color-magnitude-redshift relations. *The Astrophysical Journal Supplement Series*, 94:63–115.

Brocato, E., Castellani, V., Poli, F. M., and Raimondo, G. (2000). Predicted colours for simple stellar populations. II. The case of old stellar clusters. *Astronomy & Astrophysics Supplement*, 146:91–101.

Bruzual, G. and Charlot, S. (2003). Stellar population synthesis at the resolution of 2003. *Monthly Notices of the Royal Astronomical Society*, 344(4):1000–1028.

Bruzual A., G. (1983). Spectral evolution of galaxies. I - Early-type systems. *The Astrophysical Journal*, 273:105–127.

Bruzual A., G. and Charlot, S. (1993). Spectral evolution of stellar populations using isochrone synthesis. *The Astrophysical Journal*, 405:538–553.

Burbidge, E. M., Burbidge, G. R., Fowler, W. A., and Hoyle, F. (1957). Synthesis of the elements in stars. *Reviews of modern physics*, 29(4):547.

Burstein, D., Bender, R., Faber, S., and Nolthenius, R. (1997). Global Relationships Among the Physical Properties of Stellar Systems. *AJ*, 114:1365.

Burstein, D., Faber, S., and Gonzalez, J. (1986). Old stellar populations. iii-the metallicities of m5, m71, and m67. *The Astronomical Journal*, 91:1130–1139.

Buzzoni, A. (1989). Evolutionary population synthesis in stellar systems. I - A global approach. *The Astrophysical Journal Supplement Series*, 71:817–869.

Caldwell, N. (1983). Structure and stellar content of dwarf elliptical galaxies. *The Astronomical Journal*, 88:804–812.

Calura, F. and Menci, N. (2009). Chemical evolution of local galaxies in a hierarchical model. *MNRAS*, 400:1347–1365.

Calura, F. and Menci, N. (2011). A possible solution to the [α/Fe]-σ problem in early-type galaxies within a hierarchical galaxy formation model. *MNRAS*, 413:L1–L5.

Calura, F., Pipino, A., Chiappini, C., Matteucci, F., and Maiolino, R. (2009). The evolution of the mass-metallicity relation in galaxies of different morphological types. *Astronomy & Astrophysics*, 504(2):373–388.

Cappellari, M., Bacon, R., Bureau, M., Damen, M. C., Davies, R. L., de Zeeuw, P. T., Emsellem, E., Falcón-Barroso, J., Krajnović, D., Kuntschner, H., McDermid, R. M., Peletier, R. F., Sarzi, M., van den Bosch, R. C. E., and van de Ven, G. (2006). The SAURON project - IV. The mass-to-light ratio, the virial mass estimator and the Fundamental Plane of elliptical and lenticular galaxies. *MNRAS*, 366:1126–1150.

Cappellari, M., McDermid, R. M., Alatalo, K., Blitz, L., Bois, M., Bournaud, F., Bureau, M., Crocker, A. F., Davies, R. L., Davis, T. A., de Zeeuw, P. T., Duc, P.-A., Emsellem, E., Khochfar, S., Krajnović, D., Kuntschner, H., Lablanche, P.-Y., Morganti, R., Naab, T., Oosterloo, T., Sarzi, M., Scott, N., Serra, P., Weijmans, A.-M., and Young, L. M. (2012). Systematic variation of the stellar initial mass function in early-type galaxies. *Nature*, 484:485–488.

Cappellari, M., Scott, N., Alatalo, K., Blitz, L., Bois, M., Bournaud, F., Bureau, M., Crocker, A. F., Davies, R. L., Davis, T. A., de Zeeuw, P. T., Duc, P.-A., Emsellem, E., Khochfar, S., Krajnović, D., Kuntschner, H., McDermid, R. M., Morganti, R., Naab, T., Oosterloo, T., Sarzi, M., Serra, P., Weijmans, A.-M., and Young, L. M. (2013). The ATLAS^{3D} project - XV. Benchmark for early-type galaxies scaling relations from 260 dynamical models: mass-to-light ratio, dark matter, Fundamental Plane and Mass Plane. *MNRAS*, 432:1709–1741.

Cappellaro, E., Evans, R., and Turatto, M. (1999). A new determination of supernova rates and a comparison with indicators for galactic star formation. *A&A*, 351:459–466.

Carollo, C. M. and Danziger, I. J. (1994a). Colours, line strengths and stellar kinematics of ngc 2663 and 5018. *Monthly Notices of the Royal Astronomical Society*, 270(4):743–768.

Carollo, C. M. and Danziger, I. J. (1994b). Dynamics and stellar populations in early-type galaxies. *Monthly Notices of the Royal Astronomical Society*, 270(3):523–569.

Carollo, C. M., Danziger, I. J., and Buson, L. (1993). Metallicity Gradients in Early Type Galaxies. *MNRAS*, 265:553.

Carroll, B. W. and Ostlie, D. A. (2017). *An introduction to modern astrophysics*. Cambridge University Press.

Cenarro, A., Gorgas, J., Vazdekis, A., Cardiel, N., and Peletier, R. (2003). Near-infrared line-strengths in elliptical galaxies: evidence for initial mass function variations? *Monthly Notices of the Royal Astronomical Society*, 339(1):L12–L16.

Chabrier, G. (2003). Galactic Stellar and Substellar Initial Mass Function. *PASP*, 115:763–795.

Chabrier, G., Hennebelle, P., and Charlot, S. (2014). Variations of the stellar initial mass function in the progenitors of massive early-type galaxies and in extreme starburst environments. *The Astrophysical Journal*, 796(2):75.

Charlot, S. and Bruzual, A. G. (1991). Stellar population synthesis revisited. *The Astrophysical Journal*, 367:126–140.

Charlot, S., Worthey, G., and Bressan, A. (1996). Uncertainties in the modeling of old stellar populations. *The Astrophysical Journal*, 457:625.

Chiappini, C., Matteucci, F., and Padoan, P. (1997). Chemical Evolution of the Solar Neighbourhood with a Variable IMF. In Valls-Gabaud, D., Hendry, M. A., Molaro, P., and Chamcham, K., editors, *From Quantum Fluctuations to Cosmological Structures*, volume 126 of *Astronomical Society of the Pacific Conference Series*, page 545.

Chiosi, C., Bertelli, G., and Bressan, A. (1988). Integrated colours and ages of LMC clusters - The nature of the bimodal distribution of the (B-V) colours. *Astronomy & Astrophysics*, 196:84–108.

Cioffi, D. F., McKee, C. F., and Bertschinger, E. (1988). Dynamics of radiative supernova remnants. *ApJ*, 334:252–265.

Ciotti, L. and Pellegrini, S. (2018). Isothermal bondi accretion in two-component jaffe galaxies with a central black hole. *arXiv preprint arXiv:1808.00871*.

Clayton, D. D., Fowler, W. A., Hull, T., and Zimmerman, B. (1961). Neutron capture chains in heavy element synthesis. *Annals of Physics*, 12(3):331–408.

Collobert, M., Sarzi, M., Davies, R. L., Kuntschner, H., and Colless, M. (2006). Central stellar populations of early-type galaxies in low-density environments. *Monthly Notices of the Royal Astronomical Society*, 370(3):1213–1222.

Conroy, C., Graves, G. J., and Van Dokkum, P. G. (2013). Early-type galaxy archeology: ages, abundance ratios, and effective temperatures from full-spectrum fitting. *The Astrophysical Journal*, 780(1):33.

Conroy, C., Graves, G. J., and van Dokkum, P. G. (2014). Early-type Galaxy Archeology: Ages, Abundance Ratios, and Effective Temperatures from Full-spectrum Fitting. *ApJ*, 780:33.

Conroy, C. and van Dokkum, P. (2012a). Counting Low-mass Stars in Integrated Light. *ApJ*, 747:69.

Conroy, C. and van Dokkum, P. G. (2012b). The Stellar Initial Mass Function in Early-type Galaxies From Absorption Line Spectroscopy. II. Results. *ApJ*, 760:71.

Crain, R. A., Theuns, T., Dalla Vecchia, C., Eke, V. R., Frenk, C. S., Jenkins, A., Kay, S. T., Peacock, J. A., Pearce, F. R., Schaye, J., Springel, V., Thomas, P. A., White, S. D. M., and Wiersma, R. P. C. (2009). Galaxies-intergalactic medium interaction calculation - I. Galaxy formation as a function of large-scale environment. *MNRAS*, 399:1773–1794.

Croton, D. J., Springel, V., White, S. D., De Lucia, G., Frenk, C. S., Gao, L., Jenkins, A., Kauffmann, G., Navarro, J., and Yoshida, N. (2006). The many lives of active galactic nuclei: cooling flows, black holes and the luminosities and colours of galaxies. *Monthly Notices of the Royal Astronomical Society*, 365(1):11–28.

Cyburt, R. H., Fields, B. D., Olive, K. A., and Yeh, T.-H. (2016). Big bang nucleosynthesis: Present status. *Reviews of Modern Physics*, 88(1):015004.

Davies, R. L., Sadler, E. M., and Peletier, R. F. (1993). Line-strength gradients in elliptical galaxies. *MNRAS*, 262:650–680.

Dayal, P., Ferrara, A., and Dunlop, J. S. (2013). The physics of the fundamental metallicity relation. *Monthly Notices of the Royal Astronomical Society*, 430(4):2891–2895.

de Carvalho, R. and Djorgovski, S. (1990). The mass-metallicity - Luminosity density relation for elliptical galaxies. In Kron, R. G., editor, *Evolution of*

the Universe of Galaxies, volume 10 of *Astronomical Society of the Pacific Conference Series*, pages 106–108.

de La Rosa, I. G., La Barbera, F., Ferreras, I., and de Carvalho, R. R. (2011). The link between the star formation history and [α/fe]. *Monthly Notices of the Royal Astronomical Society: Letters*, 418(1):L74–L78.

De Lucia, G., Fontanot, F., Wilman, D., and Monaco, P. (2011). Times, environments and channels of bulge formation in a Lambda cold dark matter cosmology. *MNRAS*, 414:1439–1454.

De Lucia, G., Springel, V., White, S. D., Croton, D., and Kauffmann, G. (2006). The formation history of elliptical galaxies. *Monthly Notices of the Royal Astronomical Society*, 366(2):499–509.

De Masi, C., Matteucci, F., and Vincenzo, F. (2018). The effects of the initial mass function on the chemical evolution of elliptical galaxies. *MNRAS*, 474:5259–5271.

De Masi, C., Vincenzo, F., Matteucci, F., Rosani, G., Barbera, F. L., Pasquali, A., and Spitoni, E. (2019). Is the imf in ellipticals bottom-heavy? clues from their chemical abundances. *Monthly Notices of the Royal Astronomical Society*, page sty3127.

de Vaucouleurs, G. (1948). Recherches sur les Nebuleuses Extragalactiques. *Annales d'Astrophysique*, 11:247.

de Vaucouleurs, G. (1961). Integrated Colors of Bright Galaxies in the u, b, V System. *ApJS*, 5:233.

Delgado-Serrano, R., Hammer, F., Yang, Y., Puech, M., Flores, H., and Rodrigues, M. (2010). How was the hubble sequence 6 gyr ago? *Astronomy & Astrophysics*, 509:A78.

Denicolo, G., Terlevich, R., Terlevich, E., Forbes, D. A., and Terlevich, A. (2005). Group, field and isolated early-type galaxies–ii. global trends from nuclear data. *Monthly Notices of the Royal Astronomical Society*, 358(3):813–832.

Diaz, A. I., Terlevich, E., and Terlevich, R. (1989). Near-IR features in late type stars - Their relation with stellar atmosphere parameters. *MNRAS*, 239:325–345.

Djorgovski, S. (1995). The fundamental plane correlations for globular clusters. *The Astrophysical Journal*, 438:L29–L32.

Djorgovski, S. and Davis, M. (1987). Fundamental properties of elliptical galaxies. *ApJ*, 313:59–68.

Dressler, A., Lynden-Bell, D., Burstein, D., Davies, R. L., Faber, S. M., Terlevich, R., and Wegner, G. (1987). Spectroscopy and photometry of elliptical galaxies. I - A new distance estimator. *ApJ*, 313:42–58.

Dutton, A. A., Conroy, C., van den Bosch, F. C., Simard, L., Mendel, J. T., Courteau, S., Dekel, A., More, S., and Prada, F. (2011). Dark halo response and the stellar initial mass function in early-type and late-type galaxies. *MNRAS*, 416:322–345.

Dutton, A. A., Macciò, A. V., Mendel, J. T., and Simard, L. (2013). Universal IMF versus dark halo response in early-type galaxies: breaking the degeneracy with the Fundamental Plane. *MNRAS*, 432:2496–2511.

Dutton, A. A., Mendel, J. T., and Simard, L. (2012). Evidence for a non-universal stellar initial mass function in low-redshift high-density early-type galaxies. *MNRAS*, 422:L33–L37.

Eisenstein, D. J. (2003). Deprojecting densities from angular cross-correlations. *The Astrophysical Journal*, 586(2):718.

Ellis, R. S., Smail, I., Dressler, A., Couch, W. J., Oemler Jr, A., Butcher, H., and Sharples, R. M. (1997). The homogeneity of spheroidal populations in distant clusters. *The Astrophysical Journal*, 483(2):582.

Erb, D. K., Shapley, A. E., Pettini, M., Steidel, C. C., Reddy, N. A., and Adelberger, K. L. (2006). The Mass-Metallicity Relation at z>˜2. *ApJ*, 644:813–828.

Faber, S. (1973). Variations in spectral-energy distributions and absorption-line strengths among elliptical galaxies. *The Astrophysical Journal*, 179:731–754.

Faber, S., Friel, E., Burstein, D., and Gaskell, C. (1985). Old stellar populations. ii-an analysis of k-giant spectra. *The Astrophysical Journal Supplement Series*, 57:711–741.

Faber, S., Worthey, G., and Gonzalez, J. J. (1992). Absorption-line spectra of elliptical galaxies and their relation to elliptical formation. In *Symposium-International Astronomical Union*, volume 149, pages 255–265. Cambridge University Press.

Faber, S. M. and French, H. B. (1980). Possible M dwarf enrichment in the semistellar nucleus of M31. *ApJ*, 235:405–412.

Faber, S. M. and Jackson, R. E. (1976). Velocity dispersions and mass-to-light ratios for elliptical galaxies. *ApJ*, 204:668–683.

Ferreras, I., La Barbera, F., de la Rosa, I. G., Vazdekis, A., de Carvalho, R. R., Falcón-Barroso, J., and Ricciardelli, E. (2013). Systematic variation of the stellar initial mass function with velocity dispersion in early-type galaxies. *MNRAS*, 429:L15–L19.

Ferreras, I., Weidner, C., Vazdekis, A., and La Barbera, F. (2015). Further evidence for a time-dependent initial mass function in massive early-type galaxies. *MNRAS*, 448:L82–L86.

Fontanot, F., Barbera, F. L., De Lucia, G., Pasquali, A., and Vazdekis, A. (2018a). On the shape and evolution of a cosmic ray regulated galaxy-wide stellar initial mass function. *MNRAS*.

Fontanot, F., De Lucia, G., Hirschmann, M., Bruzual, G., Charlot, S., and Zibetti, S. (2017). Variations of the stellar initial mass function in semi-analytical models: implications for the mass assembly and the chemical enrichment of galaxies in the GAEA model. *MNRAS*, 464:3812–3824.

Fontanot, F., De Lucia, G., Monaco, P., Somerville, R. S., and Santini, P. (2009). The many manifestations of downsizing: hierarchical galaxy formation models confront observations. *Monthly Notices of the Royal Astronomical Society*, 397(4):1776–1790.

Fontanot, F., De Lucia, G., Xie, L., Hirschmann, M., Bruzual, G., and Charlot, S. (2018b). Variations of the stellar initial mass function in semi-analytical models - II. The impact of cosmic ray regulation. *MNRAS*, 475:2467–2479.

Fontanot, F., Pasquali, A., De Lucia, G., van den Bosch, F. C., Somerville, R. S., and Kang, X. (2011). The dependence of agn activity on stellar and halo mass in semi-analytic models. *Monthly Notices of the Royal Astronomical Society*, 413(2):957–970.

Gargiulo, I. D., Cora, S. A., Padilla, N. D., Muñoz Arancibia, A. M., Ruiz, A. N., Orsi, A. A., Tecce, T. E., Weidner, C., and Bruzual, G. (2015). Chemoarchaeological downsizing in a hierarchical universe: impact of a top-heavy IGIMF. *MNRAS*, 446:3820–3841.

Garnett, D. R. (2002). The luminosity-metallicity relation, effective yields, and metal loss in spiral and irregular galaxies. *The Astrophysical Journal*, 581(2):1019.

Garnett, D. R. and Shields, G. A. (1987). The composition gradient across M81. *ApJ*, 317:82–101.

Geha, M., Blanton, M., Masjedi, M., and West, A. (2006). The baryon content of extremely low mass dwarf galaxies. *The Astrophysical Journal*, 653(1):240.

Gibson, B. K. (1997). Galactic winds and the photochemical evolution of elliptical galaxies: the classic model revisited. *MNRAS*, 290:471–489.

Goswami, A. and Reddy, B. E. (2010). Principles and perspectives in cosmochemistry. *Astrophysics and Space Science Proceedings*, 16.

Greggio, L. and Renzini, A. (1983). The binary model for type I supernovae - Theoretical rates. *A&A*, 118:217–222.

Grevesse, N. and Sauval, A. J. (1998). Standard Solar Composition. *Space Sci. Rev.*, 85:161–174.

Grillo, C. and Gobat, R. (2010). On the initial mass function and tilt of the fundamental plane of massive early-type galaxies. *MNRAS*, 402:L67–L71.

Gunawardhana, M. L. P., Hopkins, A. M., Sharp, R. G., Brough, S., Taylor, E., Bland-Hawthorn, J., Maraston, C., Tuffs, R. J., Popescu, C. C., Wijesinghe, D., Jones, D. H., Croom, S., Sadler, E., Wilkins, S., Driver, S. P., Liske, J., Norberg, P., Baldry, I. K., Bamford, S. P., Loveday, J., Peacock, J. A., Robotham, A. S. G., Zucker, D. B., Parker, Q. A., Conselice, C. J., Cameron, E., Frenk, C. S., Hill, D. T., Kelvin, L. S., Kuijken, K., Madore, B. F., Nichol, B., Parkinson, H. R., Pimbblet, K. A., Prescott, M., Sutherland, W. J., Thomas, D., and van Kampen, E. (2011). Galaxy and Mass Assembly (GAMA): the star formation rate dependence of the stellar initial mass function. *MNRAS*, 415:1647–1662.

Guo, Q., White, S., Boylan-Kolchin, M., De Lucia, G., Kauffmann, G., Lemson, G., Li, C., Springel, V., and Weinmann, S. (2011). From dwarf spheroidals to cD galaxies: simulating the galaxy population in a ΛCDM cosmology. *MNRAS*, 413:101–131.

Henry, A., Scarlata, C., Domínguez, A., Malkan, M., Martin, C. L., Siana, B., Atek, H., Bedregal, A. G., Colbert, J. W., Rafelski, M., Ross, N., Teplitz,

H., Bunker, A. J., Dressler, A., Hathi, N., Masters, D., McCarthy, P., and Straughn, A. (2013). Low Masses and High Redshifts: The Evolution of the Mass-Metallicity Relation. *ApJ*, 776:L27.

Hopkins, P. F. (2013). Variations in the stellar cmf and imf: from bottom to top. *Monthly Notices of the Royal Astronomical Society*, 433(1):170–177.

Hoyle, F. (1946). The synthesis of the elements from hydrogen. *Monthly Notices of the Royal Astronomical Society*, 106(5):343–383.

Hubble, E. (1936). Realm of the nebulae (realm of the nebulae, by ep hubble. new haven.

Hunter, D. A., Elmegreen, B. G., Dupuy, T. J., and Mortonson, M. (2003). Cluster Mass Functions in the Large and Small Magellanic Clouds: Fading and Size-of-Sample Effects. *AJ*, 126:1836–1848.

Iwamoto, K., Brachwitz, F., Nomoto, K., Kishimoto, N., Umeda, H., Hix, W. R., and Thielemann, F.-K. (1999). Nucleosynthesis in Chandrasekhar Mass Models for Type IA Supernovae and Constraints on Progenitor Systems and Burning-Front Propagation. *ApJS*, 125:439–462.

Jaffe, W. (1983). A simple model for the distribution of light in spherical galaxies. *MNRAS*, 202:995–999.

Jerabkova, T., Zonoozi, A., Kroupa, P., Beccari, G., Yan, Z., Vazdekis, A., and Zhang, Z. (2018). The impact of the metallicity and star formation rate on the time-dependent galaxy-wide stellar initial mass function. *arXiv preprint arXiv:1809.04603*.

Johansson, J., Thomas, D., and Maraston, C. (2012). Chemical element ratios of Sloan Digital Sky Survey early-type galaxies. *MNRAS*, 421:1908–1926.

Jorgensen, I., Franx, M., and Kjaergaard, P. (1996). The Fundamental Plane for cluster E and S0 galaxies. *MNRAS*, 280:167–185.

Kauffmann, G. and Charlot, S. (1998). Chemical enrichment and the origin of the colour-magnitude relation of elliptical galaxies in a hierarchical merger model. *MNRAS*, 294:705.

Kauffmann, G. and White, S. D. M. (1993). The merging history of dark matter haloes in a hierarchical universe. *MNRAS*, 261.

Kennicutt, Jr., R. C. (1998). The Global Schmidt Law in Star-forming Galaxies. *ApJ*, 498:541–552.

Kewley, L. J. and Dopita, M. (2002). Using strong lines to estimate abundances in extragalactic h ii regions and starburst galaxies. *The Astrophysical Journal Supplement Series*, 142(1):35.

Kewley, L. J. and Ellison, S. L. (2008). Metallicity calibrations and the mass-metallicity relation for star-forming galaxies. *The Astrophysical Journal*, 681(2):1183.

Kobayashi, C., Springel, V., and White, S. D. (2007). Simulations of cosmic chemical enrichment. *Monthly Notices of the Royal Astronomical Society*, 376(4):1465–1479.

Komatsu, E., Smith, K. M., Dunkley, J., Bennett, C. L., Gold, B., Hinshaw, G., Jarosik, N., Larson, D., Nolta, M. R., Page, L., Spergel, D. N., Halpern, M., Hill, R. S., Kogut, A., Limon, M., Meyer, S. S., Odegard, N., Tucker, G. S., Weiland, J. L., Wollack, E., and Wright, E. L. (2011). Seven-year Wilkinson Microwave Anisotropy Probe (WMAP) Observations: Cosmological Interpretation. *The Astrophysical Journal Supplement Series*, 192:18.

Kormendy, J., Bender, R., and Cornell, M. (2011). Supermassive black holes do not correlate with galaxy disks or pseudobulges. *Nature*, 469(7330):374.

Kovac, J. M., Leitch, E. M., Pryke, C., Carlstrom, J. E., Halverson, N. W., and Holzapfel, W. L. (2002). Detection of polarization in the cosmic microwave background using DASI. *Nature*, 420:772–787.

Kroupa, P. (2001). On the variation of the initial mass function. *MNRAS*, 322:231–246.

Kroupa, P. (2002). The Initial Mass Function of Stars: Evidence for Uniformity in Variable Systems. *Science*, 295:82–91.

Kroupa, P., Tout, C. A., and Gilmore, G. (1993). The distribution of low-mass stars in the Galactic disc. *MNRAS*, 262:545–587.

Kroupa, P. and Weidner, C. (2003). Galactic-Field Initial Mass Functions of Massive Stars. *ApJ*, 598:1076–1078.

Kroupa, P., Weidner, C., Pflamm-Altenburg, J., Thies, I., Dabringhausen, J., Marks, M., and Maschberger, T. (2013). *The Stellar and Sub-Stellar Initial Mass Function of Simple and Composite Populations*, page 115.

Krumholz, M. R. (2011). On the Origin of Stellar Masses. *ApJ*, 743:110.

Kuntschner, H. (2000). The stellar populations of early-type galaxies in the Fornax cluster. *MNRAS*, 315:184–208.

La Barbera, F., de Carvalho, R. R., de La Rosa, I. G., Lopes, P. A. A., Kohl-Moreira, J. L., and Capelato, H. V. (2010). SPIDER - I. Sample and galaxy parameters in the grizYJHK wavebands. *MNRAS*, 408:1313–1334.

La Barbera, F., Ferreras, I., Vazdekis, A., de la Rosa, I. G., de Carvalho, R. R., Trevisan, M., Falcón-Barroso, J., and Ricciardelli, E. (2013). SPIDER VIII - constraints on the stellar initial mass function of early-type galaxies from a variety of spectral features. *MNRAS*, 433:3017–3047.

La Barbera, F., Vazdekis, A., Ferreras, I., Pasquali, A., Cappellari, M., Martín-Navarro, I., Schönebeck, F., and Falcón-Barroso, J. (2016). Radial constraints on the initial mass function from TiO features and Wing-Ford band in early-type galaxies. *MNRAS*, 457:1468–1489.

Lada, C. J. and Lada, E. A. (2003). Embedded Clusters in Molecular Clouds. *ARA&A*, 41:57–115.

Larson, R. B. (1974). Dynamical models for the formation and evolution of spherical galaxies. *MNRAS*, 166:585–616.

Larson, R. B. (1998). Early star formation and the evolution of the stellar initial mass function in galaxies. *MNRAS*, 301:569–581.

Larson, R. B. (2005). Thermal physics, cloud geometry and the stellar initial mass function. *MNRAS*, 359:211–222.

Lequeux, J., Peimbert, M., Rayo, J. F., Serrano, A., and Torres-Peimbert, S. (1979). Chemical composition and evolution of irregular and blue compact galaxies. *A&A*, 80:155–166.

Lian, J., Thomas, D., Maraston, C., Goddard, D., Comparat, J., Gonzalez-Perez, V., and Ventura, P. (2017). The mass–metallicity relations for gas and stars in star-forming galaxies: strong outflow versus variable imf. *Monthly Notices of the Royal Astronomical Society*, 474(1):1143–1164.

Lidman, C., Rosati, P., Tanaka, M., Strazzullo, V., Demarco, R., Mullis, C., Ageorges, N., Kissler-Patig, M., Petr-Gotzens, M., and Selman, F. (2008). Hawk-i imaging of the x-ray luminous galaxy cluster xmmu j2235. 3-2557-the red sequence at z= 1.39. *Astronomy & Astrophysics*, 489(3):981–988.

Longhetti, M., Bressan, A., Chiosi, C., and Rampazzo, R. (2000). Star formation history of early-type galaxies in low density environments. iv. what do we learn from nuclear line-strength indices? *Astronomy and Astrophysics*, 353:917–929.

Mannucci, F., Cresci, G., Maiolino, R., et al. (2010). A fundamental relation between mass, star formation rate and metallicity in local and high-redshift galaxies. *Monthly Notices of the Royal Astronomical Society*, 408(4):2115–2127.

Maraston, C. (1998). Evolutionary synthesis of stellar populations: a modular tool. *Monthly Notices of the Royal Astronomical Society*, 300:872–892.

Maraston, C. (2003). Stellar population models. In *Extragalactic Globular Cluster Systems*, pages 237–248. Springer.

Martín-Navarro, I. (2016). Revisiting the classics: is [Mg/Fe] a good proxy for galaxy formation time-scales? *MNRAS*, 456:L104–L108.

Martinelli, A., Matteucci, F., and Colafrancesco, S. (1998). A possible theoretical explanation of metallicity gradients in elliptical galaxies. *MNRAS*, 298:42–52.

Matteucci, F. (1992). The influence of dark matter on the chemical evolution of elliptical galaxies. *ApJ*, 397:32–37.

Matteucci, F. (1994). Abundance ratios in ellipticals and galaxy formation. *A&A*, 288:57–64.

Matteucci, F. (1997). The Chemical Evolution of Galaxies. In Valls-Gabaud, D., Hendry, M. A., Molaro, P., and Chamcham, K., editors, *From Quantum Fluctuations to Cosmological Structures*, volume 126 of *Astronomical Society of the Pacific Conference Series*, page 495.

Matteucci, F. (2012). *Chemical Evolution of Galaxies*.

Matteucci, F. and Gibson, B. K. (1995). Chemical abundances in clusters of galaxies. *A&A*, 304:11.

Matteucci, F. and Greggio, L. (1986). Relative roles of type I and II supernovae in the chemical enrichment of the interstellar gas. *A&A*, 154:279–287.

Matteucci, F., Ponzone, R., and Gibson, B. K. (1998). On the trend of [Mg/Fe] among giant elliptical galaxies. *A&A*, 335:855–866.

Matteucci, F. and Recchi, S. (2001). On the Typical Timescale for the Chemical Enrichment from Type Ia Supernovae in Galaxies. *ApJ*, 558:351–358.

Matteucci, F. and Vettolani, G. (1988). Chemical abundances in galaxy clusters - A theoretical approach. *A&A*, 202:21–26.

McGaugh, S. S. and De Blok, W. (1997). Gas mass fractions and the evolution of spiral galaxies. *The Astrophysical Journal*, 481(2):689.

Meneguzzi, M., Audouze, J., and Reeves, H. (1971). The production of the elements Li, Be, B by galactic cosmic rays in space and its relation with stellar observations. *A&A*, 15:337–359.

Monaco, P., Fontanot, F., and Taffoni, G. (2007). The morgana model for the rise of galaxies and active nuclei. *Monthly Notices of the Royal Astronomical Society*, 375(4):1189–1219.

Neyman, J. and Scott, E. L. (1952). A Theory of the Spatial Distribution of Galaxies. *ApJ*, 116:144.

Nusser, A. and Dekel, A. (1992). Tracing large-scale fluctuations back in time. *The Astrophysical Journal*, 391:443–452.

Okamoto, T., Nagashima, M., Lacey, C. G., and Frenk, C. S. (2017). The metal enrichment of passive galaxies in cosmological simulations of galaxy formation. *MNRAS*, 464:4866–4874.

Oswalt, T. D. and Keel, W. C. (2013). *Planets, Stars and Stellar Systems Vol. 6*.

Padovani, P. and Matteucci, F. (1993). Stellar Mass Loss in Elliptical Galaxies and the Fueling of Active Galactic Nuclei. *ApJ*, 416:26.

Pagel, B. E. J. (1997). *Nucleosynthesis and Chemical Evolution of Galaxies*.

Pagel, B. E. J. and Patchett, B. E. (1975). Metal abundances in nearby stars and the chemical history of the solar neighborhood. *MNRAS*, 172:13–40.

Peebles, P. J. E. (1980). *The large-scale structure of the universe*. Princeton university press.

Peletier, R. F. (2013). Stellar populations. *Secular Evolution of Galaxies*, 1:353.

Peng, Y.-j. and Maiolino, R. (2014). From haloes to galaxies–i. the dynamics of the gas regulator model and the implied cosmic ssfr history. *Monthly Notices of the Royal Astronomical Society*, 443(4):3643–3664.

Perivolaropoulos, L. (2011). ΛCDM: Triumphs, Puzzles and Remedies. *Journal of Cosmology*, 15:6054–6064.

Pettini, M. and Pagel, B. E. (2004). [o iii]/[n ii] as an abundance indicator at high redshift. *Monthly Notices of the Royal Astronomical Society*, 348(3):L59–L63.

Pilyugin, L. (2001). On the oxygen abundance determination in hii regions.-high-metallicity regions. *Astronomy & Astrophysics*, 369(2):594–604.

Pilyugin, L. S. and Thuan, T. X. (2005). Oxygen abundance determination in h ii regions: The strong line intensities-abundance calibration revisited. *The Astrophysical Journal*, 631(1):231.

Pilyugin, L. S., Vílchez, J. M., and Contini, T. (2004). Oxygen and nitrogen abundances in nearby galaxies. Correlations between oxygen abundance and macroscopic properties. *A&A*, 425:849–869.

Pipino, A., Devriendt, J. E. G., Thomas, D., Silk, J., and Kaviraj, S. (2009). GALICS. II: the [α/Fe] -mass relation in elliptical galaxies. *A&A*, 505:1075–1086.

Pipino, A., Lilly, S. J., and Carollo, C. (2014). On the relation between specific star formation rate and metallicity. *Monthly Notices of the Royal Astronomical Society*, 441(2):1444–1456.

Pipino, A. and Matteucci, F. (2004). Photochemical evolution of elliptical galaxies - I. The high-redshift formation scenario. *MNRAS*, 347:968–984.

Pipino, A. and Matteucci, F. (2008). Are dry mergers of ellipticals the way to reconcile model predictions with downsizing? *A&A*, 486:763–769.

Pipino, A., Matteucci, F., Borgani, S., and Biviano, A. (2002). SNe heating and the chemical evolution of the intra-cluster medium. *New Astron.*, 7:227–247.

Planck Collaboration (2016). Planck 2015 results. XIII. Cosmological parameters. *A&A*, 594:A13.

Poggianti, B. M., Bridges, T. J., Carter, D., Mobasher, B., Doi, M., Iye, M., Kashikawa, N., Komiyama, Y., Okamura, S., Sekiguchi, M., et al. (2001). Ages of s0 and elliptical galaxies in the coma cluster. *The Astrophysical Journal*, 563(1):118.

Rakos, K., Schombert, J., and Odell, A. (2007). Age and metallicities of cluster galaxies: A1185 and coma. *The Astrophysical Journal*, 658(2):929.

Recchi, S., Calura, F., Gibson, B. K., and Kroupa, P. (2014). The [α/Fe] ratios of very metal-poor stars within the integrated galactic initial mass function theory. *MNRAS*, 437:994–1008.

Recchi, S., Calura, F., and Kroupa, P. (2009). The chemical evolution of galaxies within the IGIMF theory: the [α/Fe] ratios and downsizing. *A&A*, 499:711–722.

Recchi, S., Matteucci, F., and D'Ercole, A. (2001). Dynamical and chemical evolution of gas-rich dwarf galaxies. *MNRAS*, 322:800–820.

Renzini, A. (2006). Stellar population diagnostics of elliptical galaxy formation. *Annu. Rev. Astron. Astrophys.*, 44:141–192.

Renzini, A. and Buzzoni, A. (1986). Global properties of stellar populations and the spectral evolution of galaxies. In Chiosi, C. and Renzini, A., editors, *Spectral Evolution of Galaxies*, volume 122 of *Astrophysics and Space Science Library*, pages 195–231.

Renzini, A. and Greggio, L. (2012). *Stellar populations: a guide from low to high redshift*. John Wiley & Sons.

Roberts, M. S. and Haynes, M. P. (1994). Physical parameters along the hubble sequence. *Annual Review of Astronomy and Astrophysics*, 32(1):115–152.

Robertson, B., Cox, T. J., Hernquist, L., Franx, M., Hopkins, P. F., Martini, P., and Springel, V. (2006). The fundamental scaling relations of elliptical galaxies. *The Astrophysical Journal*, 641(1):21.

Romano, D., Chiappini, C., Matteucci, F., and Tosi, M. (2005). Quantifying the uncertainties of chemical evolution studies-i. stellar lifetimes and initial mass function. *Astronomy & Astrophysics*, 430(2):491–505.

Rosani, G., Pasquali, A., La Barbera, F., Ferreras, I., and Vazdekis, A. (2018). The influence of galaxy environment on the stellar initial mass

function of early-type galaxies. *Monthly Notices of the Royal Astronomical Society*, page sty528.

Saglia, R. P., Maraston, C., Thomas, D., Bender, R., and Colless, M. (2002). The Puzzlingly Small Ca II Triplet Absorption in Elliptical Galaxies. *ApJ*, 579:L13–L16.

Salaris, M. and Cassisi, S. (2005). *Evolution of stars and stellar populations*. John Wiley & Sons.

Salpeter, E. E. (1955). The Luminosity Function and Stellar Evolution. *ApJ*, 121:161.

Sandage, A. and Visvanathan, N. (1978a). The color-absolute magnitude relation for e and s0 galaxies. ii-new colors, magnitudes, and types for 405 galaxies. *The Astrophysical Journal*, 223:707–729.

Sandage, A. and Visvanathan, N. (1978b). Color-absolute magnitude relation for e and s0 galaxies. iii-fully corrected photometry for 405 galaxies: Comparison of color distributions for e and s0 field and cluster galaxies. *The Astrophysical Journal*, 225:742–750.

Scalo, J. (1997). The imf revisited: a case for variations. *arXiv preprint astro-ph/9712317*.

Scalo, J. M. (1986). The stellar initial mass function. *Fundamentals Cosmic Phys.*, 11:1–278.

Schawinski, K., Kaviraj, S., Khochfar, S., Yoon, S.-J., Yi, S., Deharveng, J.-M., Boselli, A., Barlow, T., Conrow, T., Forster, K., et al. (2007). The effect of environment on the ultraviolet color-magnitude relation of early-type galaxies. *The Astrophysical Journal Supplement Series*, 173(2):512.

Schawinski, K., Urry, C. M., Simmons, B. D., Fortson, L., Kaviraj, S., Keel, W. C., Lintott, C. J., Masters, K. L., Nichol, R. C., Sarzi, M., Skibba, R., Treister, E., Willett, K. W., Wong, O. I., and Yi, S. K. (2014). The green valley is a red herring: Galaxy Zoo reveals two evolutionary pathways towards quenching of star formation in early- and late-type galaxies. *MNRAS*, 440:889–907.

Schaye, J., Dalla Vecchia, C., Booth, C. M., Wiersma, R. P. C., Theuns, T., Haas, M. R., Bertone, S., Duffy, A. R., McCarthy, I. G., and van de Voort, F. (2010). The physics driving the cosmic star formation history. *MNRAS*, 402:1536–1560.

Seeger, P. A., Fowler, W. A., and Clayton, D. D. (1965). Nucleosynthesis of heavy elements by neutron capture. *The Astrophysical Journal*.

Segers, M. C., Schaye, J., Bower, R. G., Crain, R. A., Schaller, M., and Theuns, T. (2016). The origin of the α-enhancement of massive galaxies. *Monthly Notices of the Royal Astronomical Society: Letters*, 461(1):L102–L106.

Silk, J. (1995). A theory for the initial mass function. *ApJ*, 438:L41–L44.

Smith, R. J., Lucey, J. R., and Conroy, C. (2015). The SINFONI Nearby Elliptical Lens Locator Survey: discovery of two new low-redshift strong lenses and implications for the initial mass function in giant early-type galaxies. *MNRAS*, 449:3441–3457.

Spiniello, C., Trager, S., Koopmans, L. V. E., and Conroy, C. (2014). The stellar IMF in early-type galaxies from a non-degenerate set of optical line indices. *MNRAS*, 438:1483–1499.

Spiniello, C., Trager, S. C., Koopmans, L. V. E., and Chen, Y. P. (2012). Evidence for a Mild Steepening and Bottom-heavy Initial Mass Function in Massive Galaxies from Sodium and Titanium-oxide Indicators. *ApJ*, 753:L32.

Spitoni, E. (2015). New chemical evolution analytical solutions including environment effects. *MNRAS*, 451:1090–1103.

Spitoni, E., Calura, F., Matteucci, F., and Recchi, S. (2010). The origin of the mass-metallicity relation: an analytical approach. *Astronomy & Astrophysics*, 514:A73.

Spitoni, E., Vincenzo, F., and Matteucci, F. (2017). New analytical solutions for chemical evolution models: characterizing the population of star-forming and passive galaxies. *A&A*, 599:A6.

Stanford, S., Eisenhardt, P. R., and Dickinson, M. (1998). The evolution of early-type galaxies in distant clusters. *The Astrophysical Journal*, 492(2):461.

Stasinska, G. (2004). Abundance determinations in h n regions and planetary nebulae. *Cosmochemistry: The Melting Pot of the Elements*, page 115.

Strateva, I., Ivezić, Ž., Knapp, G. R., Narayanan, V. K., Strauss, M. A., Gunn, J. E., Lupton, R. H., Schlegel, D., Bahcall, N. A., Brinkmann,

J., Brunner, R. J., Budavári, T., Csabai, I., Castander, F. J., Doi, M., Fukugita, M., Győry, Z., Hamabe, M., Hennessy, G., Ichikawa, T., Kunszt, P. Z., Lamb, D. Q., McKay, T. A., Okamura, S., Racusin, J., Sekiguchi, M., Schneider, D. P., Shimasaku, K., and York, D. (2001). Color Separation of Galaxy Types in the Sloan Digital Sky Survey Imaging Data. *AJ*, 122:1861–1874.

Strauss, M. A., Weinberg, D. H., Lupton, R. H., Narayanan, V. K., Annis, J., Bernardi, M., Blanton, M., Burles, S., Connolly, A., Dalcanton, J., et al. (2002). Spectroscopic target selection in the sloan digital sky survey: the main galaxy sample. *The Astronomical Journal*, 124(3):1810.

Suess, H. E. and Urey, H. C. (1956). Abundances of the elements. *Reviews of Modern Physics*, 28(1):53.

Talbot Jr, R. J. and Arnett, W. D. (1971). The evolution of galaxies. i. formulation and mathematical behavior of the one-zone model. *The Astrophysical Journal*, 170:409.

Tantalo, R., Chiosi, C., and Bressan, A. (1998). Ages and metallicities in elliptical galaxies from the H_beta, <Fe>, and Mg_2 diagnostics. *A&A*, 333:419–432.

Tantalo, R., Chiosi, C., Bressan, A., and Fagotto, F. (1996). Spectrophotometric evolution of elliptical galaxies. II. Models with infall. *Astronomy & Astrophysics*, 311:361–383.

Terlevich, A. and Forbes, D. A. (2002). A catalogue and analysis of local galaxy ages and metallicities. *Monthly Notices of the Royal Astronomical Society*, 330(3):547–562.

Thielemann, F.-K., Nomoto, K., and Hashimoto, M.-A. (1996). Core-Collapse Supernovae and Their Ejecta. *ApJ*, 460:408.

Thomas, D. (1999). Abundance ratios in hierarchical galaxy formation. *MNRAS*, 306:655–661.

Thomas, D., Greggio, L., and Bender, R. (1999). Constraints on galaxy formation from alpha-enhancement in luminous elliptical galaxies. *MNRAS*, 302:537–548.

Thomas, D., Maraston, C., and Bender, R. (2003). Stellar population models of Lick indices with variable element abundance ratios. *MNRAS*, 339:897–911.

Thomas, D., Maraston, C., Bender, R., and Mendes de Oliveira, C. (2005). The Epochs of Early-Type Galaxy Formation as a Function of Environment. *ApJ*, 621:673–694.

Thomas, D., Maraston, C., Schawinski, K., Sarzi, M., and Silk, J. (2010). Environment and self-regulation in galaxy formation. *MNRAS*, 404:1775–1789.

Thomas, J., Saglia, R. P., Bender, R., Thomas, D., Gebhardt, K., Magorrian, J., Corsini, E. M., and Wegner, G. (2007). Dynamical modelling of luminous and dark matter in 17 Coma early-type galaxies. *MNRAS*, 382:657–684.

Tinsley, B. (1974). Constraints on models for chemical evolution in the solar neighborhood. *The Astrophysical Journal*, 192:629–641.

Tinsley, B. M. (1980). Evolution of the stars and gas in galaxies. *Fundamentals of cosmic physics*, 5:287–388.

Trager, S. C., Worthey, G., Faber, S. M., Burstein, D., and González, J. J. (1998). Old Stellar Populations. VI. Absorption-Line Spectra of Galaxy Nuclei and Globular Clusters. *ApJS*, 116:1–28.

Tremonti, C. A., Heckman, T. M., Kauffmann, G., et al. (2004). The origin of the mass-metallicity relation: insights from 53,000 star-forming galaxies in the sloan digital sky survey. *The Astrophysical Journal*, 613(2):898.

Treu, T., Auger, M. W., Koopmans, L. V. E., Gavazzi, R., Marshall, P. J., and Bolton, A. S. (2010). The Initial Mass Function of Early-Type Galaxies. *ApJ*, 709:1195–1202.

van den Hoek, L. B. and Groenewegen, M. A. T. (1997). New theoretical yields of intermediate mass stars. *A&AS*, 123.

Van Dokkum, P., Stanford, S., Holden, B., Eisenhardt, P., Dickinson, M., and Elston, R. (2001). The galaxy population of cluster rx j0848+ 4453 at z= 1.27. *The Astrophysical Journal Letters*, 552(2):L101.

van Dokkum, P. G. and Conroy, C. (2010). A substantial population of low-mass stars in luminous elliptical galaxies. *Nature*, 468:940–942.

van Dokkum, P. G. and Conroy, C. (2011). Confirmation of Enhanced Dwarf-sensitive Absorption Features in the Spectra of Massive Elliptical Galaxies: Further Evidence for a Non-universal Initial Mass Function. *ApJ*, 735:L13.

van Dokkum, P. G., Franx, M., Kelson, D. D., and Illingworth, G. D. (1998). Luminosity evolution of early-type galaxies to z= 0.83: Constraints on formation epoch and ω. *The Astrophysical Journal Letters*, 504(1):L17.

Vazdekis, A., Cenarro, A. J., Gorgas, J., Cardiel, N., and Peletier, R. F. (2003). Empirical calibration of the near-infrared CaII triplet - IV. The stellar population synthesis models. *MNRAS*, 340:1317–1345.

Vazdekis, A., Coelho, P., Cassisi, S., Ricciardelli, E., Falcón-Barroso, J., Sánchez-Blázquez, P., La Barbera, F., Beasley, M. A., and Pietrinferni, A. (2015). Evolutionary stellar population synthesis with MILES - II. Scaled-solar and α-enhanced models. *MNRAS*, 449:1177–1214.

Vazdekis, A., Koleva, M., Ricciardelli, E., Röck, B., and Falcón-Barroso, J. (2016). UV-extended E-MILES stellar population models: young components in massive early-type galaxies. *MNRAS*, 463:3409–3436.

Vazdekis, A., Peletier, R. F., Beckman, J. E., and Casuso, E. (1997). A New Chemo-evolutionary Population Synthesis Model for Early-Type Galaxies. II. Observations and Results. *ApJS*, 111:203–232.

Vincenzo, F., Matteucci, F., de Boer, T. J. L., Cignoni, M., and Tosi, M. (2016). Lighting up stars in chemical evolution models: the CMD of Sculptor. *MNRAS*, 460:2238–2244.

Vincenzo, F., Matteucci, F., Recchi, S., Calura, F., McWilliam, A., and Lanfranchi, G. A. (2015). The IGIMF and other IMFs in dSphs: the case of Sagittarius. *MNRAS*, 449:1327–1339.

Vincenzo, F., Matteucci, F., Vattakunnel, S., and Lanfranchi, G. A. (2014). Chemical evolution of classical and ultra-faint dwarf spheroidal galaxies. *MNRAS*, 441:2815–2830.

Wang, L., Yang, X., Shen, S., Mo, H. J., van den Bosch, F. C., Luo, W., Wang, Y., Lau, E. T., Wang, Q. D., Kang, X., and Li, R. (2014). Measuring the X-ray luminosities of SDSS DR7 clusters from ROSAT All Sky Survey. *MNRAS*, 439:611–622.

Weidner, C., Ferreras, I., Vazdekis, A., and La Barbera, F. (2013). The (galaxy-wide) IMF in giant elliptical galaxies: from top to bottom. *MNRAS*, 435:2274–2280.

Weidner, C. and Kroupa, P. (2004). Evidence for a fundamental stellar upper mass limit from clustered star formation. *MNRAS*, 348:187–191.

Weidner, C. and Kroupa, P. (2005). The Variation of Integrated Star Initial Mass Functions among Galaxies. *ApJ*, 625:754–762.

Weidner, C., Kroupa, P., and Bonnell, I. A. D. (2010). The relation between the most-massive star and its parental star cluster mass. *MNRAS*, 401:275–293.

Weidner, C., Kroupa, P., and Pflamm-Altenburg, J. (2011). Top-heavy integrated galactic stellar initial mass functions in starbursts. *MNRAS*, 412:979–986.

Whelan, J. and Iben, Jr., I. (1973). Binaries and Supernovae of Type I. *ApJ*, 186:1007–1014.

White, S. D. M. and Frenk, C. S. (1991). Galaxy Formation through Hierarchical Clustering. *ApJ*, 379:52.

White, S. D. M. and Rees, M. J. (1978). Core condensation in heavy halos: a two-stage theory for galaxy formation and clustering. *MNRAS*, 183:341–358.

Wing, R. F. and Ford, Jr., W. K. (1969). The Infrared Spectrum of the Cool Dwarf Wolf 359. *PASP*, 81:527–529.

Worthey, G., Faber, S., Gonzalez, J. J., et al. (1994). Old stellar populations. 5: Absorption feature indices for the complete lick/ids sample of stars. *The Astrophysical Journal Supplement Series*, 94:687–722.

Worthey, G., Faber, S. M., and Gonzalez, J. J. (1992). MG and Fe absorption features in elliptical galaxies. *ApJ*, 398:69–73.

Yan, Z., Jerabkova, T., and Kroupa, P. (2017). The optimally sampled galaxy-wide stellar initial mass function-observational tests and the publicly available galimf code. *Astronomy & Astrophysics*, 607:A126.

Yang, X., Mo, H. J., van den Bosch, F. C., Pasquali, A., Li, C., and Barden, M. (2007). Galaxy Groups in the SDSS DR4. I. The Catalog and Basic Properties. *ApJ*, 671:153–170.

Yoshii, Y. and Arimoto, N. (1987). Spheroidal systems as a one-parameter family of mass at their birth. *A&A*, 188:13–23.

Zaritsky, D., Kennicutt Jr, R. C., and Huchra, J. P. (1994). H ii regions and the abundance properties of spiral galaxies. *The Astrophysical Journal*, 420:87–109.

Zhang, Q. and Fall, S. M. (1999). The Mass Function of Young Star Clusters in the "Antennae" Galaxies. *ApJ*, 527:L81–L84.

Appendix A

Light averaged metallicities

As described in Sec. 3.4, in order to compare the results of our chemical evolution model with data it is first necessary to derive the chemical composition of the stellar population; this can be done by averaging the chemical abundances in ISM, either on mass or luminosity.
We always applied mass-weighted estimates, based on the results by Yoshii and Arimoto (1987), Gibson (1997) and Matteucci et al. (1998), showing that there is no significant difference for massive galaxies ($M > 10^9\, M_\odot$) between light and mass weighted abundances.
We further tested this assumption by recomputing the light-averaged metallicity $[Z/H]$ for the sample of models obtained with the Salpeter IMF (Model 01) described in Chapter 6, and we compared them with the corresponding mass-averaged ones, as shown in Figure A.1.

As evident from the scatter plot, there is an average offset between the two quantities, with the light-weighted abundances being generally higher than the mass-averaged ones. The inserted histogram in Fig. A.1 shows the distribution of the differences between the two averages for each model (solid line), while the dotted line shows a gaussian fit to the histogram. The average difference is always less than 0,1 dex, within the observational error. Our conclusions, however, were not significantly affected by this shift, since we are not interested in absolute abundances, but in abundance trends.

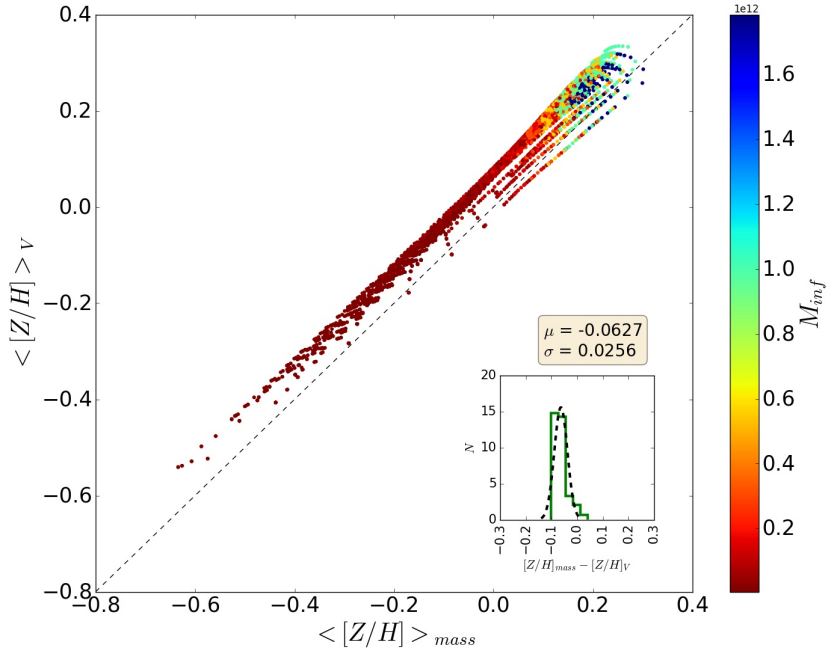

Figure A.1: Scatter plot showing the comparison between the mass and light-weighted average $< [Z/H] >_V$ for the 4400 model galaxies obtained with the Salpeter IMF (Model 01). The points are color-coded according to the initial infall mass M_{inf}. The inserted histogram shows the distribution of the differences between the two averages for each model (solid line), while the dotted line shows a gaussian fit to the histogram, whose parameters are reported in the box above.

Appendix B

Matches for central/satellites

As reported in section 6.6, we analyzed the impact of hierarchy on the matching between models and data. Figures B.1 to B.4 are analogous to figures 6.8 to 6.13, and show the results of the matching procedure with the subset of central/satellite galaxies in the dataset. As mentioned in the text, no significant difference with the general case (where we did not divide galaxies according to their hierarchy) is noticeable.

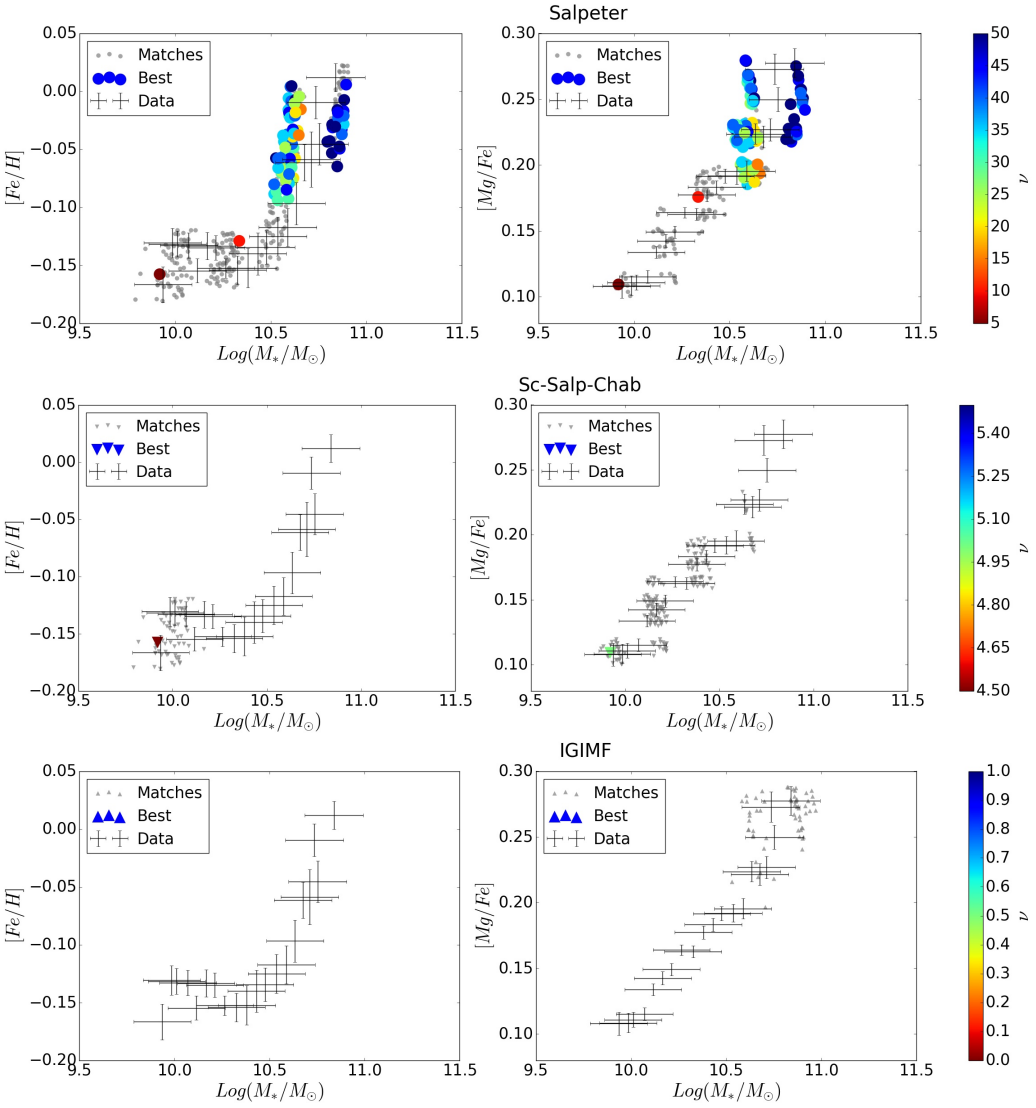

Figure B.1: Comparison between **central** galaxies in the dataset and Models01 (top row), 02 (central row) and 03 (bottom row) for the $[Fe/H]$ and $[Mg/Fe]$ abundance ratios. The black crosses represent abundances in the dataset, with the respective errors. Models matching the $[Fe/H]$-mass and the $[Mg/Fe]$-mass relations simultaneously are color-coded according to their star formation efficiency ν, while the ones matching only one of the two relations are shown with fading, smaller markers.

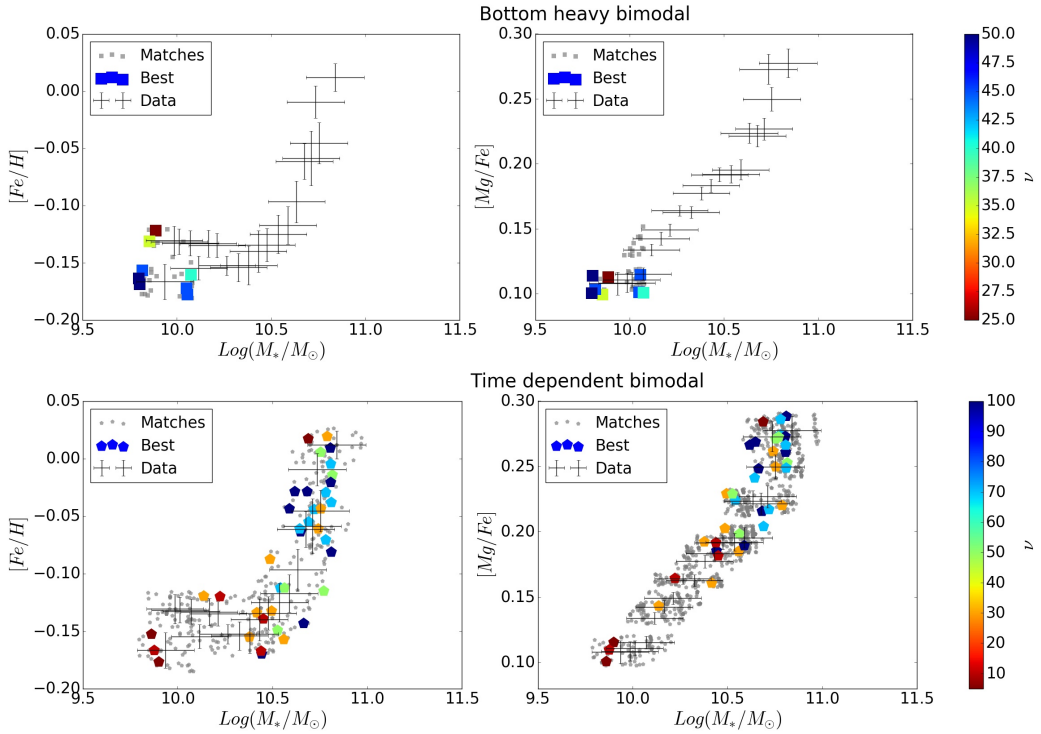

Figure B.2: Analogous to previous Figure B.1, for Models04 (top row) and 05 (bottom row).

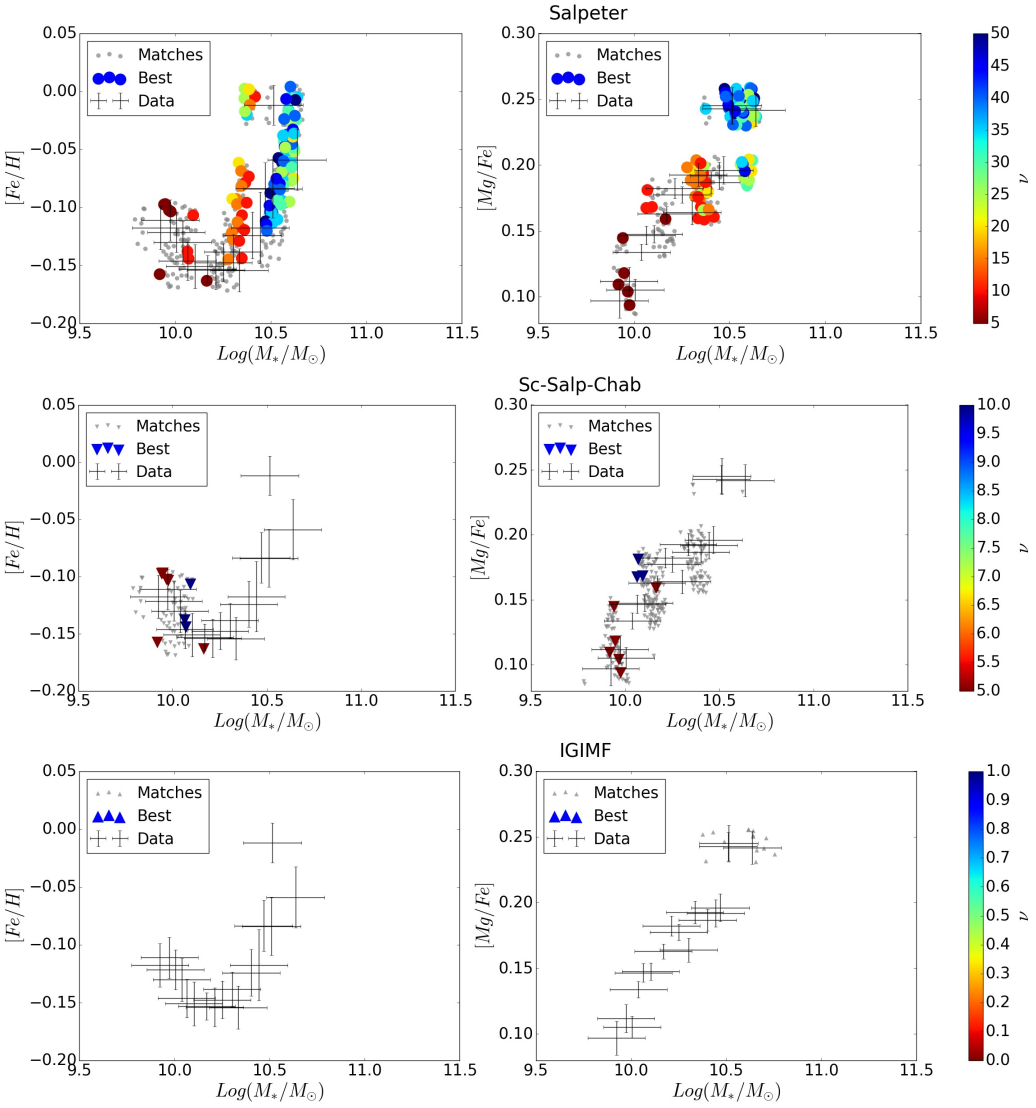

Figure B.3: Comparison between **satellite** galaxies in the dataset and Models01 (top row), 02 (central row) and 03 (bottom row) for the $[Fe/H]$ and $[Mg/Fe]$ abundance ratios. The black crosses represent abundances in the dataset, with the respective errors. Models matching the $[Fe/H]$-mass and the $[Mg/Fe]$-mass relations simultaneously are color-coded according to their star formation efficiency ν, while the ones matching only one of the two relations are shown with fading, smaller markers.

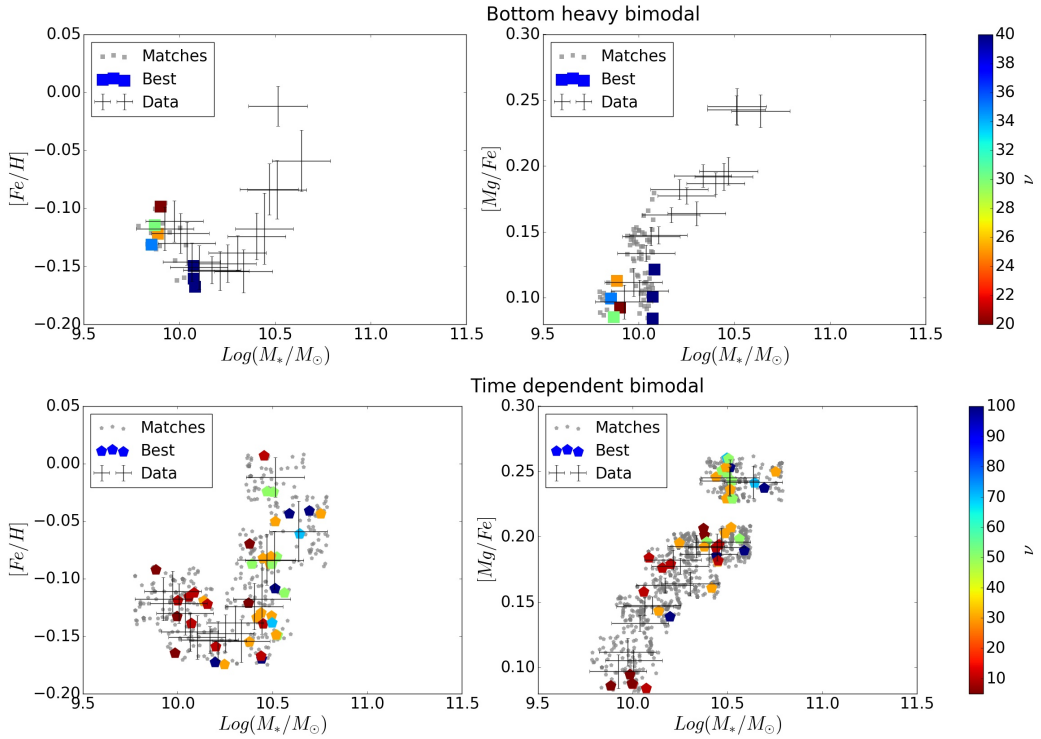

Figure B.4: Analogous to previous Figure B.3, for Models04 (top row) and 05 (bottom row).

List of Figures

List of Tables